Inorganic geochemical redox proxies - Indicators for rapid paleoenvironmental changes and related diagenetic processes in recent and ancient marine sediments

Dissertation
Zur Erlangung des Doktorgrades der Naturwissenschaften (Dr. rer. nat.)
am Fachbereich Geowissenschaften der Universität Bremen, Deutschland

Dissertation
In review for the Doctoral Degree in Natural Sciences (Dr. rer. nat.)
at the Faculty of Geosciences at Bremen University, Germany

vorgelegt von
presented by

Christian März

Bremen, Dezember 2007

Preface

This study was funded by the Deutsche Forschungsgemeinschaft (DFG) via the International Graduate College EUROPROX: Proxies in Earth History, within the subproject 8.3: *Rapid redox changes across major climate transitions – Impact on the preservation of paleoceanographic proxies*. The project has been proposed and supervised by PD Dr. Sabine Kasten (Alfred Wegener Institute for Polar and Marine Research, Bremerhaven, Germany) and Prof. Dr. Gert J. De Lange (University of Utrecht, The Netherlands). The presented work is in review as a dissertation and was mostly conducted in the working group Geochemistry and Hydrogeology headed by Prof. Dr. Horst D. Schulz at the Fachbereich 5 – Geowissenschaften (Department of Geosciences), University of Bremen, Germany.

The main part of the presented work consists of three manuscripts accepted for publication in international journals (Chapters 2-4), which are for the most part based on my own sampling, analyses, data evaluation and interpretation. The abstracts of two further manuscripts submitted to/in press for international journals are attached (Chapters 5, 6), to which I made analytical and interpretational contributions as co-author. The separate manuscripts are preceded by an abstract (in English and German) summing up the crucial foci of research, and an introduction (Chapter 1) illustrating the current state of the discussed topics and the broader scientific context. Following the manuscripts, a conclusion (Chapter 7) will sum up the most important findings and give a brief outlook and recommendation for further investigations. Finally, the many persons who contributed to this work are acknowledged.

Content

Abstract

In the context of present-day changes of atmo-, hydro-, geo- and biosphere processes, there is growing interest to decipher rapid paleoenvironmental changes in the geological past. Marine deposits provide valuable insights into paleoenvironmental conditions that prevailed during their deposition, if we know how to read the respective signals in the sedimentary record. However, caution is demanded as primary signals of past environmental conditions can be altered by postdepositional diagenetic processes. In the presented work, we will show the potentials, but also limitations of inorganic geochemical proxies to record signals of abrupt paleoenvironmental shifts in the terrestrially dominated Late Quaternary deposits of the Zambesi deep-sea fan (SE African margin), and in a fully marine Late Cretaceous black shale succession on Demerara Rise (NW South American margin).

In Zambesi deep-sea fan sediments, results of magnetic and geochemical analyses document a marked diagenetic front in ~5 m sediment depth. At this sulfate/methane transition (SMT), the anaerobic oxidation of CH_4 by SO_4^{2-} caused a marked alteration of primary sediment signals due to the production of HS^-, which in turn led to transformation of detrital Fe (oxyhydr)oxides into Fe sulfides (mostly pyrite). While this in situ dissolution-precipitation reaction left the bulk Fe record unaffected, we observed a peak in sedimentary S, a decrease of ferric Fe minerals and a related drop in magnetic susceptibility. In addition, large amounts of previously adsorbed HPO_4^{2-} got released to the pore water upon Fe (oxyhydr)oxide dissolution, creating a minimum in bulk sedimentary P. Below the SMT, the rapid drawdown of pore water HPO_4^{2-} as well as a solid P enrichment indicate formation of an authigenic P mineral. Sequential phosphate extractions suggest that a Fe(II)-phosphate mineral like vivianite precipitated below the SMT.

By applying Fick´s first law of diffusion and present-day conditions, we calculated the time of SMT fixation in its current position necessary to form the observed sedimentary S enrichment and P depletion within the SMT to amount to ~10,000 years. Around ~10,000 years B.P. the last Glacial to Holocene transition took place, and melting of large continental ice masses caused a major global sea level rise. Hence, the Mozambique shelf was largely flooded, most riverine sediment from the Zambesi was trapped close to the coastline, and sedimentation rates on the deep-sea fan were reduced significantly, leading to a fixation of the SMT at its current position.

Quaternary deposits off other large river mouths (e.g. Rio de La Plata, Amazon) show very similar geochemical patterns. Thus, rapid changes of sedimentation rates in fluvially influenced

continental margin settings may induce drastic diagenetic alterations of primary paleoenvironmental signals, especially in particular horizons, long after sediment deposition - and such features might be critical for interpreting ancient sediment successions as well.

Recording very different paleoenvironmental conditions, Late Cretaceous black shales deposited during the oceanic anoxic event (OAE) 3 in the Coniacian-Santonian on Demerara Rise are of open marine origin. Sediments investigated were obtained from ODP cores drilled at Sites 1259 and 1261 during Leg 207. As our geochemical and mineralogical analyses of two intervals of similar age (nannofossil biozone CC14) from both sites revealed, the sediments mainly consist of $CaCO_3$, marine organic matter and clinoptilolite (an alteration product of opal). Significant detrital input was most probably prevented by widely flooded continental shelves during the Late Cretaceous greenhouse. Still, the depositional regime at the shallower ODP Site 1259 was more significantly affected by turbidites, winnowing bottom currents and/or variable detrital sediment sources than at Site 1261, which was characterized by steady hemipelagic sedimentation.

Bottom waters were anoxic and even sulfidic for thousands of years across large parts of the Coniacian-Santonian Demerara Rise, indicated by redox-sensitive trace element records as well as by Fe and P speciation. However, despite overall bottom water and sediment oxygen depletion, periods with less reducing conditions occurred cyclically and were obviously triggered by astronomical eccentricity cycles. Based on our integrated high-resolution data set from two ODP sites representing different paleowater depths, and assuming linear sedimentation rates, we established a conceptual model of the development of paleoredox conditions during OAE3 at Demerara Rise.

High amounts of organic matter were deposited on the Late Cretaceous Demerara Rise, leading to progressive oxygen consumption at the sea floor, and microbial sulfate reduction created sulfidic conditions in and periodically above the sediment. Periods of sulfidic bottom waters were more pronounced and stable at Site 1261. Due to low detrital Fe input, the HS^- produced led to nearly complete pyritization (diagenetic and syngenetic) of the available ferric Fe, and excess HS^- caused extensive diagenetic sulfurization of the fresh marine organic matter in the sediment. In addition, a secondary coupling of Mo and Ni to sedimentary organic matter was created, while Mn and P were leached from the sediment. The very effective P recycling to the water column was probably one of the factors sustaining high productivity and organic matter export.

Most probably by the incursion of well-oxygenated South Atlantic water masses through the progressively opening Equatorial Atlantic Gateway, sulfidic conditions were periodically terminated, but nevertheless bottom waters stayed anoxic. Still, a close coupling of Fe and P was created - probably

induced by syngenetic formation of Fe (oxyhydr)oxides and adsorption or co-precipitation of HPO_4^{2-} to these particles - which caused HPO_4^{2-} removal from the water column and P enrichment in the sediment. After the incursion of South Atlantic water masses ceased, anoxic non-sulfidic bottom waters gradually turned sulfidic again, recorded by the rapid precipitation of large amounts of Zn and Cd sulfides and V hydroxides at low HS^- levels, before increasing syn- and diagenetic pyrite formation and organic matter sulfurization re-established.

This study shows that high-resolution records of bulk sedimentary Fe, P, S and redox-sensitive trace metals, and in particular sequential Fe and P extractions, have a large potential to trace rapid changes in paleoceanographic conditions - but can also reveal diagenetic alteration of the respective signals and preclude misinterpretations. Application of these geochemical proxies is proven successful in (sub)recent and ancient marine deposits, no matter if these are dominated by terrigenous or marine input. In addition, high sampling resolution is emphasized as one of the crucial prerequisites to capture sedimentary signals of rapid paleoenvironmental as well as diagenetic changes in their entity.

Kurzfassung

Im Kontext der sich aktuell verändernden atmo-, hydro-, geo- und biosphärischen Prozesse besteht ein wachsendes Interesse daran, rasche Umweltveränderungen in der geologischen Vergangenheit zu entschlüsseln. Marine Sedimente können wertvolle Einblicke in die Umweltbedingungen liefern, die während ihrer Ablagerung geherrscht haben, sofern wir die jeweiligen Signale in der sedimentären Abfolge interpretieren können. Allerdings ist Umsicht geboten, da ursprüngliche Signale vergangener Umweltbedingungen durch diagenetische Prozesse nach der Ablagerung verändert werden können. In der vorliegenden Arbeit werden wir die Möglichkeiten, aber auch die Grenzen anorganisch-geochemischer Proxies darstellen, die Signale abrupter Umweltveränderungen in den terrestrisch dominierten, spät-quartären Ablagerungen des Zambesi Tiefsee-Fächers (Kontinentalrand vor SE-Afrika) und den vollmarinen, spät-kretazischen Schwarzschiefern auf dem Demerara Rise (Kontinentalrand vor NW-Südamerika) aufzuzeichnen.

In Sedimenten des Zambesi Tiefsee-Fächers dokumentieren die Ergebnisse magnetischer und geochemischer Analysen eine markante diagenetische Front in etwa 5 m Sedimenttiefe. An dieser Sulfat-Methan-Übergangszone (SMT) bedingte die anaerobe Oxidation von CH_4 durch SO_4^{2-} eine deutliche Veränderung primärer Sedimentsignale durch die Produktion von HS-, welches wiederum zu einer Umwandlung detritischer Fe-(Oxyhydr)oxide zu Fe-Sulfiden (meist Pyrit) führt. Während diese in situ-Lösungs-/Fällungs-Prozesse auf die Fe-Gesamtgehalte keine Auswirkung hatten, stellten wir einen Höchstgehalt an sedimentärem S, eine Abnahme der Fe(III)-Minerale und eine dementsprechende Abnahme der magnetischen Suszeptibilität fest. Darüber hinaus wurden als Folge der Fe-(Oxyhydr)oxid-Lösung große Mengen zuvor adsorbierten HPO_4^{2-} in das Porenwasser freigesetzt, was ein P-Minimum in der Festphase erzeugte. Unterhalb der SMT deuten die rapide Abnahme von Porenwasser-Phosphat sowie eine Anreicherung von P in der Festphase auf die Bildung einer authigenen P-Mineralphase hin. Sequentielle Phosphat-Extraktionen zeigten, dass ein Fe(II)-Phosphat wie Vivianit unterhalb der SMT auszufallen scheint.

Unter Anwendung des ersten Fick´schen Diffusionsgesetzes und unter Annahme heutiger Bedingungen haben wir die Zeit der SMT-Fixierung in ihrer aktuellen Position, die zur Bildung der beobachteten S-Anreicherung und P-Abreicherung im Sediment innerhalb der SMT nötig ist, auf ca. 10.000 Jahre berechnet. Vor etwa 10.000 Jahren fand der Übergang vom letzten Glazial zum Holozän statt, und das Abschmelzen grosser kontinentaler Eismassen führte zu einem bedeutenden

globalen Meeresspiegelanstieg. Infolgedessen wurde die Schelfgebiete von Mozambique weitgehend überflutet, der grösste Teil der Sedimentfracht des Zambesi wurde küstennah abgefangen, und die Sedimentationsraten auf dem Tiefsee-Fächer wurden deutlich vermindert, was zu einer Fixierung der SMT in der aktuellen Sedimenttiefe führte.

Quartäre Ablagerungen vor anderen großen Flussmündungen (z.B. Rio de La Plata, Amazonas) zeigen sehr ähnliche geochemische Muster. Demzufolge können schnelle Änderungen der Sedimentationsraten auf fluvial geprägten Kontinentalrändern lange nach Sedimentablagerung zu drastischen diagenetischen Überprägungen primärer Umweltsignale führen können, insbesondere in spezifischen Sedimentlagen - und solche Merkmale können ebenfalls für die Interpretation älterer Sedimentabfolgen von Bedeutung sein.

Deutlich unterschiedliche Umweltbedingungen sind in spät-kretazischen, offenmarinen Schwarzschiefern dokumentiert, die während des Ozeanischen Anoxischen Ereignisses (oceanic anoxic event, OAE) 3 im Coniac-Santon auf dem Demerara Rise abgelagert wurden. Die untersuchten Sedimente stammen aus ODP-Bohrkernen, die während der Ausfahrt Leg 207 an den Sites 1259 und 1261 gewonnen wurden. Wie unsere geochemischen und mineralogischen Analysen zweier etwa gleich alter Intervalle (Nannofossilien-Biozone CC14) aus beiden Kernen zeigten, bestehen die Sedimente grösstenteils aus $CaCO_3$, mariner organischer Substanz und Clinoptilolit (ein Umwandlungsprodukt von Opal). Ein nennenswerter detritischer Eintrag wurde höchstwahrscheinlich durch die - während des Treibhausklimas in der späten Kreide weitgehend überfluteten - Schelfgebiete verhindert. Dennoch war das Ablagerungsmilieu an der vermutlich seichteren ODP Site 1259 stärker durch Trübeströme, sortierende Bodenströmungen und/oder variable detritische Liefergebiete beeinflusst als an Site 1261, die von gleichmässiger hemipelagischer Sedimentation geprägt war.

Während des Coniac-Santon war das Bodenwasser über weite Teile des Demerara Rise über Jahrtausende anoxisch und sogar sulfidisch, was durch redox-sensitive Spurenelemente sowie durch Fe- und P-Speziation belegt ist. Trotz genereller Sauerstoff-Abreicherung im Bodenwasser und Sediment gab es zyklisch auftretende Phasen mit weniger reduzierender Bedingungen, die offenbar durch astronomische Exzentrizitäts-Zyklen zeitlich gesteuert wurden. Basierend auf unserem hochauflösenden integrierten Datensatz von zwei ODP-Bohrungen, die unterschiedliche Wassertiefen repräsentieren, und unter der Annahme linearer Sedimentationsraten, haben wir ein konzeptionelles Modell der Entwicklung der Redox-Bedingungen während des OAE3 auf dem Demerara Rise erstellt.

Große Mengen organischen Materials wurden auf dem spät-kretazischen Demerara Rise abgelagert, was zu fortschreitendem Sauerstoff-Verbrauch am Meeresboden führte, und mikrobielle

Sulfat-Reduktion erzeugte sulfidische Bedingungen unterhalb und zeitweise auch oberhalb der Sedimentoberfläche. Phasen mit sulfidischem Bodenwasser waren an der Site 1261 ausgeprägter und stabiler. Aufgrund geringen detritischen Fe-Eintrags bewirkte das produzierte HS^- eine fast vollständige (diagenetische und syngenetische) Pyritisierung des verfügbaren Fe(III), und überschüssiges HS^- führte im Sediment zu beträchtlicher diagenetischer Sulfurisierung von frischer, mariner organischer Substanz. Ausserdem wurde eine sekundäre Bindung von Mo und Ni an sedimentäres organisches Material erzeugt, während Mn und P aus dem Sediment ausgelaugt wurden. Die äusserst effektive P-Regenerierung in die Wassersäule war möglicherweise einer der Faktoren, die die hohe Primärproduktion und den Export organischer Substanz aufrecht erhielten.

Vermutlich aufgrund des Einbruchs besser durchlüfteter Wassermassen aus dem Südatlantik durch den sich öffnenden „Equatorial Atlantic Gateway" wurden die sulfidischen Bedingungen zeitweise unterbrochen, wobei das Bodenwasser allerdings anoxisch blieb. Trotzdem entstand eine enge Kopplung von Fe und P - vermutlich erzeugt durch syngenetische Bildung von Fe-(Oxyhydr)oxiden und Phosphat-Adsorption an und/oder Mitfällung mit diesen Fe-(Oxyhydr)oxid-Partikeln -, die zu HPO_4^{2-}-Abnahme in der Wassersäule und P-Anreicherung im Sediment führte. Nachdem die Zufuhr südatlantischen Wassers endete, wurde das anoxischen, nicht-sulfidische Bodenwasser erneut sulfidisch, belegt durch rasche Ausfällung großer Mengen von Zn-Sulfid, Cd-Sulfid und V-Hydroxid unter niedrigen HS^--Gehalten, bevor erneut zunehmende syn- und diagenetische Pyrit-Bildung und Sulfurisierung organischer Substanz einsetzte.

Diese Arbeit belegt, dass hochauflösende Datensätze der Gesamtgehalte von sedimentärem Fe, P, S und redox-sensitiven Spurenelementen, und insbesondere sequentielle Fe- und P-Extraktionen, ein grosses Potential haben, um schnelle paläozeanograpische Veränderungen nachzuvollziehen - aber auch, um diagenetische Umwandlungen der jeweiligen Signale aufzuzeigen und damit Fehlinterpretationen vorzubeugen. Die Anwendung dieser Proxies erweist sich in (sub-)rezenten und älteren marinen Ablagerungen als erfolgreich, unabhängig davon, ob diese durch terrigenen oder marinen Eintrag geprägt sind. Ausserdem wird eine hohe Beprobungsdichte als einer der wichtigsten Parameter herausgestellt, um die sedimentären Signale rascher Wechsel von Paläoumwelt- und Diagenese-Bedingungen in ihrer Gesamtheit zu erfassen.

1.1 Motivation and objectives

Inorganic geochemistry is one of the key disciplines to decipher the record of paleoenvironmental conditions stored in marine sediments. Of particular interest are rapid changes of paleoenvironmental conditions through time, and the way that such rapid variations are recorded in marine deposits. A number of geochemical proxies - measurable properties of sediments genetically related to specific environmental parameters - has been established in paleoceanography during the last decades. They potentially document e.g. paleoproductivity, nutrient availability, assemblage of primary producers, redox conditions in water and sediment (e.g. Wefer et al., 1999). An „ideal proxy" would comprise that one measureable sediment parameter, e.g. a certain chemical element, is exclusively, quantitativly and measurably related to one defined environmental parameter. However, nature processes are more complex than that, and it has become evident that there is no such thing as an „ideal proxy".

Apart from these genetic limitations of paleoceanographic proxies, there are still many questions concerning potential post-depositional alterations of original proxy-parameter relationships. It is a major aim of this work to elucidate some of the syn- or post-depositional processes responsible for the alteration of these relationships. In particular, during times of extreme paleoenvironmental variations - triggered e.g. by plate tectonics, sea-level fluctuations, mixing of different water masses in the oceans, variations in continental runoff or primary productivity -, there are significant changes documented in the sedimentary records. But also the mode of recording and storing paleoenvironmental signals might change, and thus mislead any interpretation. The overall strategy of this study is an integrated approach, applying a variety of geochemical methods to establish the most suitable combination of measurable parameters. The integration of various proxies - sometimes referred to as multi-proxy approach - has the advantage that information obtained from various single proxies may support or exclude each other, leading to a more reliable reconstruction of paleoenvironmental conditions.

In the course of this study, we mostly applied inorganic geochemical methods (pore water and bulk sediment composition, speciation of certain chemical components), sometimes combined with mineralogical methods as X-ray diffraction (XRD) and scanning electron microscopy (SEM). In detail, pore water data yield information about the present geochemical zonation of a sediment and active diagenetic fronts (Froelich et al., 1979; Berner, 1981; Schulz et al., 1994), while the solid sediment composition rather records the „geochemical history" of a sediment succession over longer time scales, including primary (paleoenvironmental) as well as secondary (diagenetic) signals (Kasten et al., 2003; Schulz, 2006). Widely applied (paleo)redox proxies for bottom waters and sediments are Fe-S-C systematics and redox-sensitive and/or sulfide-forming trace elements. More advanced techniques are

sequential extractions of sedimentary Fe and P, giving information about the elements´ speciations in the sediment. In the following, I will give a short introduction into the geological settings and time slices investigated, discuss the geochemical parameters measured, and the way they may document rapid paleoenvironmental changes and diagenetic alterations.

1.2 Geological periods and settings investigated

Late Quaternary Zambesi deep-sea fan

Located off the coast of Mozambique (SE Africa), the Zambesi deep-sea fan has been a major depocentre for the terrigenous sediments delivered by the Zambesi river since the lower Miocene (Walford et al., 2005). Its latest very active period has been the last Glacial, when global sea level was several 10s of meters lower than today, and exposed shelf areas were bypassed by most of the riverine sediment load, resulting in high sedimentation rates on deep-sea fans like the one off the Zambesi river (Posamentier and Allen, 1993). Upon melting of large continental ice masses at the onset of the Holocene, the rising sea level flooded the Mozambique shelf, and much less sediment reached the deep-sea fan (Beiersdorf et al., 1980). A similar depositional history has also been described for many other river fans worldwide (e.g. Posamentier and Allen, 1993; Einsele, 2000). The Zambesi fan morphology is characterized by various channel-and-levee systems, but also by the activity of the strong Agulhas Current flowing southward towards the tip of Africa, and its northward countercurrent, giving the fan a coast-parallel elongated shape (Walford et al., 2005). Despite its potential to record marine and continental climate signals of SE Africa, the Zambesi fan is little investigated compared to other big deep-sea fans (e.g. Congo, Niger, Amazon, Bengal, Mississippi, Nile). During RV Meteor cruise 63/1 in 2005, among others the gravity core GeoB 9309-1 was retrieved and geochemically investigated (Chapter 2). The focus of of the study was to infer diagenetic alteration of primary sedimentary signals, related to the anaerobic oxidation of methane (AOM) at the sulfate/methane transition (SMT) that has been fixed in its current position since the last Glacial/Holocene transition.

Late Cretaceous Demerara Rise

This submarine, gently dipping plateau off the coast of Suriname and French Guyana was drilled during ODP Leg 207 in 2003 to record the development of the eastern tropical Atlantic since the Cretaceous (Erbacher et al., 2004; Mosher et al., 2007). As a major task, an extensive Middle to Late

Cretaceous black shale succession was revovered, documenting a period of extreme global greenhouse conditions that culminated in Oceanic Anoxic Events, OAEs (Schlanger and Jenkyns, 1976; Jenkyns, 1980). Climatic conditions during OAEs were characterized by high atmospheric pCO_2 (e.g. Berner and Kothavala, 2001; Bice and Norris, 2002), resulting in ice-poor or -free poles and eustatic sea level ~250 m higher than today (Haq et al., 1987), high atmosphere and ocean temperatures (Norris et al., 2002; Forster et al., 2007) and equator-pole temperature gradients lower than today (Barrera and Johnson, 1999; Takashima et al., 2006). Additionally, high CO_2 levels induced elevated marine primary productivity, high fluxes of organic matter to the sea floor followed by extensive bottom water oxygen consumption, anoxic to sulfidic conditions in the lower water column and even in the photic zone (e.g. Sinninghe Damsté and Köster, 1998; Kuypers et al., 2002), and wide-spread black shale deposition. Another scenario explaining widely anoxic/sulfidic deep Cretaceous oceans is strongly reduced vertical water exchange, leading to water column stratification and deep water oxygen depletion even without high organic matter export fluxes (e.g. Pedersen and Calvert, 1990; Calvert and Pedersen, 1990; Arthur and Sageman, 1994).

Regardless of the dominant process, the picture of a stable anoxic deep ocean over millions of years is being tackled more and more by recent data indicating rapid, most probably glacio-eustatic sea level changes (e.g. Miller et al., 2003; Miller et al., 2005) as well as redox fluctuations (e.g. Beckmann et al., 2005a, b; Kolonic et al., 2005; Nederbragt et al., 2007) in the marine realm during OAEs. Also for OAE3 (Coniacian-Santonian), astronomically forced redox fluctuations have been reported (Wagner et al., 2004; Beckmann et al., 2005a, b), but data from Demerara Rise are still lacking - although preliminary investigations of Demerara Rise black shales revealed clear indications for extremely oxygen-depleted bottom water conditions, as high organic matter contents and trace metal patterns (Erbacher et al., 2004; Böttcher et al., 2006; Hetzel et al., 2006). To close this gap, and also to confirm that detailed and integrated geochemical investigations can reveal unique details about paleoredox conditions, we investigated OAE3 black shales in high resolution (Chapters 3-5).

1.3 Marine iron cycling

The main source of Fe into the oceans is detrital input from the continents (Poulton and Raiswell, 2002; Raiswell, 2006). Most detrital Fe-containing minerals are either relatively unreactive silicates (e.g. clay minerals, pyroxenes, amphiboles), or Fe (oxyhydr)oxides as ferrihydrite, goethite, hematite and lepidocrocite. The latter can be important for biogeochemical processes in the marine environment (Cornell and Schwertmann, 1996). Under oxic conditions in the water column, iron is

hardly soluble and Fe (oxyhydr)oxides settle to the sea floor (e.g. Byrne and Kester, 1976; Liu and Millero, 2002). Upon deposition, Fe (oxyhydr)oxides may get buried in the sediment, although a certain part is reductively dissolved with or without microbial support close to the sediment surface (e.g. Froelich et al., 1979; Lovley, 1987; Burdige, 1993). In the sedimentary record, they are the main carriers of the magnetic signal. However, in the presence of HS^-, Fe (oxyhydr)oxides are transformed to Fe sulfides (as greigite, mackinawite, pyrite), and this process can occur syn- or diagenetically, i.e. in the water column or in the sediment (e.g. Berner, 1984; Morse et al., 1987; Schoonen, 2004; Lyons and Severmann, 2006). Therefore, applying sequential Fe extraction techniques is useful to distinguish between various sedimentary Fe species (amorphous or crystalline Fe (oxyhydr)oxides, Fe sulfides, Fe silicates), and thus between different syn- or post-depositional redox conditions (e.g. Haese et al., 2000; Poulton and Canfield, 2005). We investigated the biogeochemical cycling of Fe in two different continental margin settings, one being dominated by detrital Fe (oxyhydr)oxide input and well-oxygenated bottom waters (Chapter 2), the other being Fe-limited and characterised by mostly anoxic bottom water conditions (Chapters 3-5).

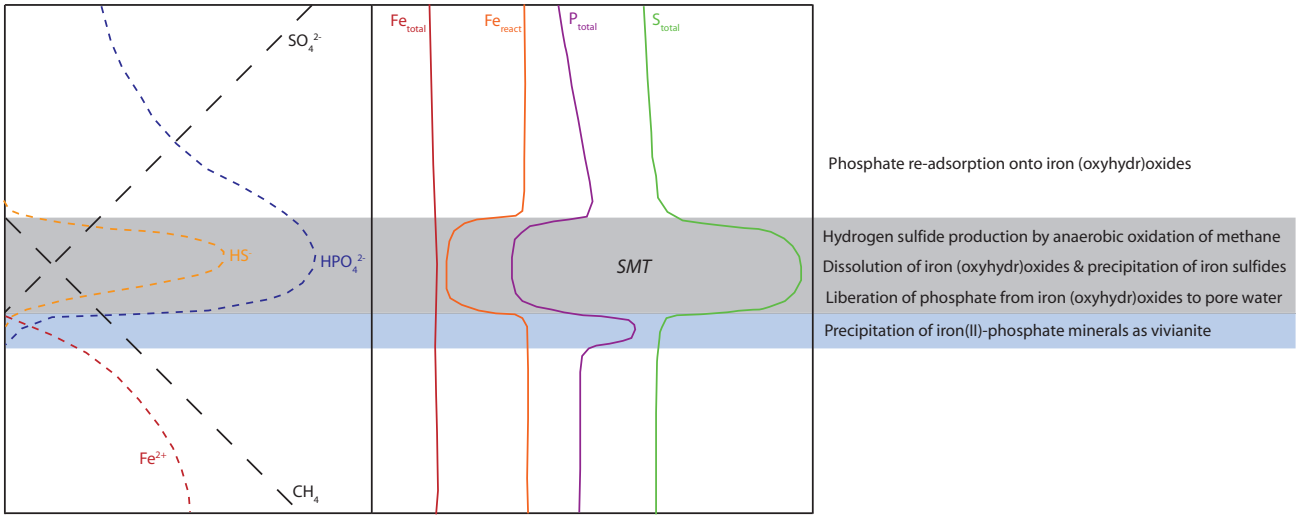

Fig. 1.1: Schematic representation of biogeochemical cycling of S, Fe and P at a sulfate/methane transition (SMT; grey bar) and below (blue bar). The left side displays pore water concentration profiles, the rights side the diagenetic solid-phase signals. Upward-diffusing CH_4 and downward-diffusing SO_4^{2-} are consumed via anaerobic oxidation of methane, and HS^- is produced. Upward-diffusing Fe^{2+} partly reacts with HS^- to form Fe sulfides in the lower SMT. In addition, HS^- leads to reductive dissolution of Fe (oxyhydr)oxides (Fe_{react}) in the SMT, and authigenic formation of Fe sulfides. This in situ transformation is invisible in the bulk sedimentary Fe record, but creates a secondary S enrichment and Fe_{react} depletion in the SMT. The dissolution of Fe (oxyhydr)oxides also liberates formerly adsorbed HPO_4^{2-} to the pore water, depleting bulk solid P within the SMT. Above the SMT, upward-diffusing HPO_4^{2-} gradually re-adsorbs onto Fe (oxyhydr)oxides. Below the SMT (blue bar), downward-diffusing HPO_4^{2-} is precipitated as authigenic P minerals, most probably Fe(II) phosphates like vivianite, leading to a secondary solid P enrichment.

1.4 Marine phosphorus cycling

In aquatic systems, P is mainly present as the stable phosphate oxy-anion HPO_4^{2-}, and is transported from the continents to the ocean mainly via rivers. Phosphate is not redox-sensitive in itself, but is strongly coupled to the redox-dependent cycles of Fe and OM. Fresh Fe (oxyhydr)oxides can not only adsorb large amounts of phosphate, but phosphate may also be co-precipitated during Fe (oxyhydr)oxide formation. Thus, Fe (oxyhydr)oxides can play a major role for the transport of P to the sea floor, and its fate in the sediment (e.g. Feely et al., 1990; Slomp et al., 1996; Poulton and Canfield, 2006). Another P carrier to the sea floor is marine OM, as marine phytoplankton contains a relatively stable amount of P atoms per carbon atom (with a mean C/P ratio of 106:1; Redfield, 1958). Under reducing conditions at the sea floor or in the sediment, a decoupling of P from both the Fe and the OM cycles takes place: As the Fe-P coupling can only be active if Fe (oxyhydr)oxides are preserved in marine waters and sediments under oxic to non-sulfidic conditions, dissolution of Fe (oxyhydr)oxides liberates phosphate to the surrounding water (Chapter 2). Additionally, under anoxic conditions organic P is regenerated from OM preferentially to organic C (e.g. Ingall et al., 1993; Ingall and Jahnke, 1997), resulting in low P burial capacities of anoxic sediments and C/P_{total} ratios >106 (review by Algeo and Ingall, 2007). This results in high C/P_{total} ratios and low P/Al values preserved in the sedimentary record of both sediments deposited under an anoxic water column and sediments affected by diagenetic processes around the SMT. If oxic to non-sulfidic conditions prevail in the sediment, both OM- and Fe-bound P can be at least partly buried - and preserved in the respective speciation - in the sedimentary record (as found in Demerara Rise black shales, Chapters 3 and 4). However, in the course of further sediment burial, OM- and Fe-bound P is usually (partly or completely) transformed into authigenic apatite at greater sediment depth ("sink switching" hypothesis; Delaney, 1998; Filippelli, 2001).

1.5 Redox-sensitive and/or sulfide-forming trace elements

The fact that certain trace element species react very sensitive and in a characteristic way to redox variations in the ambient sea or pore waters has been used for reconstructing redox conditions in recent and ancient sedimentary basins, especially in relation to extensive organic matter deposition and sulfide formation in O_2-depleted environments (e.g. Algeo and Maynard, 2004; Brumsack, 2006; Tribovillard et al., 2006). In such oxygen-free to sulfidic environments, widespread black shale deposition occurred during certain periods in the Paleozoic and Mesozoic (e.g. the Devonian Kupferschiefer, the Jurassic Posidonia Shale and Kimmeridge Clay, and various Cretaceous OAE black

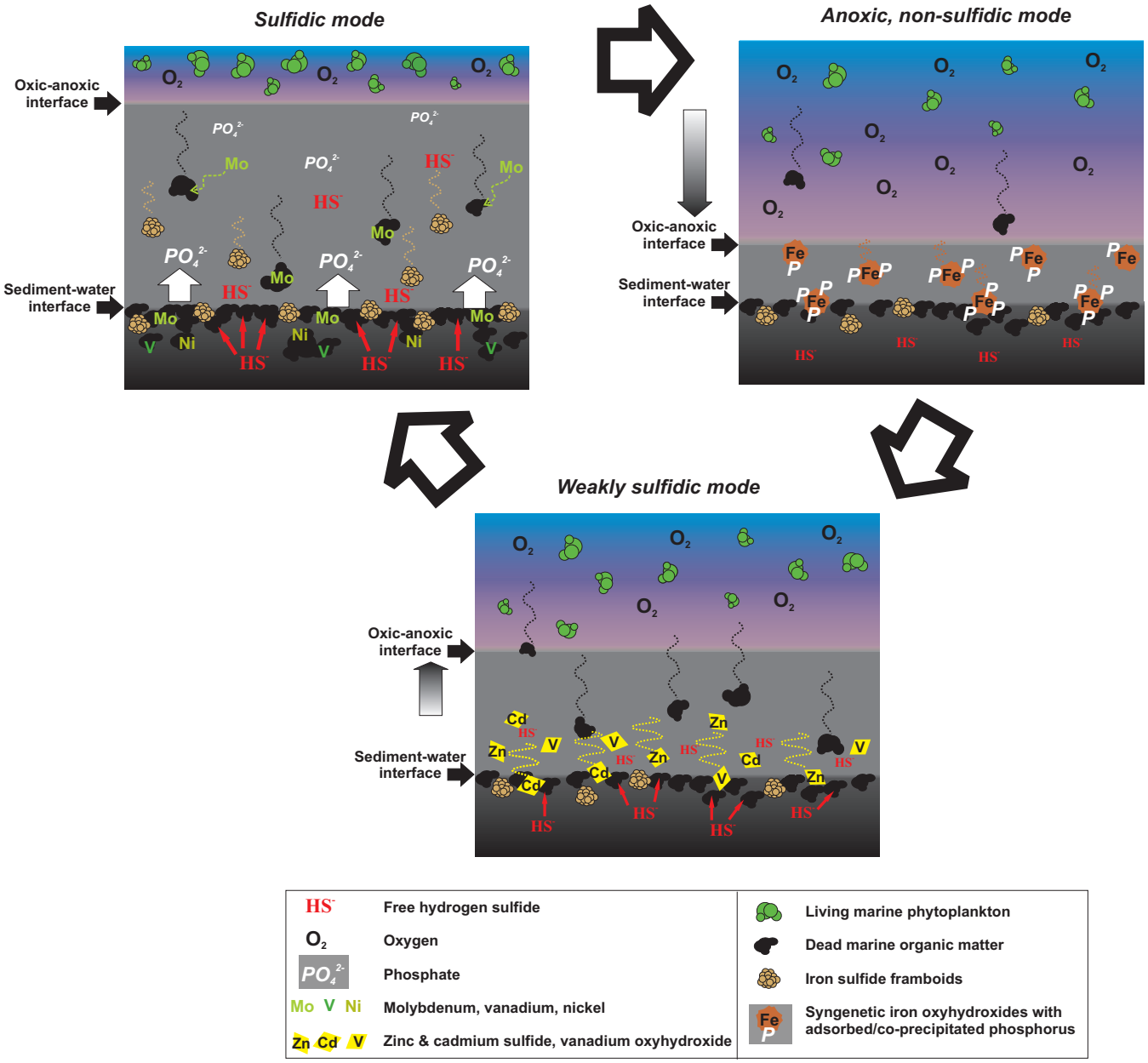

Fig. 1.2: Simplified representation of the biogeochemical cycling of S, Fe, P and redox-sensitive trace metals Cd, Mo, Ni, V and Zn in a sulfidic to anoxic, non-sulfidic deep ocean. Note that only processes occurring in the water column and in relatively shallow sediment depth are displayed. Sulfidic mode: Shallow oxic-anoxic interface (OAI); high primary production and organic matter (OM) export to the sea floor; sulfidic bottom and intermediate waters; syngenetic framboidal pyrite formation; settling OM scavenges particle-reactive thiomolybdates; strong phosphate regeneration from the sediment to the water column; diagenetic sulfurization of OM in the sediment by excess HS^- production; incorporation of Ni and V into geoporphyrins. Anoxic, non-sulfidic mode: Deepening of the OAI, lower primary production; reduced OM export to the sea floor; reduced HS^- production restricting sulfidic conditions and pyrite formation to the sediment; syngenetic formation of Fe (oxyhydr)oxide particles at the OAI; phosphate scavenging by and/or co-precipitation with these particles, creating a Fe-P coupling and enhanced P burial. Weakly sulfidic mode: Rising OAI; elevated OM export to the sea floor; enhanced HS^- production in the sediment; evolving weakly sulfidic conditions in the bottom waters; rapid precipitation of Cd and Zn sulfides and V hydroxides under low HS^- concentrations; (local?) drawdown of Cd, V and Zn bottom water concentrations.

	Oxic	Anoxic, non-sulfidic	Anoxic, weakly sulfidic	Sulfidic
OM	bad preservation	good preservation,		very good preservation, OM sulfurization
Mo	MoO_4^{2-}			thiomolybdate (MoO_xS_{4-x}, x = 0-3)
Cd, Zn	Cd^{2+}, Zn^{2+}		CdS, ZnS	
V	HVO_4^{2-}, H_2VO^{4-}	VO^{2-}, $VO(OH)_3^-$, $VO(OH)_2$	V_2O_3, $V(OH)_3$	
Fe, Mn	Fe -/ Mn-(oxyhydr)oxides	Fe^{2+}, Mn^{2+}	Fe^{2+}, FeS Mn^{2+}	FeS_2, Mn^{2+}
P	HPO_4^{2-} sorbed to Fe - (oxyhydr)oxides	HPO_4^{2-}		
Blue = dissolved in sea water, red = accumulated in sediment				

Tab. 1.1: Simplified overview of the behaviour of organic matter (OM), the redox-sensitive/ sulfide-forming elements Mo, Cd, Zn, V, Fe and Mn, and the element P under oxic - anoxic, non-sulfidic - anoxic, weakly sulfidic - sulfidic conditions.

shales). In modern oceans, anoxic to euxinic water masses are rare and limited to semi-restricted basins (e.g. Black Sea, Cariaco Basin, Saanich Inlet, Framvaren) and extreme upwelling regions (e.g. off Peru, Namibia, Pakistan). The recognition that certain trace elements are strongly enriched/depleted in organic matter-rich deposits in comparison to average marine sediments was the starting point of their systematic use as redox proxies. Of great importance for understanding the processes that caused the observed element enrichments/depletions, and the paleo-information they could (or could not) provide, were comparisons of ancient black shale deposits with modern „analogues" as far as these exist (e.g. Nijenhuis et al., 1999; Brumsack, 2006; Meyers, 2006). Based on these valuable investigations, a relatively limited number of trace elements was found to be most valuable as paleoredox proxies.

In short, Mn is an element generally depleted under anoxic conditions, while elements like Cd, Cu, Mo, Ni, V and Zn are enriched due to formation of organometallic complexes or sulfide minerals (e.g. Tribovillard et al., 2006; this work, Chapters 3-6). The degree of enrichment/depletion is usually based on the element/Al ratio in a sample, and calculated relative to the respective element/Al ratio of a common standard material, e.g. average marine shale (Turekian and Wedepohl, 1961). Although such comparisons have to be handled with care, as the composition of any common standard material is not necessarily representative for a certain erosional source area (Van der Weijden, 2002), they are unproblematic for elements with very high degrees of enrichment/depletion and/or low concentrations in the standard material. Still, one has to be aware that redox-sensitive trace metals records may not document bottom water and sediment redox conditions during the time of sediment deposition - they may also be altered by post-depositional processes as „oxygen burndown" events, i.e. oxidation fronts prograding from the bottom water into the sediment, which may hamper a correct paleoredox interpretation (e.g. Wilson et al., 1985; Thomson et al., 1995).

1.6 References

Algeo, T.J., Maynard, J.B. (2004) Trace element behaviour and redox facies in core shales of the Upper Pennsylvanian Kansas-type cyclothems. Chem. Geol. 206, 289-318.

Algeo, T.J., Ingall, E. (2007) Sedimentary C_{org}:P ratios, paleocean ventilation, and Phanerozoic pO_2. Palaeogeogr. Palaeoclimatol. Palaeoecol. 256, 130-155.

Arthur, M.A., Sageman, B.B. (1994) Marine black shales: depositional mechanisms and environments of ancient deposits: Annual Review of Earth and Planetary Sciences, v. 22, p. 499–551.

Barrera, E., Johnson, C.C. (Eds.) *Evolution of the Cretaceous Ocean-Climate System*. Boulder, Colorado, Geol. Soc. Am. Spec. Paper 332, 445 pp.

Beckmann, B., Flögel, S, Hofmann, P., Schulz, M., Wagner, T. (2005a) Orbital forcing of Cretaceous river discharge in tropical Africa and ocean response. Nature, 437, 241-244.

Beckmann, B., Wagner, T., Hofmann, P. (2005b) Linking Coniacian-Santonian (OAE3) black shale formation to African climate variability: a reference section from the eastern tropical Atlantic at orbital time scales (ODP Site 959, off Ivory Coast/Ghana). In: Harris, N.B. (Ed.) *The Deposition of Organic Carbon-Rich Sediments: Models, Mechanisms, and Consequences*. SEPM Spec. Publ. 82, 125-143.

Beiersdorf, H., Kudrass, H.-R., von Stackelberg, U. (1980) Placer deposits of ilmenite and zircon on the Zambezi shelf. Geol. Jb. D 36, 85 pp.

Berner, R.A. (1981) A new geochemical classification of sedimentary environments. J. Sediment. Petrol. 51, 259-265.

Berner, R.A. (1984) Sedimentary pyrite formation: An update. Geochim. Cosmochim. Acta 48, 605-615.

Berner, R.A., Kothavala, Z. (2001) GEOCARB III: A revised model of atmospheric CO_2 over Phanerozoic time. Am. J. Sci. 301, 182-204.

Bice, K.L., R.D. Norris (2002) Possible atmospheric CO_2 extremes of the middle Cretaceous (late Albian-Turonian). Paleoceanography 17, doi:1029/2002PA000778.

Böttcher, M. E., Hetzel, A., Brumsack, H.-J., Schipper, A. (2006) Sulfur-iron-carbon geochemistry in sediments of the Demerara Rise. In: Mosher, D.C., Erbacher, J., Malone, M.J. (Eds.) *Proc. ODP Sci. Results 207,* 1-23. doi:10.2973/odp.proc.sr.207.108.2006.

Brumsack, H.-J. (2006) The trace metal content of recent organic carbon-rich sediments: Implications for Cretaceous black shale formation. Palaeogeogr. Palaeoclimatol. Palaeoecol. 232, 344-361.

Burdige, D.J. (1993) The biogeochemistry of manganese and iron reduction in marine sediments. Earth-Sci. Rev. 35, 249-284.

Byrne, R.H., Kester, D.R. (1976) Solubility of hydrous ferric oxide and iron speciation in sea water. Mar. Chem. 4, 255-274.

Calvert, S.E., Pedersen, T.F. (1992) Organic carbon accumulation and preservation in marine sediments: how important is anoxia? In: Whelan, J.K., Farrington, J.W. (Eds.) *Productivity, Accumulation, and Preservation of Organic Matter in Recent and Ancient Sediments.* Columbia University Press, New York, pp. 231–263.

Cornell, R.M., Schwertmann, U. (1996) *The Iron Oxides - Structure, Properties, Reactions, Occurrence and Uses*. VHC Verlagsgesellschaft, 573 pp.

Delaney, M.L. (1998) Phosphorus accumulation in marine sediments and the oceanic phosphorus cycle. Global Biogeochem. Cycles 12, 563-572.

Einsele, G. (2000) *Sedimentary Basins - Evolution, Facies and Sedimentary Budget*. Springer Berlin Heidelberg New York, 792 pp.

Erbacher, J., Mosher, D.C., Malone, M.J., Shipboard Scientific Party (2004) *Proc. ODP In. Reports 207*. doi: 10.2973/odp.proc.ir.207.2004.

Feely, R.A., Massoth, G.J., Baker, E.T., Cowen, J.P., Lamb, M.F., Krogslund, K.A. (1990) The effect of hydrothermal processes on midwater phosphorus distributions in the northeast Pacific. Earth Planet. Sci. Lett. 96, 305-318.

Filippelli, G.M. (2001) Carbon and phosphorus cycling in anoxic sediments of the Saanich Inlet, British Columbia. Mar. Geol. 174, 307-321.

Forster, A., Schouten, S., Baas, M., Sinnighe Damsté, J.S. (2007) Mid-Cretaceous (Albian-Santonian) sea surface temperature records of the tropical Atlantic Ocean. Geology 35, 919-922.

Froelich, P.N., Klinkhammer, G.P., Bender, M.L., Luetge, N.A., Heath, G.R., Cullen, D., Dauphin, P. (1979) Early oxidation of organic matter in pelagic sediments of the eastern equatorial Atlantic: suboxic diagenesis. Geochim. Cosmochim. Acta 43, 1075-1090.

Haese, R.R., Schramm, J., Rutgers van der Loeff, M.M., Schulz, H.D. (2000) A comparative study of iron and manganese diagenesis in continental slope and deep sea basin sediments off Uruguay (SW Atlantic). Int. J. Earth Sci. 88, 619-629.

Haq, B.U., J. Hardenbol, P.R. Vail (1987) Chronology of fluctuating sea levels since the Triassic. Science 235, 1156-1167.

Hetzel, A., Brumsack, H.-J., Schnetger, B., Böttcher, M., (2006) Inorganic geochemical characterization of lithologic units recovered during ODP Leg 207 (Demerara Rise). In: Mosher, D.C., Erbacher, J., Malone, M.J. (Eds.) *Proc. ODP Sci. Results 207*, 1-37. doi:10.2973/odp.proc.sr.207.107.2006.

Ingall, E.D., Bustin, R.M., Van Cappellen, P. (1993) Influence of water column anoxia on the burial and preservation of carbon and phosphorus in marine shales. Geochim. Cosmochim. Acta 57, 303-316.

Ingall, E.D., Jahnke, R.A. (1997) Influence of water-column anoxia on the elemental fractionation of carbon and phosphorus during sediment diagenesis. Mar. Geol. 139, 219-229.

Jenkyns, H. C. (1980) Cretaceous anoxic events: From continents to oceans, J. Geol. Soc. London, 137, 171–188.

Kasten, S., Zabel, M., Heuer, V., Hensen, C. (2003) Processes and signals of nonsteady-stae diagenesis in deep-sea sediments and their pore waters. In: Wefer, G., Mulitza, S., Ratmeyer, V. (Eds.) *The South Atlantic in the Late Quaternary*. Springer Berlin Heidelberg New York, pp. 431-459.

Kolonic, S., Wagner, T., Forster, A., Sinninghe Damsté, J.S., Walsworth-Bell, B., Turgeon, S.C., Brumsack, H.-J., Kuhnt, W., Tsikos, H., Kuypers, M.M.M. (2005) Black shale deposition on the northwest African Shelf during the Cenomanian/Turonian oceanic anoxic event: climate coupling and global organic carbon burial. Palaeoceanography 20, PA3002. doi: 10.1029/2003PA000930.

Kuypers, M.M.M., Pancost, R.D., Nijenhuis, I.A., Sinninghe Damsté, J.S. (2002) Enhanced productivity led to increased organic carbon burial in the euxinic North Atlantic basin during the Late Cenomanian oceanic anoxic event. Paleoceanography 17, doi:10.1029/2000PA000569.

Liu, X., Millero, F.J. (2002) The solubility of iron in seawater. Mar. Chem. 77, 43-54.

Lyons, T.W., Severmann, S. (2006) A critical look at iron paleoredox proxies: New insights from modern euxinic marine basins. Geochim. Cosmochim. Acta 70, 5698-5722.

Meyers, P.A. (2006) Paleoceanographic and paleoclimtic similarities between Mediterranean sapropels and Cretaceous black shales. Palaeogeogr. Palaeoclimatol. Palaeoecol. 235, 305-320.

Miller, K.G., Sugarman, P.J., Browning, J.V., Kominz, M.A., Hernández, J.C., Olsson, R.K., Wright, J.D., Feigenson, M.D., Van Sickel, W. (2003) Late Cretaceous chronology of large, rapid sea-level changes: glacioeustasy during the greenhouse world. Geology 31, 585–588.

Miller, K.G., J.D. Wright, J.V. Browning (2005) Visions of ice sheets in a greenhouse world. Marine Geology 217, 215-231.

Morse, J.W., Millero, F.J., Cornwell, J.C., Rickard, D. (1987) The chemistry of hydrogen sulphide and iron sulphide systems in natural waters. Earth-Sci. Rev. 24, 1-42.

Mosher, D.C., Erbacher, J., Malone, M.J., Shipboard Scientific Party (2007) *Proc. ODP Sci. Results 207*. doi: 10.2973/odp.proc.sr.207.2007.

Nederbragt, A.J., Thurow, J., Pearce, R. (2007) Sediment composition and cyclicity in the Mid-Cretaceous at Demerara Rise, ODP Leg 207. In: Mosher, D.C., Erbacher, J., Malone, M.J. (Eds.) *Proc. ODP Sci. Results 207*, 1-31. doi:10.2973/odp.proc.sr.2007.103.2007.

Nijenhuis, I.A., Bosch, H.J., Sinninghe Damsté, J.S., Brumsack, H.-J., de Lange, G.J. (1999) Organic matter and trace element rich sapropels and black shales: a geochemical comparison. Earth Planet. Sci. Lett. 169, 277-290.

Norris, R. D., K. L. Bice, E. A. Magno, P. A. Wilson (2002) Jiggling the tropical thermostat in the Cretaceous hothouse: Geology 30, 299-302.

Pedersen, T.F., Calvert, S.E. (1990) Anoxia vs. productivity: what controls the formations of organic-carbon-rich sediments and sedimentary rocks? AAPG Bull. 74, 454–466.

Posamentier, H.W., Allen, G.P. (1993) Variability of the sequence stratigraphic model: effects of local basin factors. Sed. Geol. 86, 91-109.

Poulton, S.W., Raiswell, R. (2002) The low-temperature geochemical cycle of iron: from continental fluxes to marine sediment deposition. Am. J. Sci. 302, 774-805.

Poulton, S.W., Canfield, D.E. (2005) Development of a sequential extraction procedure for iron: implications for iron partitioning in continentally derived particulates. Chem. Geol. 214, 209-221.

Poulton, S.W., Canfield, D.E. (2006) Co-diagenesis of iron and phosphorus in hydrothermal sediments from the southern East Pacific rise: Implications for the evaluation of paleoseawater phosphate concentrations. Geochim. Cosmochim. Acta 70, 5883-5898.

Raiswell, R. (2006) Towards a global highly reactive iron cycle. J. Geochem. Eplor. 88, 436-439.

Redfield, A.C. (1958) The biological control of chemical factors in the environment. Am. Sci. 64, 205-221.

Schlanger, S.O., Jenkyns, H.C. (1976) Cretaceous oceanic anoxic events: Causes and consequences. Geol. Mijnbouw 55, 179-184.

Schoonen, M.A.A. (2004) Mechanisms of sedimentary pyrite formation. In: Amend, J.P., Edwards, K.J., Lyons, T.W. (Eds.) *Sulfur Biogeochemistry – Past and Present*. GSA Spec. Pap. 379, pp. 117-134.

Schulz, H.D., Dahmke, A., Schinzel, U., Wallmann, K., Zabel, M. (1994) Early diagenetic processes, fluxes, and reaction rates in sediments of the South Atlantic. Geochim. Cosmochim. Acta 58, 2041-2060.

Schulz, H.D. (2006) Quantification of early diagenesis: Dissolved constituents in pore water and signals in the solid phase. In: Schulz, H.D., Zabel, M. (Eds.) *Marine Geochemistry*, 2nd edition. Springer Berlin Heidelberg New York, pp. 73-124.

Sinninghe Damsté, J.S., Köster, J. (1998) A euxinic southern North Atlantic Ocean during the Cenomanian/Turonian oceanic anoxic event. Earth and Planetary Science Letters 158, 165-173.

Slomp, C.P., Van der Gaast, S.J. and Van Raaphorst, W. (1996) Phosphorus binding by poorly crystalline iron oxides in North sea sediments. Mar. Chem. 52, 55-73.

Takashima, R., Hiroshi, N., Huber, B.T., Leckie, R.M. (2006) Greenhouse World and the Mesozoic ocean. Oceanography 19, 82-92.

Thomson, J., Higgs, N.C., Wilson, T.R.S., Croudace, I.W., de Lange, G.J., van Santvoort, P.J.M. (1995) Redistribution and geochemical behaviour of redox-sensitive elements around S1, the most recent eastern Mediterranean sapropel. Geochim. Cosmochim. Acta 59, 3487-3501.

Tribovillard, N., Algeo, T.J., Lyons, T., Riboulleau, A. (2006) Trace metals as paleoredox and paleoproductivity proxies: An update. Chem. Geol. 232, 12-32.

Turekian, K.K., Wedepohl, K.H. (1961) Distribution of the elements in some major units of the Earth´s crust. Geol. Soc. Am. Bull. 72, 175-192.

Van der Weijden, C. (2002) Pitfalls of normalization of marine geochemical data using a common divisor. Mar. Geol. 184, 167-187.

Wagner, T., Sinninghe Damsté, J.S., Hofmann, P., Beckmann, B. (2004) Euxinia and primary production in Late Cretaceous eastern equatorial Atlantic surface waters fostered orbitally driven formation of marine black shales. Paleoceanography 19, PA3009.

Walford, H.L., White, N.J., Sydow, J.C. (2005) Solid sediment load history of the Zambezi Delta. Earth Planet. Sci. Lett. 238, 49-63.

Wefer, G., Berger, W.H., Bijma, J., Fischer, G. (1999) Clues to ocean history: a brief overview of proxies. In: Wefer, G., Berger, W.H. (Eds.) *Use of Proxies in Paleoceanography - Examples from the South Atlantic*. Springer Berlin Heidelberg New York, pp. 1-68.

Wilson, T.R.S., Thomson, J., Colley, S., Hydes, D.J., Higgs, N.C. (1985) Early organic diagenesis: The significance of progressive subsurface oxidation fronts in pelagic sediments. Geochim. Cosmochim. Acta 49, 811-822.

2. Diagenetic changes of magnetic and geochemical signals by anaerobic methane oxidation in sediments of the Zambesi deep-sea fan (SW Indian Ocean)

C. März (1*), J. Hoffmann (1), U. Bleil (1), G.J. de Lange (2), S. Kasten (3)

(1) Department of Geosciences, University of Bremen, Klagenfurter Strasse, 28359 Bremen, Germany (corresponding author: cmaerz@uni-bremen.de)*

(2) Institute of Earth Sciences, Department of Geochemistry, University of Utrecht, Budapestlaan 4, 3584 Utrecht, The Netherlands

(3) Alfred Wegener Institute for Polar and Marine Research, Am Handelshafen 12, 27570 Bremerhaven, Germany

Abstract

The Zambesi deep-sea fan, the largest of its kind along the east African continental margin, was a major target of RV *Meteor* cruise M63/1 in 2005. Gravity core GeoB 9309-1, retrieved from 1219 m water depth, was investigated for various geophysical (magnetic susceptibility, porosity, color reflectance) and geochemical (pore water and sediment geochemistry, Fe and P speciation) properties. Onboard and onshore data documented a sulfate/methane transition (SMT) zone at ~450-530 cm sediment depth, where the simultaneous consumption of pore water sulfate and methane liberates hydrogen sulfide and bicarbonate into the pore space. This leads to characteristic changes in the sediment an pore water chemistry, as the reduction of primary iron (oxyhydr)oxides, the precipitation of iron sulfides, and the mobilization of iron (oxyhydr)oxide-bound. These chemical processes also affect the other sediment properties at the SMT, such as a marked decrease in magnetic susceptibility and. Below the SMT, we find a reduction of porosity, possibly due to pore space cementation by authigenic minerals. Formation of the observed diagenetic patterns requires a fixation of the SMT at this distinct sediment depth for a considerable time - which we calculated to be ~10 000 years assuming steady-state conditions -, following a period of rapid upward migration towards this interval. We postulate that the worldwide sea-level rise at the last glacial/interglacial transition (~10 000 years B.P.) most probably resulted in the fixation of the SMT at its present position, through drastically

reduced sediment delivery to the continental slope. In addition, we report an internal redistribution of phosphate occurring around the SMT, closely linked to the (de)coupling of sedimentary iron and phosphorus, and leaving a characteristic pattern in the solid P record. By phosphate re-adsorption onto iron (oxyhydr)oxides above, and formation of authigenic phosphate minerals (e.g. vivianite) below the SMT, deep-sea fan deposits can potentially act as long-term sinks for phosphate.

Keywords: deep-sea fan, early diagenesis, iron, phosphate, susceptibility, anaerobic oxidation of methane.

Introduction

Marine sediments, especially along continental margins, are known to be one of the major archives for paleoenvironmental signals. Among others, geochemical as well as magnetic sedimentary proxies have often been used for paleoceanographic and paleoclimatic reconstructions (e.g. Müller and Suess, 1979; Thompson et al., 1980; Boyle and Keigwin, 1982; Kent, 1982; Canfield and Berner, 1987; von Dobeneck and Schmieder, 1999; Frederichs et al., 1999; Reitz et al., 2004). The sediment composition, however, is generally affected by early diagenetic processes, leading to alteration - and possibly misinterpretation - of sedimentary signals. The mostly microbially catalyzed reactions, although occurring throughout the sediment column, often leave their imprints within distinct zones where dissolution and/or precipitation of minerals takes place. One of the latter is the sulfate/methane transition (SMT) zone, where consortia of highly specific microorganisms simultaneously reduce downward diffusing sulfate and oxidize methane produced deeper in the sediment (e.g. Reeburgh, 1976; Murray et al., 1978; Hoehler et al., 1994; Boetius et al., 2000). This biogeochemical process, referred to as the anaerobic oxidation of methane (AOM), can leave a significant imprint not only in the pore water chemistry, but also in the solid phase composition. Especially lithogenically dominated sediments rich in reactive iron and manganese phases can be substancially altered. As the former are also the main carriers of the sedimentary magnetic signal, their alteration affects not only the geochemical, but also the magnetostratigraphic and paleomagnetic record (e.g. Karlin and Levi, 1983; Karlin, 1990; Tarduno, 1994; Garming et al., 2005; Riedinger et al., 2005). In this work, we present results of geochemical and geophysical investigations on gravity core GeoB 9309-1 from the Zambesi deep-sea fan, focussing on the biogeochemical cycling of iron, sulfur, phosphorus, calcium and manganese at the SMT, and to quantify the redistribution of these elements that may lead to secondary signals in the sediment. Going one step further, we will discuss our results in comparison with other deep-sea fan deposits to

demonstrate the similarity of depositional and diagenetic processes, and evaluate their implications for interpreting the sedimentary record.

Location and geological setting

The northernmost area studied during RV *Meteor* cruise M63/1 in January/February 2005 was the continental margin off Mozambique, and in particular the Zambesi (or Mozambique) deep-sea fan (Fig. 2.1). Its extension of ~1800 x 400 km (Walford et al., 2005) makes it the largest deep-sea fan off southern Africa. Sediment is mostly derived from the Zambesi River catchment, which has an average elevation of 1009 m (Hay, 1998) and a drainage area of 1.21 - 1.4 x 106 km^2 (Walford et al., 2005). In terms of Pleistocene sediment accumulation rates, Walford et al. (2005) and Beusen et al. (2005) consistently report a total solid sediment yield of ~10 t km^{-2} y^{-1}. In a review on detrital sediment fluxes from continents to oceans (Hay, 1998), detrital sediment yields of the Zambesi estimated by various authors show a large variation (16.7 - 77.2 t km^{-2} y^{-1}), but are overall in the same order of magnitude as those given for the Nile and Congo rivers. Long-term sediment deposition on the continental slope off the Zambesi river mouth is governed by two main processes. The first is the topographic elevation of the drainage area, which is at present >1000 m (Summerfield and Hulton, 1994), most probably due to a zone of active upwelling in the mantle („African Superswell") beneath southern Africa (Walford et al., 2005). This led to high sediment discharge since the Miocene, and especially during the Pleistocene. The second factor controlling sedimentation is the activity of the Agulhas (or Mozambique) Current, a strong western boundary current (peak current speeds of ~2.5 m/s; Lutjeharms,

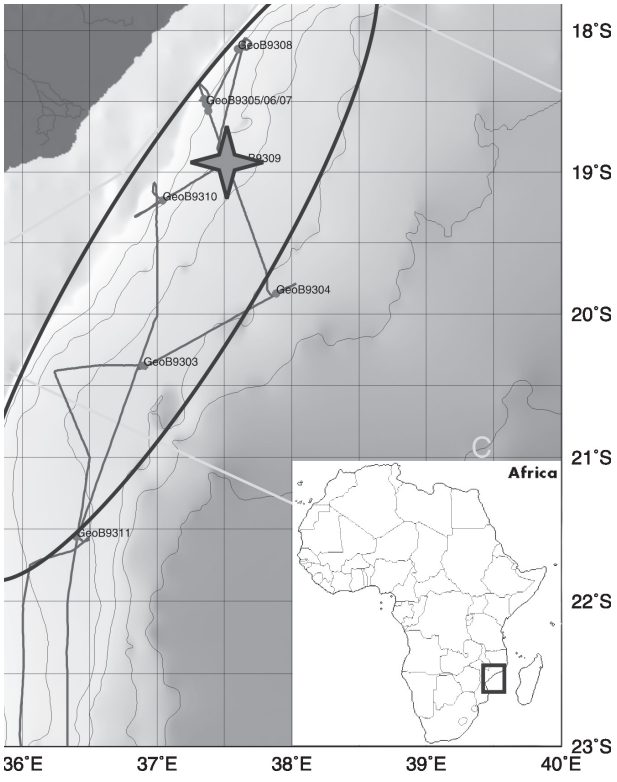

Fig. 2.1: Schematic map of the working area. The black ellipsoid indicates the elongated shape of the Pleistocene Zambesi Fan, based on a seismic reflection survey (Walford et al., 2005). The star marks the approximate position of gravity core GeoB 9309-1 on the central eastern slope of the fan.

1996) flowing in southwestern direction through the Mozambique Channel and towards the southern tip of Africa. At its confluence with the Atlantic Ocean, part of the warm water masses transported by this current are shed into the Atlantic, while another part is retroflected and flows back into the Indian Ocean, thereby creating a strong countercurrent flowing below the Agulhas Current backwards along the southwest African continental slope (Kolla et al., 1980). As a result, sediment deposited on the continental shelf and slope is distributed parallel to the countercurrent direction as a roughly SW-NE-orientated sediment body (Fig. 2.1). In isochore maps derived from a high-resolution seismic survey of the Zambesi fan (Walford et al., 2005), this elongated sediment body is observed in early Miocene times for the first time, documenting the initiation of the present Agulhas Current system.

In comparison to the western African continental margin, its (south)eastern parts - off Mozambique, Tanzania and Kenia - are only little investigated from a geological point of view. As a result, there are few data available concerning the Quaternary sedimentology and stratigraphy of the region investigated. Data on the last glacial and Holocene sea-level history on the Zambesi shelf and the western Indian Ocean can be obtained from Beiersdorf et al. (1980) and Camoin et al. (2005), respectively. Their ^{14}C age data indicate a sea-level of 60 m below the present one during the late last glacial around 10 000 years B.P., followed by a rapid transgression (0.6 - 2.4 m/100 years) during the early Holocene, until the present level was reached around 4000 years B.P. As the present shelf break is located at water depths of 50-120 m, large parts of the shelf were exposed during the last glacial. Systematic studies on marine primary productivity off the Zambesi river mouth, to our knowledge, are still lacking. Relatively low carbonate contents have been noticed in most sediment samples taken on the Zambesi deep-sea fan (H. Kuhlmann, pers. comm.; < 20 wt.% CaCO3 in GeoB 9309-1, Fig. 2.2), indicating low productivity of calcareous plankton in surface waters. Satellite data on global chlorophyll distributions in surface waters (e.g. Behrenfeld and Falkowski, 1997) indicate a primary productivity of <100 g C m^{-2} a^{-1}, which is comparable to oligotrophic open ocean settings.

Materials and Methods

Sampling

Gravity core GeoB 9309-1 was retrieved from 1219 m water depth east of the Zambesi River mouth, on the northeastern part of the fan (Fig. 2.1). After recovery, the gravity core was immediately cut into segments of 1 m length. For methane analysis, directly after cutting, 5 ml of sediment were taken with a plastic syringe and transferred into 50 ml vials prepared with 20 ml of saturated NaCl

solution. After gas-tight sealing, the samples were stored at -20 °C. Subsequently, the 1 m core segments were stored and lateron processed in a cooling laboratory under a constant temperature of 4 °C. Within one day, the core segments were cut into two halves, and pH and Eh were measured with punch-in electrodes prior to further sampling (Fig. 2.3 a). Pore water sampling was carried out in 25 cm depth resolution under an inert argon atmosphere in a glove box. The Teflon pore water squeezers were operated with argon at a gradually increased pressure (maximum 5 bar) and 0.2 µm cellulose acetate membrane filters, providing 5 to 20 ml pore water. Solid phase samples were taken every 10 cm under argon atmosphere with plastic syringes and stored in argon-filled, gas-tight glass bottles at a temperature of -20 °C. These solid phase samples are referred to as anoxic samples in the following text. In addition, the sedimentary solid phase of core GeoB 9309-1 was continuously sampled with a depth resolution of 2 cm at the University of Bremen. The samples were frozen, freeze-dried and ground in an agate mortar.

Pore water analysis

Onboard RV Meteor, the following chemical parameters were measured within a few hours after pore water sampling: ammonium, alkalinity, phosphate, iron(II) and hydrogen sulfide (Figs. 2.3 a and 2.4). A detailed description of the standard analytical procedures is given by Schulz (2006) and is also available on www.geochemie.uni-bremen.de/koelling/index.html. Subsamples of pore water were diluted 1:10 with de-ionized water and acidified with 1% HNO_3 (diluted 65% HNO_3 s.p.) for later analysis, except subsamples for sulfate determination. Sulfate was determined by HPLC at the Alfred Wegener Institute for Polar and Marine Research in Bremerhaven (Fig. 2.4). All further analyses were carried out at the University of Bremen. Pore water cations were determined from the diluted and acidified aliquots by Inductively Coupled Plasma Atomic Emission Spectrometry (ICP-AES, Perkin Elmer Optima 3300 RL). Measured constituents presented here are Ca, Fe, Mn, and P (Fig. 2.4). Methane was analysed using a gas chromatograph (Varian 3400) with splitless injector. After injection of 20 µl of gas from the headspace vials, the measured concentrations were calculated relative to total sediment.

Solid phase analysis

For total dissolution of all sedimentary components, ~50 mg of each sample (2 cm depth resolution) were digested with a HNO_3/HCl/HF mixture (3 ml, 2 ml and 2 ml, respectively).

The digestion was performed within a microwave system (MLS-MEGA II and MLS-Ethos 1600) at up to 215 °C and ~20 bar. Subsequently, the acid solution was evaporated to complete dryness. The sample was then redissolved and homogenized with 0.5 ml HNO_3 and 4.5 ml MilliQ water, and filled up to 50 ml with MilliQ water. Elemental concentrations of Al, Fe, Mn, P, S, Ti and Zr (Figs. 2.2 and 2.5) were analysed in the digestion solutions via ICP-AES. Application of standard reference material (USGS standard MAG-1, in-house standard MAX) assured the accuracy of measurements, as their element concentrations were within certified ranges. The precision of ICP-AES analyses was better than 3%.

A sequential extraction procedure to identify the different iron phases was applied to the anoxic sediment samples taken onboard. For the purpose of a quantitative approach, existing extraction schemes were slighly modified (Table 2.1; Kostka and Luther, 1994; Haese et al., 2000 and references therein). We only applied the ascorbate and dithionite steps, leading to reduction of amorphous Fe-oxyhydroxies (Fe_{Asc}) and crystalline Fe-oxides (Fe_{Dith}), respectively. These steps are regarded sufficient to quantitatively extract the iron phases most reactive towards HS^- (Fe_{react}, referring to the sum of both extraction steps; Fig. 2.5). Extraction and washing steps were carried out in an argon-flooded glove box to prevent any oxidation of sedimentary Fe-sulfides. Each extraction step was followed by a washing step with the respective buffer solution (Table 2.1) to recover all of the extracted iron. Extraction and washing solutions were analysed via ICP-AES after 1:10 dilution with MilliQ water, respective calibration standards were prepared with the corresponding buffer solution. After determination of the

Step	Extracted fraction	Extraction procedure (for 25 samples)
I-a (Ascorbate extraction step)	Easily reducable (amorphous) iron oxyhydroxides, iron in pore water	200-250 mg of wet anoxic sample, shaken over 20h wth 20ml of solution of 30g sodium citrate, 30g sodium bi-carbonate and 600ml oxygen-free bi-distilled water (buffer solution), to which 12g ascorbic acid was lowly added (degassing of carbon dioxide, final pH 7.5, Eh -150mV; extraction solution)
I-b (Washing step)		Residuum from I-a, shaken over 2h with 20ml of I-a buffer solution
II-a (Dithionite extraction step)	Crystalline iron (oxyhydr)oxides	Residuum from I-b, shaken over 4h with 20ml of solution of 42.28g sodium citrate, 12ml acetic acid and 600ml oxygen-free bi-distilled water (buffer solution), to which 18.02g sodium dithionite was added (final pH 4.8, Eh -500mV; extraction solution)
II-b (Washing step)		Residuum from II-a, shaken over 2h with 20ml of step II-a buffer solution

Table 2.1: Sequential iron extraction scheme (modified after Kostka and Luther, 1994; Haese et al., 1997, 2000). All extraction steps were performed under anoxic conditions. After each step, the extraction/washing solutions were centrifuged and filtered (0.2 µm).

water contents of the wet samples, concentrations of the extracted fractions were calculated in mg/g of dry sediment.

In order to identify major sedimentary P species at and below the SMT, a sequential phosphate extraction procedure was applied to 16 samples from the lowermost part of the core. Note that this phosphate extraction, following the methodology of Ruttenberg (1992), is usually not performed on anoxic samples or under anoxic conditions. This, however, may have an influence on the operationally defined fractions extracted in each step, as will be discussed lateron. Referring to the SEDEX extraction scheme of Ruttenberg (1992), modified by de Lange (1992) and Schenau and de Lange (2000), we applied three extraction steps (Table 2.2) to distinguish between the loosely sorbed/exchangeable/carbonate-bound phosphate (Ruttenberg, 1992) plus amorphous apatite/fish debris (Schenau and de Lange, 2000), iron (oxyhydr)oxide-bound phosphate, and authigenic apatite, respectively (Fig. 2.6).

Step	Extracted fraction	Extraction procedure
I-a (NH_4Cl step)	Exchangeable/loosely sorbed/carbonate-bound PO_4, fish bones, amorphous apatite, pore water PO_4	0.5g dry, ground sample, shaken over 12h with 50ml of solution of 106.98g ammonium chloride in 1l bi-distilled water (pH 7)
I-b (washing step)		Residuum from I-a, shaken over 2h with 50ml bi-distilled water
II-a (CDB step)	Iron(III)-bound PO_4	Residuum from I-b, shaken over 8h of solution of 22.63g sodium dithionite, 64.7g sodium citrate, 9.24g sodium bi-carbonate in 1l bi-distilled water (pH 7.5)
II-b (dithionite oxidation step)		Residuum from II-a, 8h reaction with 1ml conc. sulfuric acid in open vial; suspension filtered with acid-resistant filter
II-c (washing step)		Residuum from II-b, shaken over 2h with 50ml NH_4Cl solution (I-a)
II-d (washing step)		Residuum from II-c, shaken over 2h with 50ml bi-distilled water
III-a (acetate step)	Authigenic apatite	Residuum from II-d, shaken over 6h with 50ml of solution of 82.03g sodium acetate in 700ml bi-distilled water, brought to pH 4 with acetic acid, then filled up with bi-distilled water to 1l volume
III-b (washing step)		Residuum from III-a, shaken over 2h with 50ml NH_4Cl solution (I-a)
III-c (washing step)		Residuum from III-a, shaken over 2h with 50ml NH_4Cl solution (I-a)
III-d (washing step)		Residuum from III-a, shaken over 2h with 50ml bi-distilled water

Table 2.2: Sequential phosphate extraction scheme (modified after Ruttenberg, 1992; de Lange, 1992; Schenau and de Lange, 2000). After each step, the extraction /washing suspension were centrifuged and filtered (0.2 µm), if not stated otherwise

Phosphate concentrations in the respective extraction and washing solutions were determined via ICP-AES.

The analysis of inorganic carbon (IC) and total organic carbon (TOC) (Fig. 2.2) was performed on the homogenized and freeze-dried samples in a depth resolution of 6 cm. Total carbon (TC) was determined using a LECO CS 200 carbon sulfur analyzer. Subsequently, the sediment was decalcified with 12.5% HCl, washed twice with MilliQ and dried at 60 °C. The remaining TOC fraction was again measured with a LECO CS 200. The $CaCO_3$ content (IC) of the sediment was calculated by applying the equation: $CaCO_3$ (%) = (TC - TOC) x 8.33. Marble standards with a C content in the range of 0.5-12% were applied to track the accuracy of the measurements which was ~ 3%.

Physical sediment properties (porosity, colour reflectance, magnetic susceptibility) were investigated onboard RV Meteor using an automated core conveyor system (Fig. 2.3 b). The GEOTEK multi-sensor core logger works after the non-contact principle. It is equipped with a commercial susceptibility meter (Bartington Instruments MS2) with a loop sensor, an electrical conductivity measurement tool (to obtain porosity) and a line scanner system with digital image analysis for reflectance and colour measurements.

Results and Discussion

Sediment composition

Core GeoB 9309-1 was taken from an area on the Zambesi fan that has not been part of an active channel-levee system for at least the time interval documented in the core (T. Schwenk, pers. comm.). The muddy hemipelagic sediment of the core appears relatively uniform and homogeneous, apart from a thin sandy turbidite layer at ~180 cm sediment depth. At first glance, the sparsity of turbidites is unexpected, as continuous detrital input should trigger frequent mass movements and turbidite deposition off The Zambesi mouth. However, sedimentary mass movements on the Zambesi deep-sea fan are obviously confined to channels that deliver the material to deeper parts of the basin (Kolla et al., 1980). Thus, mostly fine-grained sediments of the river plume settle between the active channels. Similar findings have been reported from ODP sites on the Congo fan (Wefer et al., 1998) and the Amazon fan (Schneider et al., 1997), and from gravity cores taken on the Niger fan (Adegbie et al., 1998). Furthermore, Kolla et al. (1980) stated that in sediments of the „Inner Mozambique Fan" - which includes the location of core GeoB 9309-1 - turbidites almost exclusively occur in deposits older than 11 000 years, i.e. prior to the Holocene. As reviewed by Wien (2006), the rareness of turbidites in

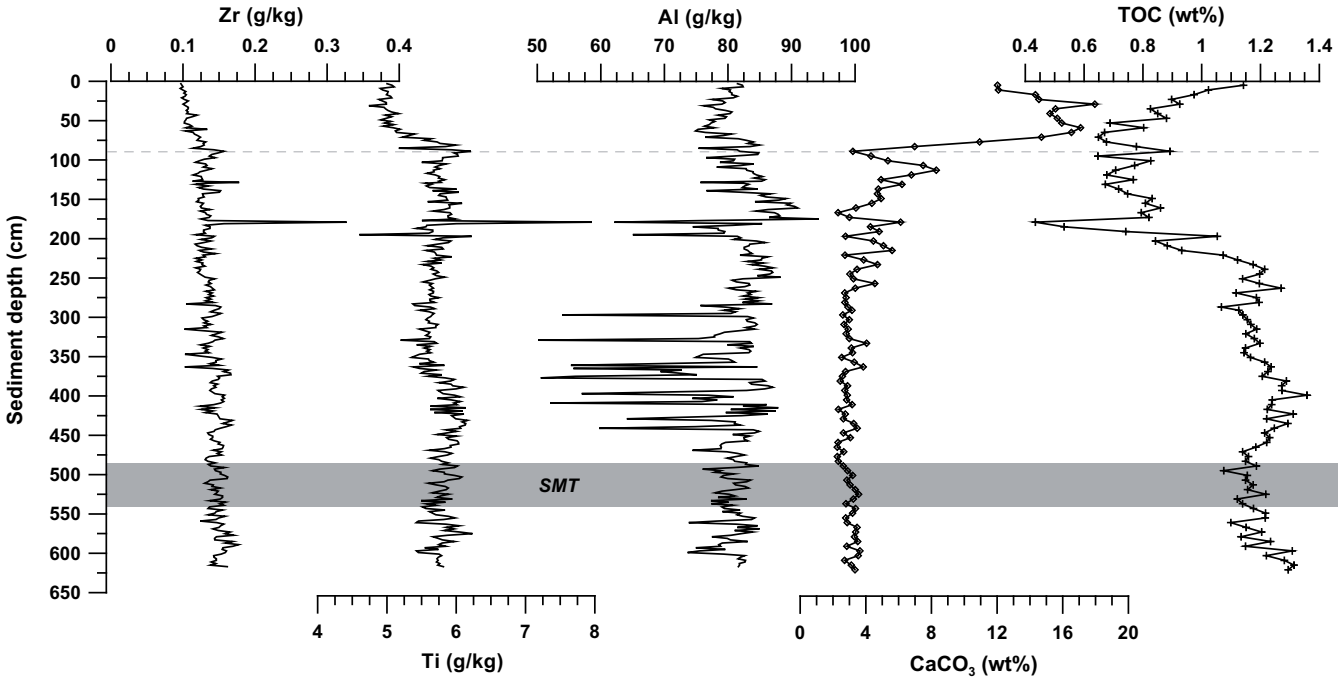

Fig. 2.2: Total solid phase concentrations of Zr, Al and Ti as well as calcium carbonate and total organic carbon (TOC) contents, all plotted against sediment depth.

Holocene sediments also fits into the traditional view of mass flow deposition, attributing major phases of turbidite emplacement to glacial periods with a low eustatic sea level (Shanmugan and Moiola, 1982; Vail et al., 1991; Einsele, 1996).

The generally grey sediment colour of core GeoB 9309-1 gradually changes downcore from light to dark. This colour trend is also documented in total reflectance and red-blue color reflectance ratio profiles (Fig. 2.3 b). It is interpreted as the visual expression of both downcore increase of TOC (from 0.7 to 1.4 wt%) and decrease of carbonate content (from 18.0 to 3.0 wt%, Fig. 2.2). Carbonate contents calculated from IC analysis match the carbonate contents calculated from bulk Ca contents obtained by acid digestion procedure (correlation coefficient $R^2 = 0.97$). Thus, $CaCO_3$ seems to be the major Ca-containing mineral in the deposits. The overall low carbonate concentrations in core GeoB 9309-1 (mean of 4.9 wt%) point to a minor importance of marine carbonate productivity or detrital carbonate input to the sediment budget. Additionally, high sedimentary contents of Al, Ti and Zr (mean of 80.6 g/kg, 5.7 g/kg and 137 ppm, respectively) point at a system dominated by terrigenous input (Fig. 2). However, there is only weak linear correlation between these lithogenic elements throughout the core (R^2 is 0.02 for Al/Ti, 0.06 for Al/Zr, 0.56 for Ti/Zr), implying variable sediment sources and/or processes that have been active during or after deposition, e.g. the winnowing activity of northeast-directed bottom currents (Kolla et al., 1980). The observed enrichments of Ti and Zr above upper

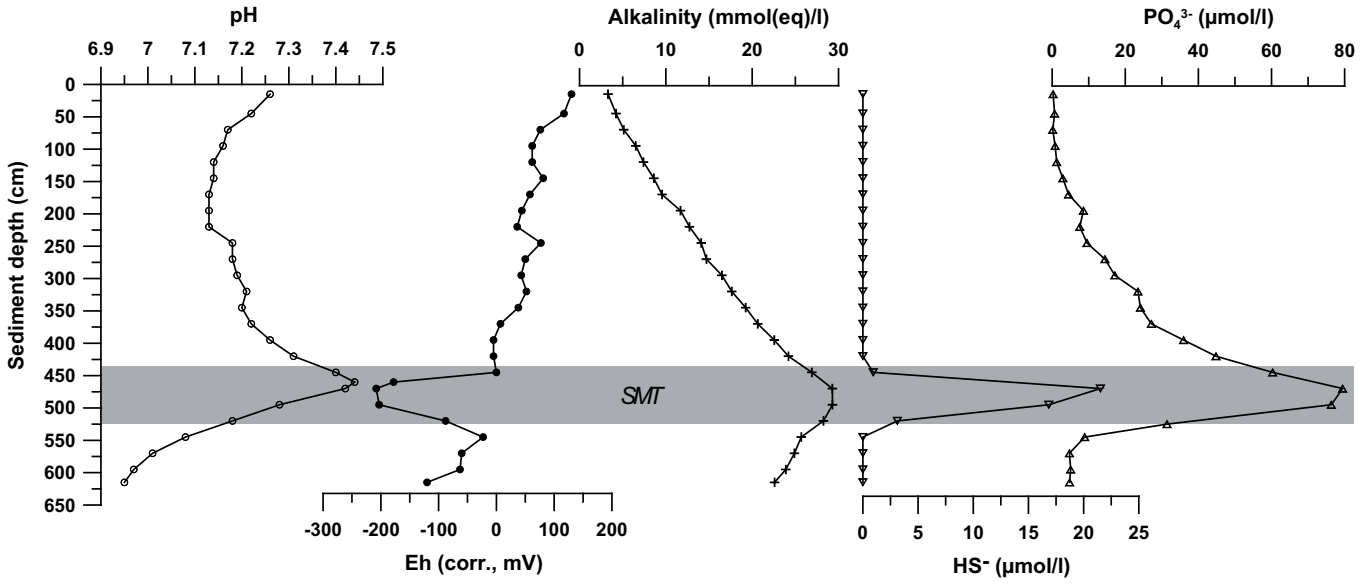

Fig. 2.3: Onboard geochemical and geophysical data obtained by pore water extraction and multisensor core logging, respectively. (a) punch-in pH, Eh, alkalinity, sulfide and phosphate concentrations; (b) magnetic susceptibility, porosity and red/blue colour reflectance ratio. The position of the sulfate/methane transition (SMT) is indicated by grey bar.

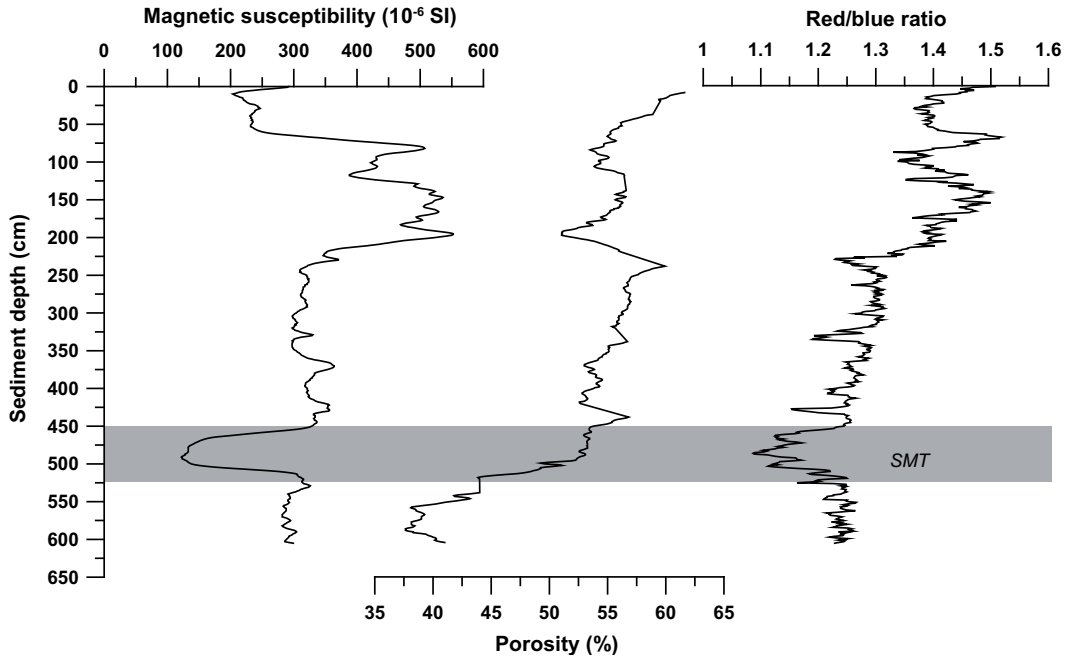

continental crust values (e.g. Condie, 1993) are most probably linked to heavy mineral placer deposits (mainly ilmenite, rutile, zircon) along the Mozambique coastline, adjacent to the Zambesi mouth (Beiersdorf et al., 1980; H. Kudrass, pers. comm.). The initial sources of these deposits are Precambrian magmatic and metamorphic rocks in the Zambesi catchment area (Kolla et al., 1980; Dürr et al., 2005),

namely the Rhodesian and Kaapvaal Cratons and the Mozambique, Limpopo and Zambesi mobile belts (Beiersdorf et al., 1980).

There are striking similarities in the development of carbonate and TOC concentrations of core GeoB 9309-1 (Fig. 2.2) with deposits of the Rio de la Plata offshore depocenter (e.g. GeoB 6308-4, Riedinger et al., 2005), the Congo fan (e.g. GeoB 1008, Schneider et al., 1997; GeoB 1401, Gingele et al., 1998), the Amazon fan (e.g. GeoB 1514-6, Kasten et al., 1998; ODP Site 942, Schlünz et al., 1999) and older data from the Mozambique Channel (Kolla et al., 1980). As a common pattern of all these sedimentary systems, there is a maximum of calcium carbonate around 50-80 cm depth, followed by a rapid downcore decrease within the uppermost 80-200 cm of sediment. The carbonate trend in the uppermost 100-200 cm usually anticorrelates with the TOC content. These findings indicate similar processes controlling sedimentation patterns, at least during the Quaternary, in deep-sea fans worldwide. At site GeoB 9309, below ~90 cm sediment depth, carbonate contents decrease rapidly from ~18 wt% to ~3 wt%, and further downcore mostly stay below 5 wt%. Concomitantly, TOC contents start to rise at 90 cm sediment depth from ~0.6 wt% to ~1.2 wt% (Fig. 2.2). Based on these findings, the position of the last glacial/interglacial transition (Termination I) at site GeoB 9309 is in ~90 cm sediment depth. Thus, the sedimentation rate to be derived since the last glacial/interglacial transition is ~9 cm kyr^{-1}. The downcore shift to carbonate-poor deposits below 90 cm is interpreted as a dilution of calcareous material by increased terrigenous input during the last glacial, probably due to increased continental erosion and/or increased sediment bypass across the shelf, in combination with lower carbonate productivity. Despite the lack of a detailed age model for GeoB 9309-1, ^{14}C data of two other gravity cores (Kuhlmann et al., 2007; J. Pätzold, pers. comm.) retrieved in ~500 m water depth closer to the Zambesi river mouth confirm the suggestions made above. Sedimentation rates seem to drop rapidly from ~100 cm kyr^{-1} around the Last Glacial Maximum (LGM, ~11 000 years B.P.) to ~20 cm kyr^{-1} for the Holocene. The greater water depth and longer distance to the detrital sediment source of station GeoB 9309 could explain the lower Holocene sedimentation rates in core GeoB 9309-1, as derived from carbonate and TOC records, which are additionally consistent with other submarine river fans (see references above). Further, though indirect support for Termination I in core GeoB 9309-1 at 90 cm sediment depth is given by Kolla et al. (1980). At sites from the „Inner Mozambique Fan", they found almost all turbidites in sediments older than 11 000 years. At site GeoB 9309, the only turbidite is found in ~180 cm sediment depth, indicating that Termination I is located above this sediment depth.

Diagenetic processes

The sulfate/methane transition (SMT) zone in core GeoB 9309-1 is situated at a sediment depth of ~450-530 cm (Figs. 2.3-2.5). The anaerobic oxidation of methane (AOM) is triggering a suite of biogeochemical reactions around the SMT that will be discussed lateron. The overall AOM reaction can be formulated as:

$$CH_4 + SO_4^{2-} \rightarrow HCO_3^- + HS^- + H_2O \quad (1)$$

This process is mediated by a consortium of methane-oxidizing archaea and sulfate-reducing bacteria (Boetius et al., 2000; Orphan et al., 2001). Crucial factors controlling the depth location of the SMT and the shape of the sulfate profile are the fluxes of sulfate and methane (e.g. Niewöhner et al., 1998; Hensen et al., 2003; Riedinger et al., 2005) and the sedimentation rate (Riedinger et al., 2005). Sulfate is derived from sea water diffusing downward through the sediment pore space. Methane originates from deeper parts of the sediment, where it is either produced by microbial degradation of organic matter, or by thermal hydrocarbon generation during deeper sediment burial (in the zone of metagenesis). The AOM influences the carbonate system of the pore water, leading to higher alkalinity and pH (Fig. 2.3 a), and liberates free HS^- into the pore water (see eq. (1), Fig. 2.3 a). This not only decreases the redox potential of the pore water, but can also have a significant impact on the solid sediment composition via several secondary reactions. In the following, processes and products of these reactions as detected at site GeoB 9309 will be discussed, based on solid phase and pore water data of selected elements (Ca, Fe, Mn, S, P; Fig. 2.4).

Calcium, manganese

These elements are potentially influenced by early diagenesis around the SMT, but are of minor importance in core GeoB 9309-1.

Precipitation of authigenic calcium carbonate as a byproduct of AOM (e.g. Bohrmann et al., 1998; Peckmann et al., 2001) could neither be detected macroscopically nor via pore water and solid phase analyses in core GeoB 9309-1 (Figs. 2.2 and 2.3 a). Obviously, the rates of AOM are low, so concentrations of HCO_3^- produced are not high enough to induce a significant precipitation of authigenic calcium carbonates.

Manganese, as indicated by pore water data, seems to be affected by free HS^- and/or alkalinity

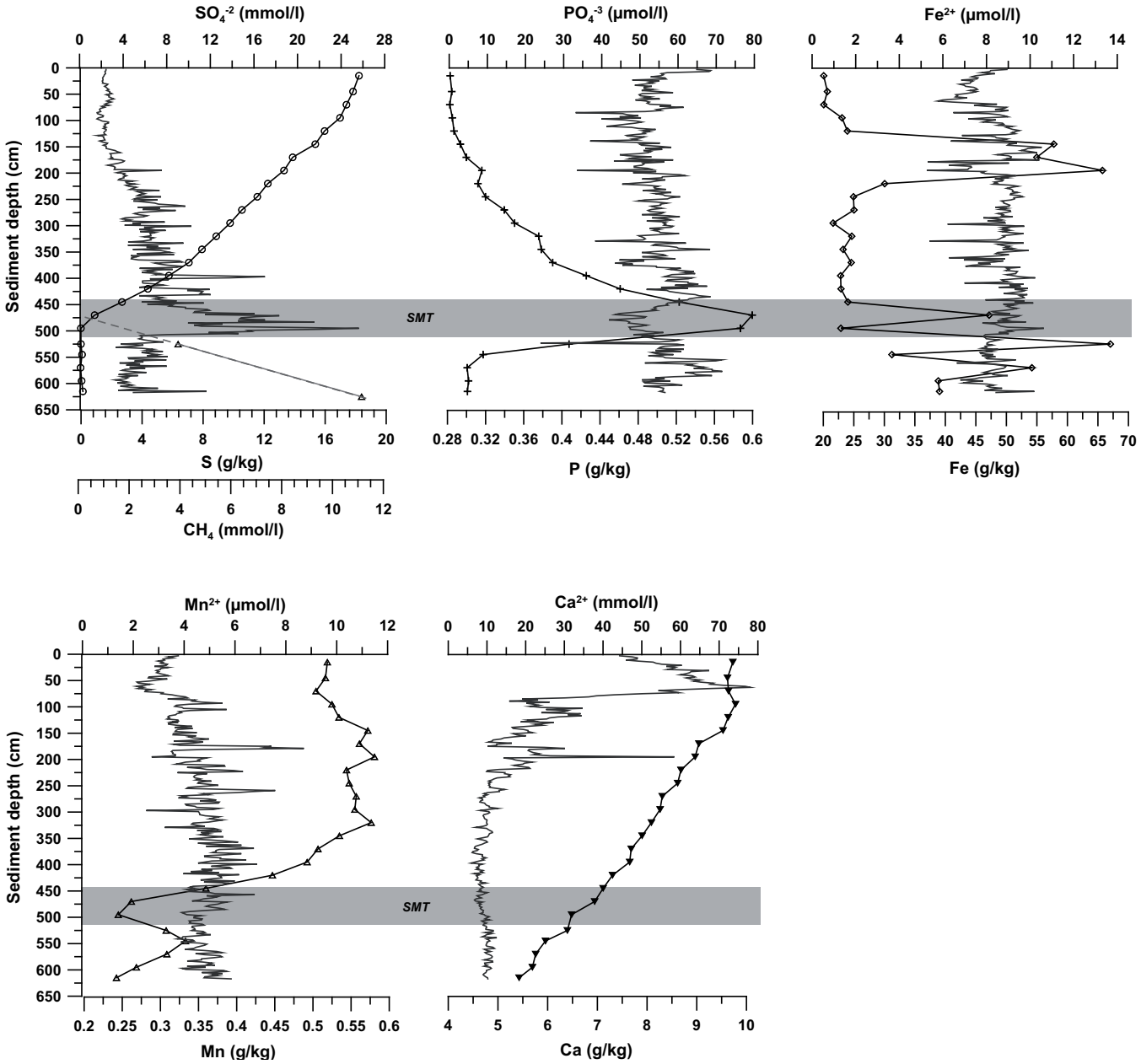

Fig. 2.4: Pore water concentrations of SO_4^{2-}, CH_4, PO_4^{3-}, Fe^{2+}, Mn^{2+} and Ca^{2+} (25 cm depth resolution) and solid sediment contents of total sulfur, phosphorus, iron, manganese and calcium (1 cm depth resolution), all plotted against sediment depth.

(Fig. 2.4). It generally occurs in the sediment as Mn-oxides and -carbonates. The former are primarily supplied to the sediment or re-precipitated at the Mn redox boundary. Manganese (oxyhydr)oxides on average make up ~30% of bulk Mn in core GeoB 9309-1, as indicated by analyses of Mn in the sequential iron extraction solutions. It has been found that Mn oxides can be reduced, dissolved and re-precipitated as sulfides and carbonates around the SMT (Böttcher and Huckriede, 1997; Lepland and Stevens, 1998). However, solid phase Mn concentrations in core GeoB 9309-1 are in general

considerably lower (2 orders of magnitude) than those of Fe and average around 0.35 g/kg sediment (Fig. 2.4). Thus, potential Mn sulfide precipitation around the SMT is considered to be quantitatively of minor importance. Diagenetic Mn sulfides have up to now only been reported from local anoxic depressions of the Derugin Basin, Sea of Okhotsk (Derkachev et al., 2007), and in greater detail from deposits of the Landsort Deep and Gotland Deep, two oxygen-depleted subbasins of the Baltic Sea (Böttcher and Huckriede, 1997; Lepland and Stevens, 1998). In the latter sediments, manganese plays an exceptionally important role in the sediment redox system due to its high background concentration in combination with relatively low reactive iron in the sediment. However, in Landsort Deep deposits, Lepland and Stevens (1998) do not regard manganese availability, but high alkalinity and hydrogen sulfide production during extremely reducing conditions in the sediment as limiting factors in Mn carbonate and sulfide precipitation, respectively (in contrast to Neumann et al., 2002). Elevated alkalinity (up to 30 mmol(eq)/l) and HS^- (up to 22 µmol/l) values are also found in GeoB 9309-1 at the SMT (Fig. 2.3 a), yet these values are still comparably low, and thus most probably insufficient for a manganese precipitation after the Lepland and Stevens model. Furthermore, due to the intermittendly anoxic character of the Baltic Sea Deeps as well as to the low reactive iron contents in their deposits, it is doubtful whether this postulated formation mechanism for authigenic Mn minerals can be fully applied to the Zambesi deep-sea fan sediments.

Recently, Riedinger (2005) found distinct solid phase Mn enrichments around the SMT in gravity cores from the Argentine Basin. They are likely to consist of Mn sulfides (e.g. alabandite) or carbonates (e.g. rhodochrosite), as they were concomitant with significant drawdowns of dissolved Mn in pore water and intervals of hydrogen sulfide and bicarbonate production. A similar Mn^{2+} drawdown around the SMT can be observed in the Mn pore water profile of GeoB 9309-1 (Fig. 2.4). The lack of a solid phase Mn peak might be due to lower background Mn contents at site GeoB 9309 compared to Argentine Basin sediments and/or an in situ transformation of Mn (oxyhydr)oxides into sulfides. Another explanation would be that the precipitation process has only been active for a relatively short time, too short for the formation of a bulk Mn peak. This is even more probable considering that, according to Lepland and Stevens (1998), Mn sulfides have a higher solubility than Fe sulfides. Therefore, they only start to form when all chemically reactive iron (oxyhydr)oxides within the HS^- production zone are already reduced and HS^- production continues. In summary, it is possible that Mn sulfides or carbonates have precipitated at the SMT, but in concentrations that do not rise significantly above the bulk solid phase Mn signal, thus remain undetectable.

Iron

The average sedimentary Fe content is ~48 g/kg in core GeoB 9309-1 (Fig. 2.4). This value is regarded as typical for tropical-subtropical river deep-sea fan systems, as off the Amazon (e.g. Burns, 1998) or the Niger (e.g. Dillon and Bleil, 2006). Most iron is probably bound to silicates, but also iron (oxyhydr)oxides can make up a significant fraction of total in Fe sediments dominated by riverine input (e.g. Poulton and Raiswell, 2002). Iron (oxyhydr)oxide minerals (e.g. ferrihydrite, goethite, magnetite) are prone to biogeochemical reduction, either connected to microbial oxidation of organic matter, or - especially at the SMT - driven by hydrogen sulfide. The latter reduction process schematically follows the multistage reaction (e.g. Berner, 1984; Canfield, 1989):

$$2FeOOH_{(s)} + HS^-_{(aq)} + 5H^+_{(aq)} \rightarrow 2Fe^{2+}_{(aq)} + S^0_{(s)} + 4H_2O_{(aq)} \quad (2)$$

$$Fe_3O_{4\ (s)} + HS^-_{(aq)} + 7H^+_{(aq)} \rightarrow 3Fe^{2+}_{(aq)} + S^0_{(s)} + 4H_2O_{(aq)} \quad (3)$$

$$Fe^{2+}_{(aq)} + HS^-_{(aq)} \rightarrow FeS_{(s)} + H^+_{(aq)} \quad (4)$$

$$FeS_{(s)} + HS^-_{(g)} + H^+_{(aq)} \rightarrow FeS_{2\ (s)} + H_{2\ (g)} \quad (5)$$

Apart from the iron monosulfide (eq. (4)) and pyrite (eq. (5)) endmembers, metastable iron sulfide phases (e.g. pyrrhotite, greigite) not mentioned above may also occur, especially in sulfide-limited systems. The „H_2S pathway“ (Rickard and Luther, 1997) described above is regarded as dominant pyrite formation mechanism in the sediments investigated. The „polysulfide pathway“ (Berner, 1970, 1984; Luther, 1991) and the „iron-loss pathway“ (Wilkin and Barnes, 1996) will not be discussed here in detail (recent reviews by Schoonen, 2004; Jørgensen and Kasten, 2006). The type of iron sulfide formed around the SMT plays a decisive role regarding the magnetic properties of the sediment. Generally, most primary iron oxides (e.g. magnetite, maghemite) are ferrimagnetic and determine the magnetic susceptibility of a sediment. The iron sulfide phases pyrrhotite and greigite, intermediates in the pyrite formation process, are also ferrimagnetic, thus their formation can create a secondary enhancement of magnetic susceptibility. Formation of paramagnetic pyrite, however, leads to a reduction of the magnetic susceptibility. The latter process is obviously documented at the SMT in core GeoB 9309-1, confirming the precipitation of pyrite and a lack of intermediate iron sulfides (Fig. 2.5). Finely dispersed pyrite also leads to a darker sediment colour at the SMT compared to the

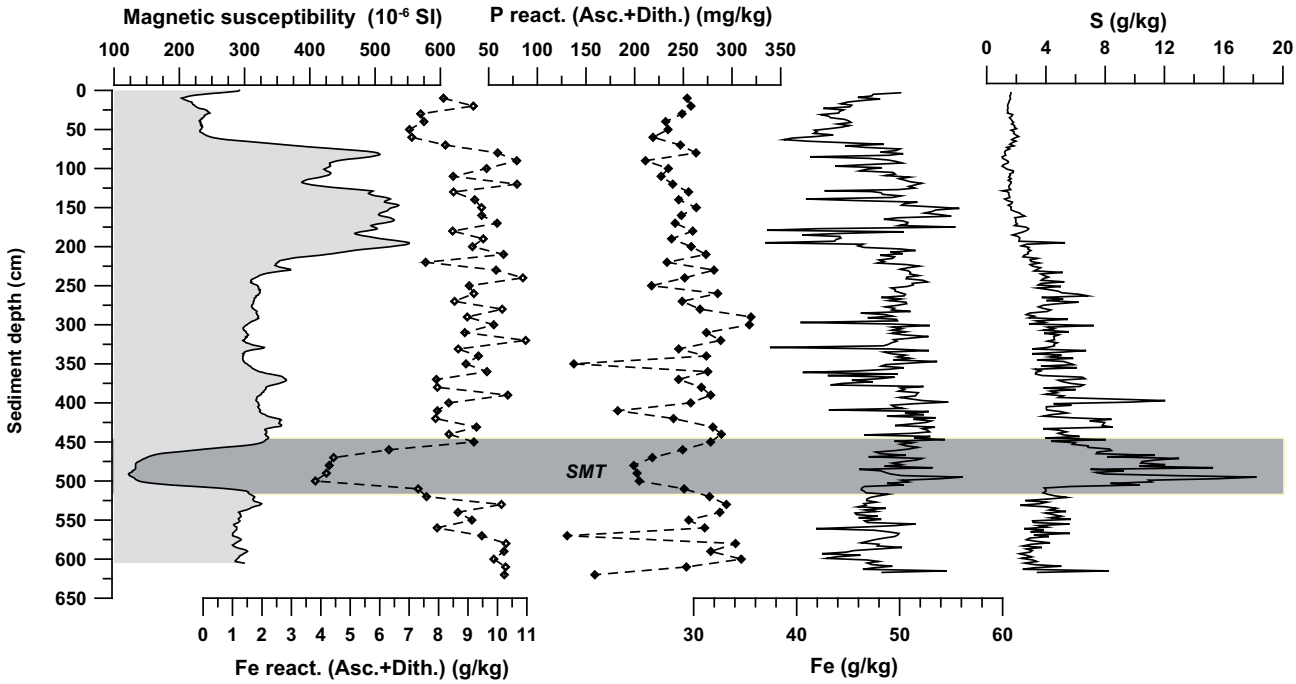

Fig. 2.5: Magnetic susceptibility, reactive iron and phosphorus contents (Fe_{react}, P_{react}), and bulk iron and sulfur contents of the sediment, all plotted against sediment depth.

surrounding sediment, as documented in the profile of the red/blue ratio (Fig. 2.3 b). Pyrite formation at the SMT is a well-known phenomenon in marine sediments (e.g. Berner, 1984; Canfield, 1989; Passier and Dekkers, 2002; Novosel et al., 2005) and also on several riverine slope depocenters (e.g. Garming et al., 2005; Riedinger et al., 2005). In these publications, pyrite formation at the SMT is indicated by a similar loss of magnetic susceptibility, an enrichment in sedimentary S, but also by marked bulk Fe enrichments. However, core GeoB 9309-1 differs from the above-mentioned examples, as it does not show a characteristic bulk Fe peak at the SMT (Fig. 2.4). To solve this discrepancy, a sequential iron extraction procedure (Table 2.1) was applied to anoxic subsamples taken throughout the core, to determine the relative contribution of reactive iron minerals ($Fe_{react.}$) to bulk solid phase iron throughout the core (Haese et al., 2000). In our definition, „reactive“ refers to the reactivity towards HS^- (Berner, 1984; Canfield, 1989; Poulton et al., 2004). This does usually not equal reactivity in the biological sense, which is referred to as „bioavailability“ and generally makes up only a fraction of the “chemically reactive” iron pool (Postma, 1993; Hyacinthe et al., 2006). As a result of the sequential extraction, iron (oxyhydr)oxides on average make up ~19.2% (ranging from 15.1% to 22.6%) of total sedimentary Fe (excluding samples within the SMT), thus a significant fraction. As shown in Figure 2.5, iron (oxyhydr)oxides have a distinct minimum at the SMT (7.6% to 12.6% of total Fe), parallel

to the drop in magnetic susceptibility. This finding is indicative for an in situ transformation of iron (oxyhydr)oxides to pyrite at the SMT, without affecting the total sedimentary Fe record.

Sulfur

A strong enrichment of sulfur is found at the SMT around ~450-530 cm sediment depth, with values 2-3 times higher than background contents (up to 18 g sulfur/kg sediment; Fig. 2.4). The sulfate depth profile exhibits an almost linear shape, indicating that a predominant sink occurs at this depth, and that a steady state pore water situation at the SMT has nearly been reached. These findings are in agreement with data from the Argentine continental margin (Riedinger et al., 2005), where a similar steady state has been reached due to low Holocene sedimentation rates (<10 cm/1000 years) and subsequent fixation of the SMT since that time. At both the Argentine margin and on the Zambesi deep-sea fan, the depth fixation of the SMT followed a period of higher glacial sediment delivery to the continental slope, during which the SMT was migrating upward parallel to the respective sediment surface. Since the last glacial/interglacial transition ~10 000 years ago, reductive dissolution of iron and/or manganese (oxyhydr)oxides and reprecipitation as sulfides (e.g. Kasten et al., 1998) has been taking place at the current SMT. However, there are no concomitant enrichments of solid phase Fe, as found e.g. by Kasten et al. (1998) on the Amazon Fan and by Riedinger et al. (2005) in the Argentine Basin. This is most probably due to in situ dissolution of ferric iron minerals and reprecipitation as sulfides, as described above. The amount of sulfur that was fixed in iron sulfides at the SMT can be used to calculate for how long the SMT has been fixed in its current position, as will be discussed lateron. Apart from the coupling of the iron and sulfur cycles around the SMT, another change in the solid phase sulfur profile occurs at ~220 cm depth (Fig. 2.4). Above this depth, sulfur remains at relatively constant values of 1-3 g/kg, while below 220 cm sediment depth, S values are generally higher and show significant variability (3-8 g/kg). However, as in the scope of this paper we want to focus on processes around the SMT, this pattern will not be discussed in more detail.

Phosphorus

Phosphate is an essential nutrient for all organisms. In aquatic sediments, it is mostly incorporated into organic matter and liberated during its biogeochemical degradation. Furthermore, phosphate strongly adsorbs onto surfaces of iron (oxyhydr)oxide minerals, thereby creating a strong link between the iron and phosphorus cycles (e.g. Slomp et al., 1996 a; Delaney, 1998; Canfield et al.,

2005), which is also documented at site GeoB 9309. Sequential iron extraction revealed that phosphate bound to iron (oxyhydr)oxides (defined here as Preact) makes up on average 51.5% of total sediment P (Fig. 2.5). Triggered by the postulated dissolution of primary iron (oxyhydr)oxides around the SMT, there is a liberation of formerly surface-bound phosphate into the pore water at the SMT (~80 µmol/l in Zambesi fan sediments; Figs. 2.3 a, 2.4). Most probably due to phosphate re-adsorption to iron (oxyhydr)oxides in the sediment above the SMT, phosphate decreases upward and reaches values below detection limit at ~120 cm below the sediment/water interface. The concave-upward shape of the PO_4^{3-} pore water profile indicates that this re-adsorption process is taking place not within a discrete horizon, but over the whole sediment interval between ~120 and 450 cm. In contrast, there is a steep gradient of dissolved phosphate directly below the SMT. Between 500 and 550 cm sediment depth, values decrease with a steep gradient from ~80 to 3 µmol/l, or 1.5 µmol/cm. Considering the comparably modest upward PO_4^{3-} gradient, a different mechanism than re-adsorption is supposed to be the cause for the steep pore water phosphate gradient below the SMT. A possible explanation for this effective phosphate sink could be the precipitation of phosphatic minerals like apatite ($Ca_5(PO_4)_3$(OH, F, Cl)) or vivianite ($Fe_3(PO_4)_2\ 8H_2O$).

Solid-phase P data correspond nicely to pore water results (Fig. 2.4), as there is a distinct minimum in sedimentary P at the SMT (450 ppm relative to 550 ppm above). Directly below the SMT, P contents reach 570 ppm, supporting the postulated precipitation of secondary phosphate minerals. Measurements of phosphate in the sequential iron extraction solution, representing the P fraction adsorbed onto iron (oxyhydr)oxides, confirm a distinct decrease in the extracted phosphate amount of ~100 ppm at the SMT (Fig. 2.5). Thus, the observed decrease in bulk solid phase P from 550 to 450 ppm can be fully attributed to dissolution of iron (oxyhydr)oxides and concomitant phosphate desorption. A further indication for authigenesis below the SMT is the rapid downward porosity decrease (from 52 to 38%) beneath ~500 cm (Fig. 2.3 b). Precipitation of authigenic minerals could partly seal the pore space, as described by Schuffert et al. (1998) in gravity cores taken off Baja California, Mexico. However, authigenic phosphate minerals alone cannot cause the observed porosity loss below the SMT. Alternatively, the reduced porosity could be attributed to selective compaction, or be a sampling artifact. We have no reasons to believe, however, that either of the latter two hypotheses has been the case.

Diagenetic reactions leading to authigenic phosphate precipitation below the SMT have been suggested by a number of authors for various locations. In Quaternary sediments recovered during ODP Leg 155 on the Amazon deep-sea fan, Burns (1997) described the precipitation of millimeter-sized vivianite nodules. At Site 944, pore water phosphate concentrations were elevated at the SMT

(100-400 µmol/l) and decreased rapidly to around zero below it. According to Burns (1997), the latter drawdown of phosphate was probably due to vivianite formation below the SMT. As an explanation for the lack of authigenic apatite, Burns (1997) proposed the lack of calcium carbonate surfaces that could promote apatite precipitation (deKanel and Morse, 1987). Rasmussen (2000) described early diagenetic alumino-phosphate precipitates in Archaean to Cretaceous marine sandstones from Australian sedimentary basins. The phosphate minerals identified by means of SEM-EDS and XRD (e.g. florencite, crandalite, gorceixite) precipitated onto detrital clay particles within the zones of sulfate reduction and methanogenesis, and incorporated significant amounts of Ca, Ba and REEs. Hence, Rasmussen (2000) postulated that, in addition to phosphate, elevated concentrations of the respective elements must have been available in the pore water during mineral formation. During ODP cruise 175, Murray et al. (1998) found a strong increase in phosphate at the depth of sulfate depletion in Congo Fan sediments, followed by a rapid downward decrease which they unspecifically attributed to phosphate uptake into apatite minerals. Schulz et al. (1994) found pore water phosphate patterns similar to core GeoB 9309-1 in sediments off the Amazon river (GeoB 1514), and attributed them to possible vivianite precipitation. Despite pore water phosphate concentrations ~4 times higher than on the Zambesi deep-sea fan (350-500 µmol/l), at both locations phosphate decreased rapidly below the SMT, within ~100 cm.

To identify the potential phosphate minerals precipitated below the SMT at site GeoB 9309, we used two different approaches. First, we applied a sequential extraction procedure after Ruttenberg (1992), de Lange (1992) and Schenau and de Lange (2000) to distinguish between major phosphate-carrying minerals below the SMT (listed in Table 2.2). The extraction results are shown in Figure 2.6, with the sequential steps (a) NH_4Cl solution (exchangeable/loosely sorbed/carbonate-bound P plus amorphous apatite/fish bones), (b) CDB solution (P bound to iron (oxyhydr)oxides) and (c) Na-Acetate solution (authigenic apatite. Comparison of P contents obtained by total digestion to those in the sequential extraction solutions shows that from all samples, nearly all sedimentary P (>88%) was recovered by the extraction steps applied, implying that other potential sedimentary P fractions (as organic matter-bound P, detrital apatite) are of minor importance. The NH_4Cl fraction (Fig. 2.6 a) shows highest PO_4^{3-} concentrations within the SMT (grey bar), but is strongly decreased and stays on a constant level below it. To a minor amount, this may be a relic of elevated pore water phosphate. A major contribution of a fast-forming, amorphous apatite precursor to the NH_4Cl-extracted fraction was proven in sediments under the Arabian Sea oxygen minimum zone (Schenau et al., 2000). The Ca^{2+} pore water profile of core GeoB 9309-1 (Fig. 2.4) does not exhibit a marked sink at the SMT that would confirm the precipitation of such a Ca-rich and F-poor mineral. Still, such a sink could be masked by

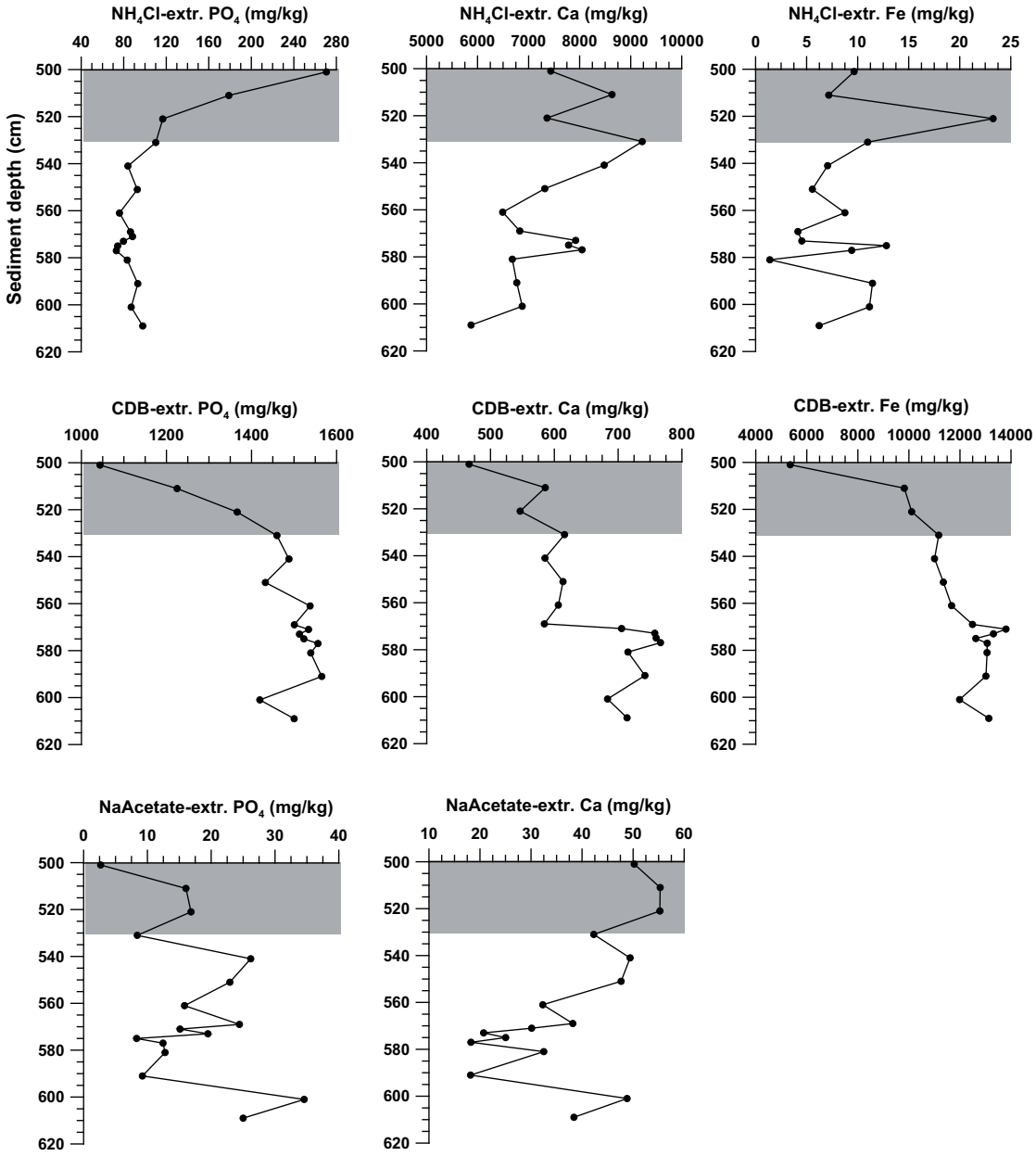

Fig. 2.6: Results of the sequential phosphate extraction procedure for selected samples from 500-620 cm sediment depth. Concentrations for phosphate, calcium and iron were measured for the sequential steps (a) NH_4Cl solution (exchangeable/loosely sorbed/carbonate-bound/fish bones/amorphous apatite fraction), (b) CDB solution (fraction bound to iron (oxyhydr)oxides) and (c) Na-Acetate solution (authigenic apatite). Note different scales for concentrations! The position of the SMT is indicated by the grey bar.

concentrations of Ca^{2+} three orders of magnitude higher than those of PO_4^{3-}. In addition, the NH_4Cl step was only applied once, so the preferentially extracted mineral might be $CaCO_3$ (Schenau et al., 2000). Amorphous apatite precursors might not have been extracted completely during this step due to saturation of the extraction solution with $CaCO_3$, and might be partly extracted in the following

CDB extraction. The CDB-extracted phosphate fraction (Fig. 2.6 b) exhibits the opposite pattern of the NH_4Cl step, with strongly increasing values below the SMT, and is the overall dominant fraction of the three steps applied. The CDB extracted phosphate profile matches well with that of iron, indicating a close iron-phosphorus coupling below the SMT. The Na-Acetate step (Fig. 2.6 c) yields no systematically higher phosphate values below the SMT than within it and exhibits lowest values of all extraction steps applied. Thus, authigenic apatite does not seem to be a quantitatively important phosphate sink. Na-Acetate-extracted calcium matches well with the respective phosphate profile, reflecting the chemical composition of calcium apatite. Iron concentrations were below detection limit.

The results of this sequential extraction procedure have to be interpreted with care. The extraction scheme is defined for crystalline phases only, masking the possible contribution and composition of amorphous P phases. Furthermore, the extraction behaviour of the mineral vivianite has not been defined by Ruttenberg (1992), de Lange (1992) and Schenau and de Lange (2000). Freudenthal (1995, unpubl. diploma thesis) experimentally investigated the dissolution behaviour of pure, hydrothermal vivianite. Although the sequential extraction procedure did not follow Ruttenberg (1992), the findings are valuable for our investigations. In theory, as an Fe(II) phosphate, vivianite should dissolve in the first, oxidative extraction step (NH_4Cl solution in Ruttenberg (1992), NaOAc solution in Freudenthal (1995)). However, if samples are not treated under strictly anoxic conditions, vivianite is quickly oxidized to blue kertschenite (Nriagu, 1972), which, in turn, is dissolved in the second, reductive extraction step (CDB solution of Ruttenberg (1992), HA solution of Freudenthal (1995)). Fagel et al. (2005) investigated the formation of vivianite in Lake Baikal sediments, and found that the original mineral was quickly oxidized to its amorphous alteration product santabarbaraite (Pratesi et al., 2003). Following the established extraction scheme , the phosphate extraction on samples from core GeoB 9309-1 has been performed under oxic conditions and on finely ground material, suggesting that any vivianite originally present must have been completely oxidized, and extracted during the CDB step. Since a major fraction of P has been extracted in the CDB step, the vivianite contribution to the bulk solid phase phosphorus below the SMT could be significant.

The second analytical approach we took was the application of X-ray diffraction (XRD) to selected sub-SMT samples of core GeoB 9309-1. This revealed the possible presence of iron-phosphate minerals, e.g. koninckite ($(Fe, Al)PO_4$), below the SMT. Vivianite is not expected to be detectable via XRD due to its high sensitivity towards oxidation, as described above. However, the detected Fe(III)-phosphate koninckite is probably an oxidation product of diagenetic vivianite. The fact that apatite was not detected via XRD confirms the results of SEDEX, which do not show a significant systematic increase of the apatite fraction below the SMT (Fig. 2.6 c). Furthermore, there may be significant

amounts of amorphous phosphate phases and/or crystalline phosphate minerals making up less than 1 wt% of the samples, that simply escaped quantitative XRD detection.

Position of the SMT and the timing of its migration and fixation

Based on the geochemical profiles presented above, the SMT at site GeoB 9309 is currently situated at a sediment depth of 450-530 cm. This is evident from the sulfate, methane and hydrogen sulfide profiles (Figs. 2.2, 2.3), and also documented by magnetic susceptibility, Fe_{react}, and total S (Fig. 2.5). All diagenetic patterns around the SMT in Zambesi deep-sea fan deposits are very similar to those described by Hensen et al. (2003) and Riedinger et al. (2005) for the Rio de la Plata depocenter, thus formation processes are believed to be similar in both settings as well. Based on detailed geochemical analyses and modelling, Riedinger et al. (2005) found that a period of high sedimentation rates (> ~100 cm/1000 years) must have caused a rapid upward migration of the SMT to its present position, leaving the underlying deposits largely unaffected by AOM and processes related to it. Subsequently, the sedimentation rate must have dropped abruptly to much lower levels (< ~10 cm/1000 years) that stayed rather constant until today, fixing the position of the SMT at a distinct position, e.g. in 450-530 cm sediment depth at site GeoB 9309. In such a case, HS^- production is strictly limited to this sediment depth since the drop in sedimentation rate ~ 10 000 years ago. Furthermore, the small and sharp pore water HS^- peak indicates that HS^- is consumed rapidly after its production, and thus inhibits diffusion out of the discrete reaction zone. This can only be achieved in a system containing high amounts of iron (oxyhydr)oxides reactive towards HS^-, which is typically the case in depocenters dominated by fluvial input. Only when HS^- production exceeds the readily dissolvable Fe_{react}, i.e. when the system becomes iron-limited, HS^- will start diffusing beyond the boundaries of the reaction zone. Considering the low HS^- concentrations (maximum of 22 µmol/l) and iron (oxyhydr)oxides still being present at the SMT, however, this state has not yet been reached at site GeoB 9309 (Figs. 2.3 a and 2.5).

With respect to the diagenetic reactions and their traces in the sediment, the questions arising are (1) for how long the SMT has been in its actual position to create e.g. the loss of magnetic susceptibility and the sulfur enrichment, (2) which processes might have been responsible for its fixation, and (3) why the deposits below the SMT are obviously largely unaffected by AOM. To answer the first question, we refer to similar findings in the Amazon deep-sea fan and Rio de la Plata depocenter (Kasten et al., 1998; Riedinger et al., 2005) and to the derived genetic implications. Assuming a nonsteady-state scenario resulting from a drastically reduced sedimentation rate for the Holocene compared to the last glacial, Kasten et al. (1998) used the enrichment in solid phase S at the present SMT as a proxy for the

duration of SMT fixation. Following their approach, we state that all solid phase S at this depth in excess of a certain background value is exclusively in the form of iron sulfides that were produced at the SMT via the „H_2S pathway“ (Rickard and Luther, 1997; eqs. (2) to (5)). Under the prerequisites of a defined S background concentration, a constant low Holocene sedimentation rate (lasting from ~10,000 years BP until the present), an estimated porosity for the time of iron sulfide formation, a diffusive sulfate flux, a linear sulfate pore water profile and the sediment depth of Termination I, we calculated the time needed to create the existing sulfur enrichment using Fick´s first law of diffusion:

$$J = -\Phi * D_s * dC/dx \qquad (6)$$

J = diffusive flux of sulfate, Φ = porosity, D_s = sediment diffusion coefficient for sulfate, and dC/dx = concentration gradient. For further details concerning the calculation, we refer to Kasten et al. (1998). Applying this calculation to core GeoB 9309-1, we defined the diffusion coefficient for sulfate in free solution (D_0) (165 $cm^2\ yr^{-1}$, calculated from values in Schulz (2006), p. 80f), the sediment dry bulk density (2.8 g cm^{-3}, as a value for detrital-dominated marine sediments; Breitzke, 2006), the temperature (4 °C), the measured mean porosity (55%), the estimated range of sedimentary sulfur background contents (2-3 wt%), and the assumed Holocene sedimentation rate (9 cm/1000 years, based on the location of Termination I in ~90 cm sediment depth). The resulting time needed to produce the observed S enrichment at the SMT is ~10,000 years (9200 and 11 000 years for solid phase S background of 3 and 2 wt%, respectively). This indicates that a drastic decrease in sedimentation rate at the last glacial/interglacial transition ~10 000 years B.P. has most likely led to a fixation of the SMT at its present depth, creating the observed S enrichment and loss in magnetic susceptibility.

In addition to the solid phase S enrichment, we used another approach to confirm the importance of the last glacial/interglacial transition for processes at the SMT in core GeoB 9309-1. As described earlier, pore water phosphate exhibits a steep gradient below the SMT, accompanied by a decrease of solid phase P at the SMT and an increase below it. The question arises how much time is needed to create the elevated P contents below the SMT, assuming that (1) desorption by iron (oxyhydr)oxide dissolution is the only source of phosphate at the SMT, and (2) the downward phosphate flux has been constant since the fixation of the SMT. Using a similar calculation as for the S enrichment, we applied Fick´s first law of diffusion (eq. 6) to the downward flux of phosphate from the SMT. Sediment dry bulk density and temperature were the same as for the solid S enrichment. The diffusion coefficient for phosphate in free solution (D_0) was set to 115 $cm^2\ yr^{-1}$ (calculated from values in Schulz (2006), p. 80f), the porosity below the SMT to 40-45% (due to uncertainty if the measured mean porosity below

the SMT of 39.8% documents the original porosity at this depth), and the sedimentary phosphorus background contents to 505 mg/kg. Application of these parameters, depending on the assumed porosity, yielded a period of ~6500-10 000 years necessary to create the P enrichment below the SMT, which matches well with the time calculated for the S enrichment at the SMT. This is strong indication that indeed, iron (oxyhydr)oxide reduction by HS^- production at the SMT is triggering P redistribution in deposits at site GeoB 9309, and diagenetic processes are linked to decreased sedimentation rate since the last glacial/interglacial transition.

The abrupt change in sediment delivery to the Zambesi deep-sea fan was most likely initiated by variations in eustatic sea level. During the last glacial, sea level was ~120 m (~18 000 years B.P.) to ~60 m (~11 000 years B.P.) lower than today, so the continental shelf off the Zambesi mouth was largely exposed (Beiersdorf et al., 1980; Camoin et al., 2005; Walford et al., 2005). Thus, sediment delivered by the Zambesi river could bypass the shelf and was deposited on the Zambesi deep-sea fan, i.e. the upper continental slope. At Termination I, melting of polar ice masses induced a rapid sea level rise (~2.4 m/100 years after Beiersdorf et al., 1980; ~0.6 m/100 years after Camoin et al., 2005), followed by a transgression on the shelf and the creation of new accomodation space. Therefore, the Zambesi sediment load was largely trapped on the shelf, leading to a strong decrease of sediment delivery to the deep-sea fan. At that time, the SMT was fixed at its present position. It is an astonishing finding that the time interval of ~10 000 years calculated for the fixation of the SMT in core GeoB 9309-1 is in good agreement with data from the Amazon deep-sea fans (Burns, 1997; Kasten et al., 1998) and the Rio de la Plata depocenter (Hensen et al., 2003; Riedinger et al., 2005). We postulate that the same sedimentary and diagenetic processes were, and still are, taking place in all three settings, and probably in other deep-sea fan deposits as well.

SMT fixation in deep-sea fan sediments - implications for the oceanic P budget

Our results demonstrate that P is strongly affected by diagenetic processes around the SMT. As it is regarded as one of the limiting nutrients for marine productivity, its fate in the sediments has a deep impact on the global marine P budget. Removal of sea water phosphate is mainly controlled by organic matter deposition, authigenic apatite formation and phosphate adsorption onto iron (oxyhydr)oxides (e.g. Froelich et al., 1982; Jahnke et al., 1983; Ruttenberg and Berner, 1993; Slomp et al., 1996 a, b; Wheat et al., 1996; Kim et al., 1999, Schenau and de Lange, 2000; Schenau et al., 2002; Faul et al., 2005). Ruttenberg and Berner (1993) and van der Zee et al. (2002) stated that - under oxic bottom water conditions - P burial is very efficient in riverine delta sediments and at the bases

of submarine canyons, respectively, due to high sedimentation rates and high iron (oxyhydr)oxide contents in these deposits. The results of our study demonstrate that this statement can be extended to river-fed deep-sea fans and other slope depocenters, i.e. transitional environments between shelf deltas and submarine canyon fans. The crucial parameters for enhanced P burial - high sedimentation rate, oxic bottom waters and high sedimentary contents of iron (oxyhydr)oxides - are also met for the last glacial upper slope deposits off the Zambesi, Amazon and Rio de la Plata rivers. However, on a longer time scale, this P sink has to be regarded as temporary, as iron (oxyhydr)oxides are subject to reductive dissolution processes in the sediment, e.g. at the SMT. Fixation of the SMT at a certain sediment depth for several thousands of years should therefore result in a gradual release of (part of the) phosphate to the pore waters, followed by diffusive transport through the overlying sediment. Ultimately, one might expect a phosphate flux from the SMT back into the water column, as described for slope sediments from the Argentine Basin (Hensen et al., 2000, 2006), where dissolution of iron (oxyhydr)oxides and degradation of organic matter in the iron reduction zone few centimeters below the sediment-water interface release phosphate to the pore water (Slomp et al., 1996 a).

However, such a phosphate release to the bottom water does not occur at Site GeoB 9309, similar to sites on the Amazon and Congo fans (GeoB 1514 and 1401, respectively; Schulz et al., 1994). In the studied sediments, there is indeed a significant phosphate source at the SMT, but phosphate is removed from the pore water again and does not reach the bottom waters in significant amounts. The mechanisms for the removal are most probably (1) re-adsorption onto iron (oxyhydr)oxides above the SMT and (2) formation of authigenic P phases below it. This is confirmed by the solid phase P profile, documenting a loss of solid P at the SMT (450-530 cm sediment depth), while P contents above (200-450 cm) and below (530-620 cm) are elevated above background values (Fig. 2.4). Notably, the P enrichment in the interval below the SMT is more than three times higher than above it, indicating sub-SMT phosphate mineral precipitation at site GeoB 9309. However, it should be noted that in core GeoB 9309-1, apatite is not regarded as the dominant authigenic P mineral occurring below the SMT, as it is described for many marine sediments (e.g. Sheldon, 1981; Ruttenberg and Berner, 1993; Filippelli, 1997; Schuffert et al., 1998; Kim et al., 1999; Schenau et al., 2000; van der Zee et al., 2002; Slomp et al., 2004). Instead, we postulate the precipitation of authigenic Fe-phosphates like vivianite, or amorphous apatite precursor minerals (Schenau et al., 2000). This mechanism of internal phosphate redistribution, including diffusive transport of desorbed phosphate out of the SMT, differs from other studies that merely state a relatively unspecified in situ transfer of organic matter- and Fe-bound P to authigenic apatite upon increasing sediment burial depth (e.g. Heggie et al., 1990; Ruttenberg and Berner, 1993; Louchouarn et al., 1997; Schuffert et al., 1998; Kim et al.,1999; Schenau et al., 2000).

By the observed phosphorus redistribution or „sink switching" processes, contrasting to the processes occurring in the suboxic iron reduction zone (Hensen et al., 2000, 2006), depocenters of large rivers can effectively bury significant amounts of iron-bound phosphorus even over long time scales. In the present oxic state of the whole water and upper sediment column (uppermost ~5 cm, derived from the Mn^{2+} pore water profile of multicorer core GeoB 9309-3, not shown here), the described reactive P burial could partly explain the low marine productivity off the Zambesi mouth, as derived from satellite data (e.g. Behrenfeld and Falkowski, 1997), in spite of permanent riverine nutrient input. Under the precondition of an adequate fluvial input of iron (oxyhydr)oxide particles, surface adsorption of sea water and riverine phosphate could outbalance its biological uptake by microorganisms, and thereby reduce primary productivity. Verifying this hypothesis, however, would require detailed geochemical investigations of sediment trap samples, which are not available in this region.

Considering the characteristic impact of SMT diagenetic processes on the composition of Quaternary sediments of riverine origin in different geographical locations (Zambesi, Amazon, Congo, Rio de la Plata) leads to implications for the interpretation of sedimentary signals in other recent and fossil deep-sea fan deposits. Features like the characteristic solid phase P pattern found in core GeoB 9309-1, showing decreased solid P contents at the SMT and increased values below (and, to a lesser extend, also above; Fig. 2.4) can be formed at the SMT if it is fixed over a considerable amount of time. Interpreting such a diagenetic pattern as a primary sedimentary signal, caused e.g. by variations in organic matter-bound or detrital P input, might lead to wrong paleoenvironmental reconstructions. We regard it as potentially important for interpretations of solid phase P data from sediment deposited off riverine systems, to consider diagenetic P redistribution specifically at the SMT. This could be of special importance in sediment cores that cover glacial/interglacial transitions, as the SMT might have been fixed at a certain level due to rapid decreases of sedimentation rates. It should further be emphasized that the observed „early" diagenetic overprint of the primary sediment composition was, and still is, occuring in sediments that were deposited tens of thousands of years ago, and are now situated in several meters sediment depth.

Conclusions

At site GeoB 9309 on the Zambesi deep-sea fan, anaerobic oxidation of methane (AOM), and related early diagenetic processes, have significantly altered the chemical and physical properties of the sediment/pore water system and thus the primary sedimentary signals. At the sulfate/methane transition (SMT) in ~450-530 cm sediment depth, reductive dissolution of primary iron (oxyhydr)oxides by

hydrogen sulfide has resulted in a drop in magnetic susceptibility and in the red/blue color reflectance ratio. This is paralleled by a decrease of ferrimagnetic reactive Fe(III) minerals and an increase of solid phase sulfur, documenting the formation of paramagnetic pyrite. Drawdown of pore water manganese at the SMT suggests precipitation of manganese sulfide or carbonate phases. Reduction of iron (oxyhydr)oxides at the SMT has led to liberation of phosphate to the pore water at this interval. Above and below the SMT, pore water phosphate concentrations decrease again, most probably due to re-adsorption onto iron (oxyhydr)oxides, and fixation of phosphate as authigenic minerals as vivianite or amorphous apatite precursors, respectively. Authigenic apatite is no quantitatively important P sink below the SMT. Koninckite, an Fe(III) phosphate, was detected below the SMT and is believed to be an oxidation product of the Fe(II) phosphate vivianite, which could be a major contributor to the reductively extracted phosphate fraction dominant below the SMT. Thus, despite its remobilization at the SMT, phosphate is locked in the sediment, making deep-sea fan sediments an effective P sink. The diagenetic patterns observed in GeoB 9309-1 suggest that the SMT has been fixed in its actual position for the last ~10 000 years. This is thought to be caused by a drastic decrease in sedimentation rate at the last glacial/interglacial transition, triggered by a rapid sea-level rise that shifted the detrital depocenter from the deep-sea fan to the shelf. This genetic model has also been inferred from the Late Quaternary Amazon and Rio de la Plata continental slope depocenters, and might well be applicable to comparable sedimentary environments.

Acknowledgements:

This study was funded by the DFG International Graduate College Proxies in Earth History (EUROPROX). The authors would like to thank the Master and the crew as well as the team of scientists of RV *Meteor* cruise M63-1 for excellent sediment material. We are indebted to Silvana Pape, Susanne Siemer, Ludmila Baumann, Kathrin Küster, Karsten Enneking, Christian Hilgenfeldt and Christoph Vogt for analytical support. Discussions with Jürgen Pätzold, Holger Kuhlmann and Horst D. Schulz improved the quality of this paper. Special thanks are to Natascha Riedinger for most helpful comments on an earlier version of this manuscript.

Literature

Adegbie, A., Klump, J., Schneider, R.R., Wagner, T. (1998) Visual core description and stratigraphy. In: Schulz, H.D. and cruise participants (Ed.) *Report and Preliminary Results of METEOR-Cruise M 41/1, Málaga-Libreville, 13.2.-15.3.1998 with Partial Results of METEOR-Cruise 41/2, Libreville-Vitória, 18.03.1998-15.04.1998*. Berichte 114, Fachbereich Geowissenschaften, Universität Bremen, pp. 28-81.

Behrenfeld, M.J., Falkowski, P.G. (1997) Photosynthetic rates derived from satellite-based chlorophyll concentration. Limnol. Oceanogr. 42, 1-20.

Beiersdorf, H., Kudrass, H.-R., von Stackelberg, U. (1980) Placer deposits of ilmenite and zircon on the Zambezi shelf. Geol. Jb. D 36, 85 pp.

Berner, R.A. (1970) Sedimentary pyrite formation. Am. J. Sci. 268, 1-23.

Berner, R.A. (1984) Sedimentary pyrite formation: An update. Geochim. Cosmochim. Acta 48, 605-615.

Beusen, A.H.W., Dekkers, A.L. M., Bouwman, A.F., Ludwig W., Harrison, J. (2005) Estimation of global river transport of sediments and associated C, N and P. Global Biogeochem. Cycles 19, GB4S05, doi: 10.1029/2005GB002453.

Boetius, A., Ravenschlag, K., Schubert, C.J., Rickert, D., Widdel, F., Gieseke, A., Amann, R., Jørgensen, B.B., Witte, U., Pfannkuche, O. (2000) A marine microbial consortium apparently mediating anaerobic oxidation of methane. Nature 407, 623-626.

Böttcher, M.E., Huckriede, H. (1997) First occurence and stable isotope composition of authigenic γ-MnS in the central Gotland Deep (Baltic Sea). Mar. Geol. 137, 201-205.

Bohrmann, G., Greinert, J., Suess, E., Torres, M. (1998) Authigenic carbonates from the Cascadia subduction zone and their relation to gas hydrate stability. Geology 26, 647-650.

Boyle, E.A., Keigwin, L.D. (1982) Deep circulation of the North Atlantic over the last 200,000 years: Geochemical evidence. Science 218, 784-787.

Breitzke, M. (2006) Physical properties of marine sediments. In: Schulz, H.D., Zabel, M. (Eds.), *Marine Geochemistry*, 2nd ed., Springer Berlin Heidelberg New York, pp. 27-71.

Brumsack, H.-J. (1989) Geochemistry of recent TOC-rich sediments from the Gulf of California and the Black Sea. Geol. Rundsch. 78, 851-882.

Burns, S.J. (1997) Early diagenesis in Amazon Fan sediments. In: Flood, R.D., Piper, D.J.W., Klaus, A., Peterson, L.C. (Eds.) *Proc. ODP Sci. Results 155*. College Station, TX (Ocean Drilling Program), pp. 497-504.

Burns, S. J. (1998) Carbon isotopic evidence for coupled sulfate reduction-methane oxidation in Amazon Fan sediments. Geochim. Cosmochim. Acta 62, 797-804.

Camoin, G.F., Montaggioni, L.F., Braithwaite, C.J.R. (2005) Late glacial to post glacial sea levels in the Western Indian Ocean. Mar. Geol. 206, 119-146.

Canfield, D.E., Berner, R.A. (1987) Dissolution and pyritization of magnetite in anoxic marine sediments. Geochim. Cosmochim. Acta 51, 645-659.

Canfield, D.E. (1989) Reactive iron in marine sediments. Geochim. Cosmochim. Acta 53, 619-632.

Canfield, D.E., Kristensen, E., Thamdrup, B. (2005) The phosphorus cycle. In: Canfield, D.E., Kristensen, E., Thamdrup, B. (Eds.) *Aquatic Geomicrobiology*. Advances in Marine Biology 48, 419-440.

Condie, K.C. (1993) Chemical composition and evolution of the upper continental crust: Contrasting results from surface samples and shales. Chem. Geol. 104, 1-37.

DeKanel, J., Morse, J.W. (1978) The chemistry of orthophosphate uptake from seawater onto calcite and aragonite. Geochem. Cosmochem. Acta 42, 1335-1340.

Delaney, M.L. (1998) Phosphorus accumulation in marine sediments and the oceanic phosphorus cycle. Global Biogeochem. Cycles 12, 563-572.

De Lange, G.J. (1992) Distribution of various extracted phosphorus compounds in the interbedded turbiditic/pelagic sediments of the Madeira Abyssal Plain, eastern North Atlantic. Mar. Geol. 109, 115-139.

Derkachev, A.N., Nikolaeva, N.A., Mozherovsky, A.V., Grigoréva, T.N., Ivanova, E.D., Pletnev, S.P., Barinov, N.N., Chubarov, V.M. (2007) Mineralogical and geochemical indicators of anoxic sedimentation conditions in local depressions within the Sea of Okhotsk in the Late Pleistocene-Holocene. Russ. J. Pac. Geol. 1, 203-229.

Dillon, M., Bleil, U. (2006) Rock magnetic signatures in diagenetically altered sediments from the Niger deep-sea fan. J. Geophys. Res. 111, B3, doi: 10.1029/2004JB003540.

Dürr, H.H., Meybeck, M., Dürr, S.H. (2005) Lithologic composition of the Earth´s continental surfaces derived from a new digital map emphasizing riverine material transfer. Global Biogeochem. Cycles 19, GB4S10, doi: 10.1029/2005GB002515.

Einsele, G. (1996) Event deposits: the role of sediment supply and relative sea-level changes - overview. Sed. Geol. 104, 11-37.

Fagel, N., Alleman, L.Y., Granina, L., Hatert, F., Thamo-Boszo, E., Cloots, R., André, L. (2005) Vivianite formation and distribution in Lake Baikal sediments. Global Planet. Change 46, 315-336.

Faul, K.L., Paytan, A., Delaney, M.L. (2005) Phosphorus distribution in sinking oceanic particulate matter. Mar. Chem. 97, 307-333.

Filippelli, G.M. (1997) Controls on phosphorus concentrations and accumulation in oceanic sediments. Mar. Geol. 139, 231-240.

Frederichs, T., Bleil, U., Däumler, K., von Dobeneck, T., Schmidt, A.M. (1999) The magnetic view on the marine paleoenvironment: Parameters, techniques and potentials of rock magnetic studies as a key to paleo-climate and paleoceanographic changes. In: Fischer, G., Wefer, G. (Eds.) *Use of Proxies in Palaeoceanography: Examples from the South Atlantic*. Springer Berlin Heidelberg New York, pp. 575-599.

Froelich, P.N., Bender, M.L., Luedtke, N.A., Heath, G.R., deVries, T. (1982) The marine phosphorus cycle. Am. J. Sci. 282, 474-511.

Garming, J.F.L., Bleil, U., Riedinger, N. (2005) Alteration of magnetic mineralogy at the sulfate-methane transition: Analysis of sediments from the Argentine continental slope. Phys. Earth Planet. In. 151, 290-308.

Gingele, F.X., Müller, P.M., Schneider, R.R. (1998) Orbital forcing of freshwater input in the Zaire Fan area - clay mineral evidence from the last 200 kyr. Palaeogeogr. Palaeoclimatol. Palaeoecol. 138, 17-26.

Haese, R.R., Schramm, J., Rutgers van der Loeff, M.M., Schulz, H.D. (2000) A comparative study of iron and manganese diagenesis in continental slope and deep sea basin sediments off Uruguay (SW Atlantic). Int. J. Earth Sci. 88, 619-629.

Hay, W.W. (1998) Detrital sediment fluxes from continents to oceans. Chem. Geol. 145, 287-323.

Heggie, D.T., Skyring, G.W., O´Brien, G.W., Reimers, C., Herczeg, A., Moriarty, D.J.W., Burnett, W.C., Milnes, A.R. (1990) Organic carbon cycling and modern phosphorite formation on the East Australian continental margin: an overview. In: Notholt, A.J.G., Jarvis, I. (Eds.) *Phosphorite Research and Development*. Geol. Soc. Spec. Publ. 52, pp. 87-117.

Hensen, C., Zabel, M., Schulz, H.D. (2000) A comparison of benthic nutrient fluxes from deep-sea sediments off Namibia and Argentina. Deep-Sea Res. II 47, 2029-2050.

Hensen, C., Zabel, M., Pfeifer, K., Schwenk, T., Kasten, S., Riedinger, N., Schulz, H.D., Boetius, A. (2003) Control of pore-water profiles by sedimentary events and the significance of anaerobic oxidation of methane for the burial of sulfur in marine sediments. Geochim. Cosmochim. Acta 67, 2631-2647.

Hensen, C., Zabel, M., Schulz, H.N. (2006) Bentic cycling of oxygen, nitrogen and phosphorus. In: Schulz, H.D., Zabel, M. (Eds.) *Marine Geochemistry,* 2nd ed. Springer Berlin Heidelberg New York, pp. 207-240.

Hoehler, T.M., Alperin, M.J., Albert, D.B., Martens, C.S. (1994) Field and laboratory studies of methane oxidation in an anoxic marine sediment: Evidence for a methanogen-sulfate reducer consortium. Global Biogeochem. Cycles 8, 451-463.

Hyacinthe, C., Bonneville, S., van Cappellen, P. (2006) Reactive iron(III) in sediments: Chemical versus microbial extractions. Geochim. Cosmochim. Acta 70, 4166-4180.

Jahnke, R.A., Emerson, S.R., Roe, K.K., Burnett, W.C. (1983) The present day formation of apatite in Mexican continental margin sediments. Geochim. Cosmochim. Acta 47, 259-266.

Jørgensen, B.B., Kasten, S. (2006) Sulfur cycling and methane oxidation. In: Schulz, H.D., Zabel, M. (Eds.) *Marine Geochemistry,* 2nd ed. Springer Berlin Heidelberg New York, pp. 271-309.

Karlin, R. (1990) Magnetic mineral diagenesis in suboxic sediments at Bettis Site W-N, NE Pacific Ocean. J. Geophys. Res. 95, 4421-4436.

Karlin, R., Levi, S. (1983) Diagenesis of magnetic minerals in recent hemipelagic sediments. Nature 303, 327-330.

Kasten, S., Freudenthal, T., Gingele, F.X., Schulz, H.D. (1998) Simultaneous formation of iron-rich layers at different redox boundaries in sediments of the Amazon deep-sea fan. Geochim. Cosmochim. Acta 62, 2253-2264.

Kent, D.V. (1982) Apparent correlation of paleomagnetic intensity and climatic records in deep-sea sediments. Nature 229, 538-539.

Kim, D., Schuffert, J.D., Kastner, M. (1999) Francolite authigenesis in California continental slope sediments and its implication for the marine P cycle. Geochim. Cosmochim. Acta 63, 3477-3485.

Kolla, V., Kostecki, J.A., Henderson L., Hess, L. (1980) Morphology and Quaternary sedimentation of the Mozambique Fan and environs, southwestern Indian Ocean. Sedimentology 27, 357-378.

Kostka, J.E., Luther, G.W. III (1994) Partitioning and speciation of solid phase iron in saltmarsh sediments. Geochim. Cosmochim. Acta 58, 1701-1710.

Kuhlmann, H., Pätzold, J., Weldeab, S., Schneider, R.R. (2007) Hydrological changes in the southeastern African tropics during the deglaciation and Holocene. Terra Nostra 1-2, 142.

Lepland, A., Stevens, R.L. (1998) Manganese authigenesis in the Landsort Deep, Baltic Sea. Mar. Geol. 151, 1-25.

Louchouarn, P., Lucotte, M., Duchemin, E., de Vernal, A. (1997) Early diagenetic processes in recent sediments of the Gulf of St-Lawrence: phosphorus, carbon and iron burial rates. Mar. Geol. 139, 181-200.

Luther III, G.W. (1991) Pyrite synthesis via polysulfide compounds. Geochim. Cosmochim. Acta 55, 2839-2849.

Lutjeharms, J.R.E. (1996) The exchange of water between the South Indian and South Atlantic Oceans. In: Wefer, G., Berger, W.H., Siedler, G., Webb, D.J. (Eds.) *The South Atlantic: Present and Past Circulation*. Springer Berlin Heidelberg New York, pp. 125-162.

Müller, P.J, Suess, E. (1979) Productivity, sedimentation rate, and sedimentary organic matter in the oceans. I. Organic carbon preservation. Deep-Sea Res. 26, 1347-1362.

Murray, J.W., Grundmanis, V., Smethie, W.M. Jr. (1978) Interstitial water chemistry in sediments of the Saanich Inlet. Geochim. Cosmochim. Acta 42, 1011-1026.

Murray, R.W., Wigley, R., Shipboard Scientific Party (1998) Interstitial water chemistry of deeply buried sediments from the southwest African margin: A preliminary synthesis of results from Leg 175. In: Wefer, G., Berger, W.H., Richter, C. (Eds.) *Proc. ODP In. Reports 175*. College Station, TX (Ocean Drilling Program), pp. 547-553.

Neumann, T., Heiser, U., Leosson, M.A., Kersten, M. (2002) Early diagenetic processes during Mn-carbonate formation: Evidence from the isotopic composition of authigenic Ca-rhodochrosites of the Baltic Sea. Geochim. Cosmochim. Acta 66, 867-879.

Niewöhner, C., Hensen, C., Kasten, S., Zabel, M., Schulz, H.D. (1998) Deep sulfate reduction completely mediated by anaerobic methane oxidation in sediments of the upwelling area off Namibia. Geochim. Cosmochim. Acta 62, 455-464.

Novosel, I., Spence, G.D., Hyndman, R.D. (2005) Reduced magnetization produced by increased methane flux at gas hydrate vent. Mar. Geol. 216, 265-274.

Nriagu, J.O. (1972) Stability of vivianite and ion-pair formation in the system $Fe_3(PO_4)_2$-H_3PO_4-H_2O. Geochim. Cosmochim. Acta 36, 459-470.

Orphan, V.J, House, C.H., Hinrichs, K.-U., McKeegan, K.D., de Long, E.F. (2001) Methane-consuming Archaea revealed by directly coupled isotopic and phylogenetic analysis. Science 293, 494-487.

Passier, H.F., Dekkers, M.J. (2002) Iron oxide formation in the active oxidation front above sapropel S1 in the eastern Mediterranean Sea as derived from low-temperature magnetism. Geophys. J. Inter. 150, 230-240.

Peckmann, J., Reimer, A., Luth, U., Luth, C., Hansen, B.T., Heincke, C., Hoefs, J., Reitner, J. (2001) Methane-derived carbonates and authigenic pyrite from the northwestern Black Sea. Mar. Geol. 177, 129-150.

Postma, D. (1993) The reactivity of iron oxides in sediments: a kinetic approach. Geochim. Cosmochim. Acta 57, 5027-5034.

Poulton, S.W., Raiswell, R. (2002) The low-temperature geochemical cycle of iron: from continental fluxes to marine sediment deposition. Am. J. Sci. 302, 774-805.

Poulton, S.W., Krom, M.D., Raiswell, R. (2004) A revised scheme for the reactivity of iron (oxyhyr)oxide minerals towards dissolved sulfide. Geochim. Cosmochim. Acta 68, 3703-3715.

Pratesi, G., Cipriana, C., Guili, G., Birch, W.D. (2003) Santabarbaraite: a new amorphous phosphate mineral. Eur. J. Mineral. 15, 185-192.

Rasmussen, B. (2000) The impact of early-diagenetic aluminophosphate precipitation on the oceanic phosphorus budget. In: Glenn, C.R., Prévot-Lucas, L., Lucas, J. (Eds.) *Marine Authigenesis: From Global to Microbial*. SEPM Spec. Publ. 66, pp. 89-101.

Reeburgh, W.S. (1976) Methane consumption in Cariaco Trench waters and sediments. Earth Planet. Sci. Lett. 47, 345-352.

Reitz, A., Hensen, C., Kasten, S., Funk, J.K., de Lange, G.J. (2004) A combined geochemical and rock-magnetic investigation of a redox horizon at the last glacial/interglacial transition. Phys. Chem. Earth 29, 921-931.

Rickard, D., Luther, G.W. III (1997) Kinetics of pyrite formation by the H_2S oxidation of iron(II) monosulfide in aqueous solutions between 25 and 125°C: The rate equation. Geochim. Cosmochim. Acta 61, 115-134.

Riedinger, N. (2005) Alteration of manganese minerals and release of ferrous iron in deeper subsurface marine sediments from the western Argentine Basin. In: Riedinger, N. *Preservation and diagenetic overprint of geochemical and geophysical signals in ocean margin sediments related to depositional dynamics*. Berichte 242, Fachbereich Geowissenschaften, Universität Bremen, pp. 40-58.

Riedinger, N., Pfeifer, K., Kasten, S., Garming, J.F.L., Vogt, C., Hensen, C. (2005) Diagenetic alteration of magnetic signals by anaerobic oxidation of methane related to a change in sedimentation rate. Geochim. Cosmochim. Acta 69, 4117-4126.

Ruttenberg, K.C. (1992) Development of a sequential extraction method for different forms of phosphorus in marine sediments. Limnol. Oceanogr. 37, 1460-1482.

Ruttenberg, K.C., Berner, R.A. (1993) Authigenic apatite formation and burial in sediments from non-upwelling, continental margin environments. Geochim. Cosmochim. Acta 57, 991-1007.

Schenau, S.J., de Lange, G.J. (2000) A novel chemical method to quantify fish debris in marine sediments. Limnol. Oceanogr. 45, 963-971.

Schenau, S.J., Slomp, C.P., de Lange, G.J. (2000) Phosphogenesis and active phosphorite formation in sediments from the Arabian Sea oxygen minimum zone. Mar. Geol. 169, 1-20.

Schlünz, B., Schneider, R.R., Müller, P.J., Showers, W.J., Wefer, G. (1999) Terrestrial organic carbon accumulation on the Amazon deep sea fan during the last glacial sea level low stand. Chem. Geol. 159, 263-281.

Schneider, R.R., Müller, P.J., Schlünz, B., Segl, M., Showers, W.J., Wefer, G. (1997) Upper Quaternary western Atlantic paleoceanography and terrigenous sedimentation on the Amazon Fan: A view from stable isotopes of planktonic foraminifers and bulk organic matter. In: Flood, R.D., Piper, D.J.W., Klaus, A., Peters, L.C. (Eds.) *Proc. ODP Sci. Results 155*. College Station, TX (Ocean Drilling Program), pp. 319-333.

Schneider, R.R., Price, B., Mueller, P.J., Kroon, D., Alexander, I. (1997) Monsoon related variations in Zaire (Congo) sediment load and influence of fluvial silicate supply on marine productivity in the east equatorial Atlantic during the last 200,000 years. Paleoceanography 12, 463-481.

Schoonen, M.A.A. (2004) Mechanisms of sedimentary pyrite formation. In: Amend, J.P., Edwards, K.J., Lyons, T.W. (Eds.) *Sulfur Biogeochemistry - Past and Present*. Geol. Soc. Am. Spec. Pap. 379, pp. 117-134.

Schuffert, J.D., Kastner, M., Jahnke, R.A. (1998) Carbon and phosphorus burial associated with modern phosphorite formation. Mar. Geol. 146, 21-31.

Schulz, H.D., Dahmke, A., Schinzel, U., Wallmann, K., Zabel, M. (1994) Early diagenetic processes, fluxes, and reaction rates in sediments of the South Atlantic. Geochim. Cosmochim. Acta 58, 2041-2060.

Schulz, H.D. (2006) Quantification of early diagenesis: Dissolved constituents in pore water and signals in the solid phase. In: Schulz, H.D., Zabel, M. (Eds.) *Marine Geochemistry,* 2nd ed. Springer Berlin Heidelberg New York, pp. 73-124.

Shanmugam, G., Moiola, R.G. (1982) Eustatic control of turbidites and winnowed turbidites. Geology 10, 231-235.

Sheldon, R.P. (1981) Ancient marine phosphorites. Ann. Rev. Earth Planet. Sci. 9, 251-284.

Slomp., C.P., van der Gaast, S.J, van Raaphorst, W. (1996a) Phosphorus binding by poorly crystalline iron oxides in North Sea sediments. Mar. Chem. 52, 55-73.

Slomp, C.P., Epping, E.H.G., Helder, W., van Raaphorst, W. (1996b) A key role for iron-bound phosphorus in authigenic apatite formation in North Atlantic continental platform sediment. J. Mar. Res. 54, 1179-1205.

Slomp, C.P., Thomson, J., de Lange, G.J. (2004) Controls of phosphorus regeneration and burial during formation of eastern Mediterranean sapropels. Mar. Geol. 203, 141-159.

Summerfield, M.A., Hulton, N.J. (1994) Natural controls of fluvial denudation rates in major world drainage basins. J. Geophys. Res. 99, 13871-13883.

Tarduno, J.A. (1994) Temporal trends of magnetic dissolution in the pelagic realm: gauging paleoproductivity? Earth Planet. Sci. Lett. 123, 39-48.

Thompson, R., Bloemendal, J., Dearing, J.A., Oldfield, F., Rummery, T.A. (1980) Environmental applications of magnetic measurements. Science 207, 481-486.

Vail, P.R., Audemard, F., Bowman, S.A., Eisner, P.N., Perez-Cruz, C. (1991) The stratigraphic signatures of tectonics, eustasy and sedimentology - an overview. In: Einsele, G., Ricker, W., Seilacher, A. (Eds.) *Cycles and events in stratigraphy*. Springer Berlin Heidelberg New York, pp. 617-659.

Valiela, I. (1995) *Marine ecological processes*, 2nd ed. Springer New York, 686 pp.

Van der Zee, C., Slomp, C.P., van Raaphorst, W. (2002) Authigenic P formation and reactive P burial in sediments of the Nazaré canyon on the Iberian margin (NE Atlantic). Mar. Geol. 185, 372-392.

Von Dobeneck, T., Schmieder, F. (1999) Using rock-magnetic proxy records for orbital tuning, and extended time series analyses into the super- and sub-Milankovitch bands. In: Fischer, G., Wefer, G. (Eds.) *Use of Proxies in Palaeoceanography: Examples from the South Atlantic*. Springer Berlin Heidelberg New York, pp. 601-633.

Walford, H.L., White, N.J., Sydow, J.C. (2005) Solid sediment load history of the Zambezi Delta. Earth Planet. Sci. Lett. 238, 49-63.

Wefer, G., Berger, W.H., Richter, C., Shipboard Scientific Party (1998) Facies patterns and authigenic minerals of upwelling deposits off southwest Africa. In: Wefer, G., Berger, W.H., Richter, C. (Eds.) *Proc. ODP In. Reports 175*. College Station, TX (Ocean Drilling Program), pp. 487-504.

Wheat, C.G., Feely, R.A., Mottl, M.J. (1996) Phosphate removal by oceanic hydrothermal processes: An update of the phosphorus budget in the oceans. Geochim. Cosmochim. Acta 60, 3593-3608.

Wien, K. (2006) Age models for the Cape Blanc Debris Flow and the Mauretania Slide Complex in the Atlantic Ocean off NW Africa. In: Wien, K. *Element stratigraphy and age models for pelagites and gravity mass flow deposits based on shipboard XRF analysis.* Berichte 248, Fachbereich Geowissenschaften, Universität Bremen, pp. 71-87.

Wilkin, R.T., Barnes, H.L. (1996) Pyrite formation by reactions of iron monosulfides with dissolved inorganic and organic sulfur species. Geochim. Cosmochim. Acta 60, 4167-4179.

3. Redox sensitivity of P cycling during marine black shale formation - dynamics of sulfidic and anoxic, non-sulfidic bottom waters

C. März (1*), S.W. Poulton (2), B. Beckmann (3), K. Küster (1),
T. Wagner (2), S. Kasten (4)

(1) Department of Geosciences, University of Bremen, Klagenfurter Str., 28359 Bremen, Germany
*(*corresponding author: Email: cmaerz@uni-bremen.de, Tel.: +421 218 3927)*
(2) School of Civil Engineering and Geosciences, Newcastle University,
Newcastle upon Tyne, NE1 7RU, UK
(3) Institute for Geology and Mineralogy, University of Cologne, Zülpicher Str. 49a,
50674 Cologne, Germany
(4) Alfred Wegener Institute for Polar and Marine Research, Am Handelshafen 12,
27570 Bremerhaven, Germany

Abstract

A high-resolution geochemical record of a 120 cm black shale interval deposited during the Coniacian-Santonian Oceanic Anoxic Event 3 (ODP Leg 207, Site 1261, Demerara Rise) has been constructed to provide detailed insight into rapid changes in deep ocean and sediment paleo-redox conditions. High contents of organic matter, sulfur and redox-sensitive trace metals (Cd, Mo, V, Zn), as well as continuous lamination, point to deposition under consistently oxygen-free and largely sulfidic bottom water conditions. However, rapid and cyclic changes in deep ocean redox are documented by short-term (~15-20 ka) intervals with decreased total organic carbon (TOC), S and redox-sensitive trace metal contents, and in particular pronounced phosphorus peaks (up to 2.5 wt% P) associated with elevated Fe oxide contents. Sequential iron and phosphate extractions confirm that P is dominantly bound to iron oxides and incorporated into authigenic apatite. Preservation of this Fe-P coupling in an otherwise sulfidic depositional environment (as indicated by Fe speciation and high amounts of sulfurized organic matter) may be unexpected, and provides evidence for temporarily non-sulfidic bottom waters. However, there is no evidence for deposition under oxic conditions. Instead, sulfidic conditions were punctuated by periods of anoxic, non-sulfidic bottom waters. During these

periods, phosphate was effectively scavenged during precipitation of iron (oxyhydr)oxides in the upper water column, and was subsequently deposited and largely preserved at the sea floor. After ~15-25 ka, sulfidic bottom water conditions were re-established, leading to the initial precipitation of CdS, ZnS and pyrite. Subsequently, increasing concentrations of H_2S in the water column led to extensive formation of sulfurized organic matter, which effectively scavenged particle-reactive Mo complexes (thiomolybdates). At Site 1261, sulfidic bottom waters lasted for ~90-100 ka, followed by another period of anoxic, non-sulfidic conditions lasting for ~15-20 ka. The observed cyclicity at the lower end of the redox scale may have been triggered by repeated incursions of more oxygenated surface- to mid-waters from the South Atlantic resulting in a lowering of the oxic-anoxic chemocline in the water column. Alternatively, sea water sulfate might have been stripped by long-lasting high rates of sulfate reduction, removing the ultimate source for HS^- production.

Keywords: OAE, black shale, iron speciation, phosphorus, trace metals, anoxia.

Introduction

Of the numerous black shale deposits throughout Earth history (e.g. Brumsack, 1980, 1986; Stein et al., 1986; Calvert and Pedersen, 1993; Wignall, 1994; Sageman et al., 2003; Riquier et al., 2006; see summary in Negri et al., 2006), some of the most prominent examples were deposited during the Mid- to Late Cretaceous as a result of expanded oxygen minimum zones in the oceans. Due to their extensive impact on ocean biogeochemistry, the predominance of oxygen-depleted conditions, and their relatively abrupt onsets and terminations, these periods of widescale black shale deposition have been termed Oceanic Anoxic Events (OAEs) (e.g. Schlanger and Jenkyns, 1976; Jenkyns, 1980).
Sediment cores through the Coniacian-Santonian OAE3 were retrieved during ODP Leg 207 (Demerara Rise off Suriname/French Guyana, equatorial Atlantic; Erbacher et al., 2004) at Site 1261 (Fig. 3.1), from the mid Coniacian nannofossil biozone CC14. Previous work on age-equivalent deposits from the eastern equatorial Atlantic (Deep Ivory Basin, ODP Site 959) has revealed pronounced precession-forced cyclicity in geochemical records, implying repetitive and wide-scale changes in surface and deep ocean redox, closely related to central African climate and associated runoff (Hofmann, 2003; Wagner et al., 2004; Beckmann et al., 2005 a; b). Similar orbital frequencies have not been recognized in Coniacian-Santonian sediments at ODP Site 1261 (Flögel et al., in review). This has been attributed to a different sensitivity of tropical South America to precessional insolation changes relative to central Africa, leading to different runoff patterns on either side of the tropical Equatorial Atlantic and

consequently different cycle patterns in the marine sedimentary record (Flögel et al., in review).

Studies on black shales of different stratigraphic age suggest that changes in climatic, oceanic and sedimentary redox conditions can strongly affect the supply and cycling of phosphorus, a limiting nutrient for ocean productivity. Previous investigations of P systematics in total organic carbon (TOC)-rich marine sediments (e.g. Föllmi, 1996; Ingall and Jahnke, 1997; Delaney, 1998; Anderson et al. 2001; Filippelli, 2001; Nederbragt et al., 2004; Slomp et al., 2004; Mort et al., 2007; review by Algeo and Ingall, 2007) have resulted in the following observations: (1) Upon progressive burial, the more labile forms of phosphorus (P bound to organic matter and iron oxides) may be partially or completely transformed into authigenic apatite ("sink switching"), which serves as the major phosphate carrier following early diagenetic transformations; (2) under oxygen-deficient conditions, P released during reductive dissolution of iron (oxyhydr)oxides and/or selective organic matter mineralization may diffuse into the overlying water column. Under such conditions, preferential regeneration of P from organic matter (relative to organic C) may further enhance oceanic productivity, and result in high sedimentary C:P ratios (>106:1; Ingall and Jahnke, 1997; Algeo and Ingall, 2007).

In order to further evaluate these processes, and their significance in terms of responses and feedbacks associated with short term changes in ocean redox, high-resolution, multi-proxy geochemical records are required through key stratigraphic intervals. The Coniacian-Santonian OAE3 sediments

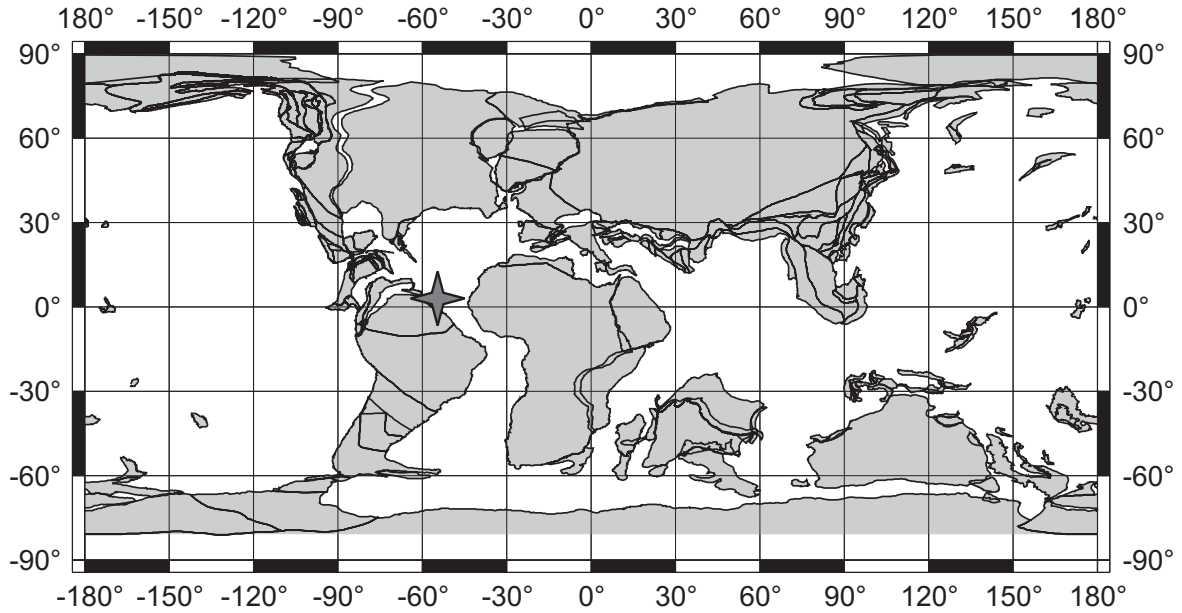

Figure 3.1: Paleogeographic map with plate configuration reconstructed for ~86 Ma B.P., with Proto-Atlantic in centre (plate tectonic reconstruction generated at http://www.odsn.de/odsn/services/paleomap/paleomap.html). Continental plates are in light grey, oceans in white. The dark grey star marks the position of Demerara Rise.

recovered at ODP Site 1261 afford an ideal opportunity for such a detailed approach, as the section consists of a continuously laminated (and thus physically undisturbed) black shale interval (Erbacher et al., 2004). The cyclic $CaCO_3$ record for nannofossil biozone CC14 (Fig. 3.2) shows spectral peaks at the eccentricity bands at ~400 kyr and ~120 kyr, however, little response is observed at the precessional band (Flögel et al., in review).

Here, we combine high-resolution geochemical records of carbonate, TOC, S and Fe speciation and the redox-sensitive/sulfide-forming (RSSF) trace metals Cd, Mo, V and Zn in order to evaluate the precise nature of short term fluctuations in deep ocean redox across the chosen section. Our high-resolution work on Fe-S-C and trace metal systematics builds upon the more general redox evaluation of the whole black shale section from ODP Sites 1257-1261, as reported by Böttcher et al. (2006). We attempt to refine their findings, which indicated generally sulfidic bottom waters throughout Cretaceous black shale deposition at Site 1261 (Böttcher et al., 2006). In addition, we particularly focus on the record of bulk sedimentary P and its speciation, in order to provide insight into the nature of P cycling during black shale formation.

Material and Methods

A core interval of ~120 cm thickness (570.2-571.4 mcd; nannofossil biozone CC14), recovered during ODP Leg 207 at Site 1261, was sampled in continuous 1 cm resolution. Details on core recovery and previous investigations are reported in the Initial Reports and Scientific Results (Erbacher et al., 2004; Mosher et al., 2007). Age determination was based on a revised nannofossil stratigraphy (Flögel et al., in review) for the timescale published in the ODP Leg 207 Initial Reports (Erbacher et al., 2004). Based on biostratigraphy, sedimentation rates show little variability across the studied section with values of 4.5 mm/ka in biozone CC14.

The core interval consists of finely laminated black claystone, rare fecal pellets and some possible fish debris (Erbacher et al., 2004). Detailed high-resolution composite photographs of the core (Fig. 3.2) provide support for preservation of primary laminations across the section. Splits of the samples were frozen, freeze-dried and ground. Carbon concentrations were analyzed with a Leco CS 200. Carbonate C was determined as the difference between total C and organic C (determined on samples pre-treated with 12.5% HCl). Several standards with C contents of 0.5-12% were applied to maintain accuracy within a range of 3%.

Aliquots of ~50 mg of each sample were subjected to a microwave total digestion procedure, completely dissolving the sediment in a mixture of suprapure HF, HCl, and HNO_3 at a temperature

of ~210°C within pressure-tight teflon cups. Contents of major and minor elements (Al, Fe, P, S, Cd, Mo, V, Zn) were measured by Inductively Coupled Plasma Atomic Emission Spectrometry (ICP-AES, Perkin-Elmer Optima 3300RL), equipped with a cross-flow nebulizer for major, and with an ultrasonic nebulizer for minor element measurements (Schulz, 2006). Standard reference materials (USGS standard MAG-1, internal lab standards MAX and CAMAX) were run parallel to the samples. Element concentrations were within certified ranges, and relative standard deviations were <3% for all elements except for Cd, which was within 5%. We display our total element data normalized to aluminum, a procedure applied to correct for dilution by variable biogenic and/or authigenic contributions, in particular carbonate. Relative enrichment factors (EFs; see reviews by Brumsack, 2006; Tribovillard et al., 2006) were also used to quantify trace metal contents relative to average shale values reported by Turekian and Wedepohl (1961).

A sequential phosphate extraction procedure (a slightly modified version of SEDEX; Ruttenberg, 1992; Schenau et al., 2000; Schenau and De Lange, 2000) was applied to selected P-rich samples (core interval 570.56-570.64 mcd), to differentiate between the various operationally-defined phosphorus-bearing phases described in Table 3.1. Phosphorus was measured photometrically (partly automatically with Skalar Autoanalyser SA 6250, partly manually with Perkin-Elmer UV/VIS Spectrophotometer 550SE), with the exception of the second extraction step, where P was measured via ICP-AES

Step	Reagents	P component extracted
I	25 ml 2M NH_4Cl (pH 7, shake for 4 h), repetition up to 20x	P_{var}: Pore water phosphate, amorphous Ca-rich apatite precursor mineral, phosphate loosely sorbed to carbonates and clay minerals, fish bones (= biogenic hydroxyapatite)
II	25 ml Na-dithionite solution, citrate-buffered (pH 7.5, shake for 8 h); wash with 25 ml 2M NH_4Cl (shake for 2 h); wash with 25 ml dem. water (shake for 2 h)	P_{iron}: Phosphate bound to iron (oxyhydr)oxides, including secondarily oxidized Fe(II)-phophates as vivianite
III	25 ml 1M Na-acetate solution (pH 4, for 6 h); wash with 25 ml 2M NH_4Cl (shake for 2 h); wash with 25 ml dem. water (shake for 2 h)	P_{auth}: Authigenic apatite (CFA, francolite)
IV	25 ml 1M HCl (shake for 24 h); wash with 25 ml dem. water (shake for 2 h)	P_{det}: Detrital apatite
V	25 ml 1M HCl (shake for 24 h) after ignition at 550°C	P_{org}: Phosphate bound to organic matter

Table 3.1: Different steps of the applied sequential phosphate extraction, the respective extraction solutions and extracted fractions of phosphate.

(Perkin-Elmer Optima 3300RL). The total recovery of the sequential extraction, calculated as the sum of P extracted from all five steps relative to bulk P, was >85% for all samples.

The speciation of iron was determined following the sequential extraction procedure of Poulton and Canfield (2005) and the Fe sulfide extraction procedure of Canfield et al. (1986). Together, these techniques allow the recognition of seven operationally-defined Fe fractions, listed in Table 3.2. Iron in the sequential extraction solutions was measured by Atomic Absorption Spectrometry (AAS), and for sulfide phases was determined stoichiometrically following precipitation of the liberated sulfide as Ag_2S. Replicate extractions indicate a reproducibility of >95% for all stages. Note that the sulfide extraction procedure of Canfield et al. (1986) does not include any contribution from organic S. However, the Canfield et al. (1986) procedure does extract sulfide from metal sulfides other than Fe, but these are generally regarded as negligible relative to Fe sulfides (e.g. Böttcher et al., 2006). In our samples, if we assume all Zn and Cd to be present as sulfides (most probably an over-estimation), this would represent an average of 2% of the total S pool. Thus, although trace metal sulfides are important, their contributions do not have a significant impact on our quantification of Fe present as sulfides.
The phases dissolved during the first three sequential Fe steps react with dissolved sulfide on early diagenetic timescales (within months to few years), and are thus considered to be highly reactive

Step	Reagents	Fe component extracted
I-a	10 ml 1 M Na-acetate solution (pH 4.5, for 24 h in water bath at 50° C)	Fe_{carb}: Iron bound to carbonate, including siderite, ankerite
I-b	10 ml Na-dithionite solution, citrate-buffered (CDB; pH 4.8, shake for 2 h)	Fe_{ox}: Iron bound as (oxyhydr)oxides (e.g. goethite, hematite)
I-c	10 ml Ammonium oxalate solution (pH 3.2; shake for 2 h)	Fe_{mag}: Iron bound as magnetite
I-d	5 ml 12 N HCl (boiling for 1 min)	FePR: Iron bound to sheet silicates
II	5 ml conc. HNO_3, ~10 ml conc. HF (boiling and evaporating at 120-150° C to dryness), redissolution with 5 ml 18% HCl	Fe_{total}: Total iron, including silicates
III-a	8 ml 18% HCl (boiling for 45 min; HS^- driven out by bubbling with N_2, precipitated in $AgNO_3$ trap)	Fe_{AVS}: Iron bound as acid-volatile sulfur AVS (e.g. greigite, pyrrothite)
III-b	~15 ml $CrCl_2$ solution (boiling for 60 min; HS^- driven out by bubbling with N_2, precipitated in $AgNO_3$ trap)	Fe_{Py}: Iron bound as chromium(II)-reducible sulfur CRS (pyrite)

Table 3.2: Different steps of the applied sequential iron extraction, the respective extraction solutions and extracted fractions of iron.

towards dissolved sulfide (Canfield et al., 1992; Poulton et al., 2004a). Therefore, when any Fe that has been converted to sulfide phases either in the water column or during diagenesis is also considered, a highly reactive Fe pool (FeHR; Raiswell and Canfield, 1998; Poulton and Raiswell, 2002) is defined ($FeHR = Fe_{carb} + Fe_{ox} + Fe_{mag} + Fe_{AVS} + Fe_{py}$). By contrast, Fe released by step 4 (boiling HCl) is only reactive towards dissolved sulfide on timescales of 10^5-10^6 years (Raiswell and Canfield, 1996) and thus defines a poorly reactive Fe pool (FePR). Finally, residual silicate Fe (FeU) is essentially unreactive towards dissolved sulfide ($FeU = Fe_{total} - (FeHR + FePR)$)

Results

Carbonate, TOC and sulfur

Carbonate is quantitatively the most significant sediment component over most of the investigated interval, with a mean content of ~59 wt% (Fig. 3.2). However, the record is highly variable, exhibiting "background" values of 55 to 75 wt% (90 samples), which are punctuated at regular intervals by samples with only 20-55 wt% carbonate (26 samples: grey bars in Fig. 3.2). Results of frequency analysis identify these breaks in the carbonate record as most probably documenting a ~120 kyr cyclicity (Flögel et al., in review). In the high-performance core photographs, these lower carbonate layers can readily be recognized by their darker sediment colour (Fig. 3.2), due to weaker dilution of the sediment by paler carbonate particles.

Total organic carbon and total S contents (Fig. 3.2) also exhibit variable values of ~4-12 wt% and ~1-2.5 wt%, respectively, and are closely correlated ($R^2 = 0.80$). However, when normalised to Al, intervals with higher TOC and total S contents have the lowest Al-ratios (grey bars). Thus, the elevated TOC and total S contents are a result of less dilution by carbonate. A marked cyclicity is also evident in the Al-normalised data, whereby TOC/Al and S/Al fluctuate periodically in a sawtooth-like pattern with a periodicity of 30-35 cm, resulting in four distinct cycles over the sampled interval. The correlation coefficient between Al-normalised TOC and S remains high ($R^2 = 0.83$). Metal sulfides, according to the sequential iron extraction applied, account for only ~25% of total sedimentary S (with a range of 15-41%), suggesting that a large fraction of the S pool is not associated with metal sulfides and is instead most likely associated with organic matter. Assuming all non-sulfidic S is present within sulfurized organic matter, the S/C ratio of this organic matter averages ~0.18 (from ~0.13-0.22) and is lowest within the carbonate-poor horizons.

Redox-sensitive trace metals Cd, Mo, V and Zn

The element/Al records of Cd, Mo, V and Zn are characterized by strong variability, and systematic enrichment above respective element/Al ratios of average shale (Fig. 3.3, average shale ratios indicated by black arrows on the x-axis). Element/Al ratios (ppm/%) are within a range of ~1-25 (mean of 7.2) for Cd, ~15-60 (mean of 38.5) for Mo, ~180-730 (mean of 453) for V and ~100-950 (mean of 333) for Zn. This gives mean EFs of 212 (up to 763) for Cd, 130 (up to 207) for Mo, 32 (up to 47) for V, and 32 (up to 87) for Zn. Such EF values are comparable to those reported for the Cenomanian/ Turonian OAE2 black shales from the same ODP Site (Brumsack, 2006).

The element/Al records show patterns partly similar to TOC/Al and S/Al (i.e. lowest overall values within low-carbonate intervals, indicated by grey bars), and exhibit the same periodicity as for TOC and S. However, while Mo/Al correlates well with TOC/Al and S/Al over the whole interval ($R^2 = 0.79$ and 0.74, respectively), the equivalent correlation coefficients of Cd, V and Zn are consistently <0.1. This discrepancy in element/Al patterns is due to the contrasting asymmetrical distributions of Cd, V and Zn compared to Mo, TOC and total S within each cycle (Figs. 3.2 and 3.3).

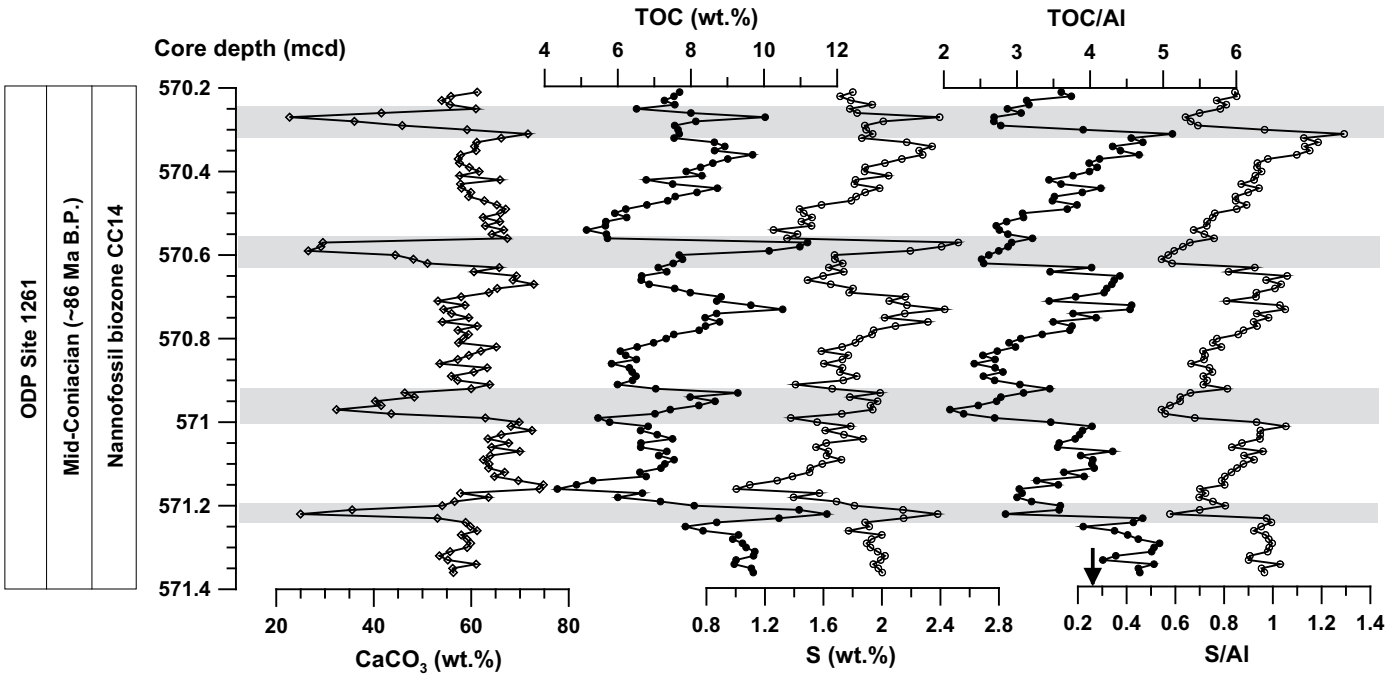

Figure 3.2: High-resolution core photograph, and sedimentary contents of carbonate, TOC and S (wt%); TOC/Al and S/Al plotted versus core depth (meters composite depth, mcd) of the investigated core interval from ODP Site 1261, with continuous sample resolution of 1 cm. Shaded intervals mark postulated intervals of anoxic non-sulfidic conditions. Arrow at X-axis of S/Al plot marks respective value for average shale (after Turekian and Wedepohl,1961).

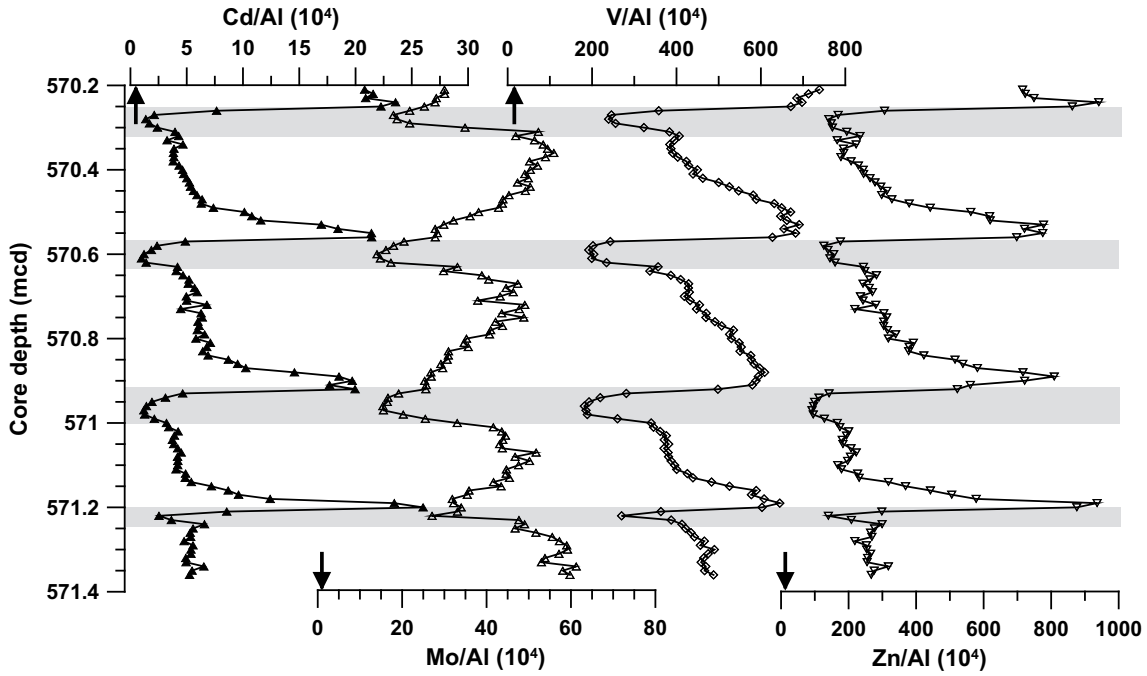

Figure 3.3: Sedimentary contents of Cd/Al (10^4), Mo/Al (10^4), V/Al (10^4) and Zn/Al (10^4) plotted versus core depth (meters composite depth, mcd) of the investigated core interval from ODP Site 1261, with continuous sample resolution of 1 cm. Shaded intervals mark postulated intervals of anoxic non-sulfidic conditions. Arrows at X-axis mark respective values for average shale (after Turekian and Wedepohl,1961).

Phosphorus and iron

Profiles of total P and P/Al (Fig. 3.4) exhibit low and remarkably constant background concentrations, but with sharp P peaks corresponding to the decreased Al-normalised TOC, total S and trace metal data (Figs. 3.2 and 3.3, grey bars). The P contents of these peaks are ~1.0-2.5 wt.%. The core photographs show that P-enriched layers contain whitish, round to elliptical concretions of up to several mm in diameter (Fig. 3.2). We infer these to be phosphatic concretions, as they are visible only within the P-rich intervals. The TOC/Ptotal ratio, expected to be between 106:1 to 117:1 in marine organic matter according to the Redfield ratio (Redfield, 1958), reaches values of up to 300 in the P-poor horizons, but approximates zero across the P peaks (Fig. 3.4). In terms of P enrichment relative to average shale, the P-rich samples are strongly enriched (EF up to 72), while the remaining samples are rather P-depleted (EF<1).

Results of the sequential P extraction procedure applied to one of the phosphorus peaks (Fig. 3.5) reveal that in general, P_{org} (Step V) is negligible (0.3-1.8 % of total P). Extraction Step I yields

2-5 wt% of bulk P, attributable to either adsorbed P, biogenic hydroxyapatite (i.e. fish bones), or to an amorphous, calcium-rich precursor of authigenic apatite (Schenau and De Lange, 2000; Schenau et al., 2000). However, as the latter is regarded as relatively unstable, we doubt its preservation in sediments ~86 Ma old and buried to several hundred meters depth. At these depths even opal, an amorphous yet comparably stable phase, is quantitatively recrystallized to clinoptilolite (Kastner, 1980; Gingele and Schulz, 1993). The P_{det} fraction (Step IV) makes up a variable, but rather small P fraction (0.2-9.3 % of total P). The overall dominant fractions of the P pool, but with a high level of variability, are the P_{iron} (23-66 wt% of total P) and P_{auth} (16-81 wt% of total P) fractions, respectively.

Highly reactive Fe on average accounts for ~59% of total Fe, but with $FeHR/Fe_{total}$ ratios that vary from 0.42 to 0.93 (Fig. 3.6). The lowest $FeHR/Fe_{total}$ ratios for each of the 4 cycles investigated generally occur in association with the periods of elevated P deposition. $FePR/Fe_{total}$ and FeU/Fe_{total} ratios also show some variation (0.17-0.44 and 0.06-0.58, respectively; Fig. 3.6) over the sampled interval (likely due to variations in syngenetic FeHR inputs to the sediment), with average values of 0.21 and 0.39, respectively. Within the FeHR pool, sulfide-associated Fe (Fe-S; i.e. $Fe_{AVS} + Fe_{py}$) is the most significant fraction, with Fe-S/FeHR average ratios of 0.71 (0.57 to 0.91; Fig. 3.6). The Fe-S/FeHR data show some scatter, but pronounced peaks occur immediately prior to each interval of P enrichment, with

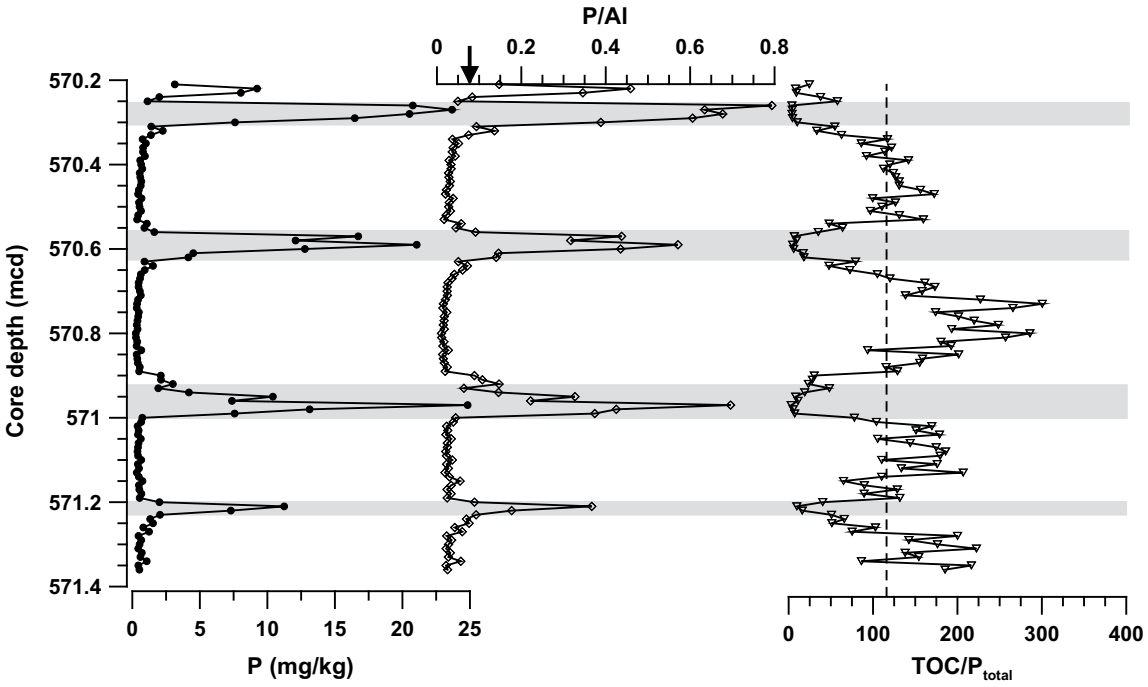

Figure 3.4: Sedimentary contents of total P (g/kg); P/Al ratio, and TOC/P_{total} ratio. Shaded intervals mark postulated intervals of anoxic non-sulfidic conditions. The arrow at the X-axis in P/Al marks respective value for average shale. In the TOC/P_{total} plot, the dashed line marks the C:P ratio for average marine organic matter (106:1, Redfield ratio; Redfield, 1958).

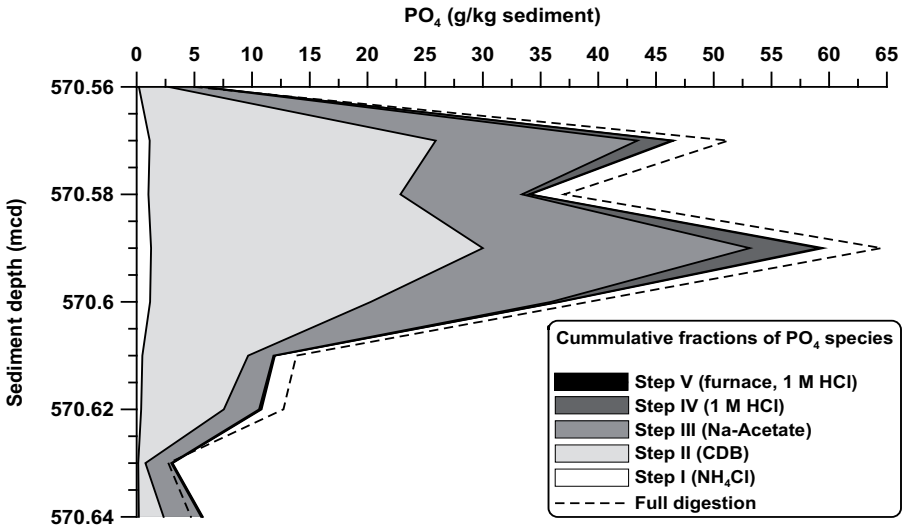

Figure 3.5: Cummulative contents of phosphate (g PO_4/kg sediment) retained in different P-carrying phases within the second P peak (downcore). The respective P-carrying phases extracted can be depicted from table 1. The dashed line shows the bulk phosphate content of the sediment, obtained by acid full digestion.

intermediate to low Fe-S/FeHR ratios found within the actual zones of P enrichment (Fig. 3.6). Fe_{carb} comprises 2.4 to 19.3% of the FeHR pool, while Fe_{ox} and Fe_{mag} account for 7.7 to 23.1% and 0-5.0% of FeHR, respectively. The Fe_{ox}/FeHR ratio generally increases within the P-enriched horizons, which arises due to relative enrichments in Fe oxide contents over these intervals (Fig. 3.6).

Discussion

Iron-Sulfur systematics

Iron speciation in marine sediments has proven to be a valuable tool for investigating redox conditions in a variety of modern (e.g. Canfield et al., 1996; Raiswell and Canfield, 1998; Poulton and Raiswell, 2002; Anderson and Raiswell, 2004) and ancient (e.g. Raiswell et al., 2001; Shen et al., 2002; 2003; Poulton et al., 2004b; Canfield et al., 2007) oceanic settings experiencing different water column redox conditions (see review by Lyons and Severmann, 2006). A particular strength of Fe speciation is the ability to distinguish between oxic, anoxic sulfidic, and anoxic non-sulfidic water column conditions (Poulton et al., 2004b; Canfield et al., 2007), thus allowing a detailed evaluation of the nature of ocean redox. In brief, FeHR/Fe_{total} ratios above 0.38 indicate anoxic bottom water

conditions, where enrichments in FeHR relative to total Fe occur due to the water column formation of either pyrite in sulfidic basins, or non-sulfidized minerals in anoxic non-sulfidic basins (Raiswell et al., 2001; Anderson and Raiswell, 2004). The ratio Fe-S/FeHR can then be used to distinguish between deposition in sulfidic and anoxic non-sulfidic basins, whereby Fe-S/FeHR ratios in sulfidic basins commonly approach 0.8-0.9 (Anderson and Raiswell, 2004; Poulton et al., 2004b; Canfield et al., 2007). These techniques are refined from those used to define the original 'Degree of Pyritization (DOP)' paleoredox indicator (Raiswell et al., 1988), and provide more detail and sensitivity in relation to the precise nature of ocean redox.

Across the entire study section, $FeHR/Fe_{total}$ ratios are consistently >0.38 (Fig. 3.6), indicating bottom water anoxia thoughout. This is in agreement with molecular analyses between 570.60 and 570.68 mcd within the same core (Beckmann et al., in press). They show lycopane/C_{31} n-alkane ratios >1, comparable to data reported from surface sediments deposited within the Arabian Sea oxygen minimum zone with lycopane/C_{31} n-alkane ratios >0.5 (Sinninghe Damsté et al., 2003), suggesting anoxic conditions. Such redox conditions persisted over much longer time scales than investigated in this study, as indicated by constantly enriched redox-sensitive trace element contents throughout

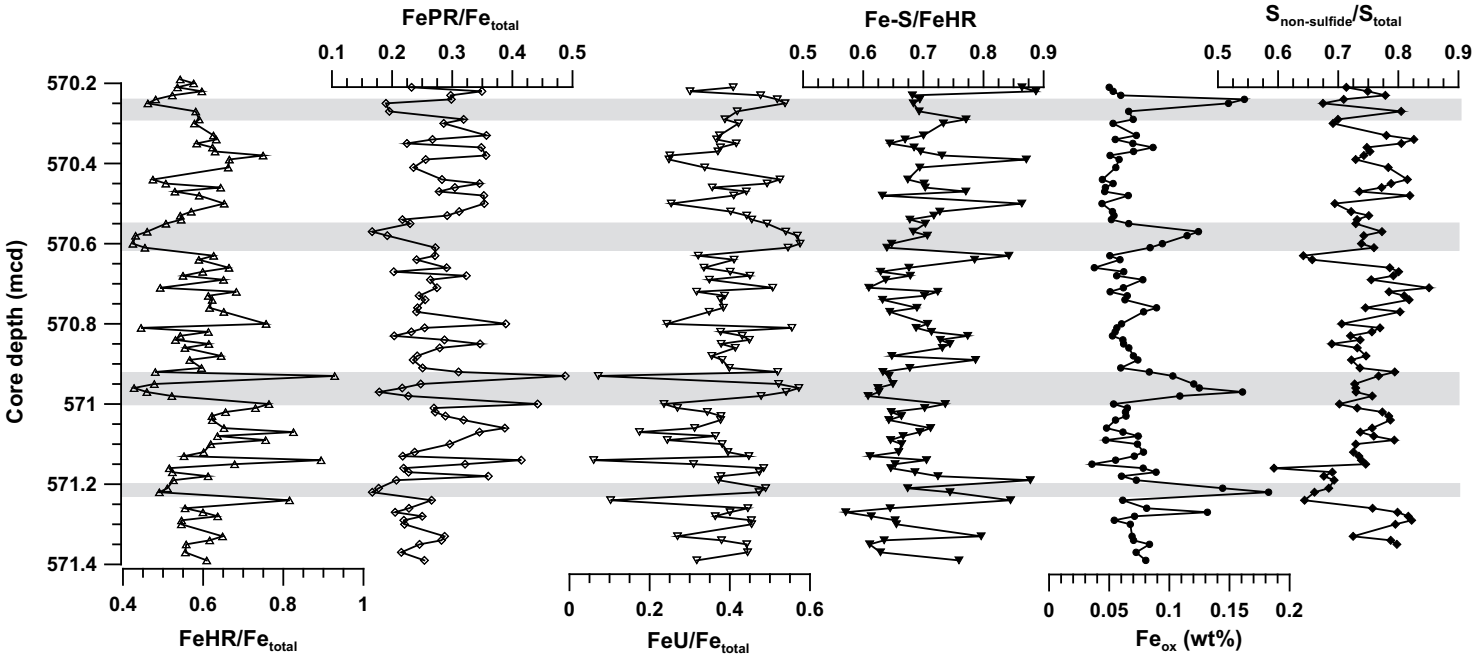

Figure 3.6: Sedimentary ratios of $FeHR/Fe_{total}$, $FePR/Fe_{total}$, FeU/Fe_{total}, representing the contribution of iron fractions that are highly reactive, poorly reactive and unreactive towards hydrogen sulfide to bulk iron. Fe-S/FeHR ratio, representing the contribution of sulfide-bound iron to the highly reactive iron pool. Fe_{ox} (wt%), sedimentary content of oxide-bound iron. Ratio of $S_{non\text{-}sulfide}/S_{total}$, the contribution of sulfur not bound to metal sulfides to the bulk sulfur pool. Shaded intervals mark postulated intervals of anoxic non-sulfidic conditions.

nannofossil biozones CC14 and CC15 (Flögel et al., in review). Interpreting Fe-S/FeHR profiles to distinguish sulfidic from anoxic non-sulfidic conditions is not always straightforward, as relatively low ratios may occur even under sulfidic bottom water conditions if, for example, some Fe oxide minerals escape sulfidization during settling through the water column. However, enrichments above 0.8 (when combined with elevated $FeHR/Fe_{total}$ ratios) clearly indicate sulfidic conditions, while values around 0.7 are more equivocal, and may indicate anoxic non-sulfidic conditions.

In the studied section, the Fe speciation data suggest periods of pronounced sulfidic conditions in bottom waters, in particular (but not solely) immediately prior to the formation of the P-enriched layers, where Fe-S/FeHR ratios tend to be relatively high (Fig. 3.6). Fe-S/FeHR ratios drop markedly in the P-enriched horizons, and these intervals correspond to somewhat elevated Fe oxide contents (Fig. 3.6), no longer supporting sulfidic conditions in these zones. Rather, elevated $FeHR/Fe_{total}$ combined with relatively low Fe-S/FeHR ratios suggest that bottom waters were anoxic and non-sulfidic across these intervals, and the elevated Fe oxide (and P) contents likely arose due to the water column precipitation of Fe oxides, which may have been a result of expanded oxic conditions in surface waters. The observed coupling between Fe speciation and P cycling is only active within relatively short-termed periods. For most of the studied section, the coupling of Fe to S, mainly in the form of pyrite (Fig. 3.6), is dominant.

However, the total sulfide contribution to bulk sedimentary S is only in the range of 15-35 %, implying that an average of ~75 % of total S is bound to phases other than Fe-sulfides (Fig. 3.6). Potential candidates are sulfurized organic matter and various sulfate minerals (e.g. barite). Sulfates are regarded as metastable in the black shales of Demerara Rise, as detailed pore water measurements (Erbacher et al., 2004) revealed continuous pore water sulfate depletion throughout the black shale interval, due to ongoing anaerobic oxidation of methane at its top (Arndt et al., 2006). Additionally, maximum estimates of barite sulfur (by assuming all bulk Ba is present as Ba sulfate) results in a negligible average barite contribution of ~1 % of total sedimentary S. Thus, diagenetically sulfurized organic material is likely the major S pool, as observed for other marine black shales (e.g. Sinninghe Damsté and de Leeuw, 1990; Sinninghe Damsté et al., 1998), and in particular (in lower resolution) for the whole Cretaceous black shale sequence at Demerara Rise (Böttcher et al., 2006). This is supported by a close coupling between non-iron-bound sulfur and TOC ($R^2 = 0.73$; or, if normalized to Al, $R^2 = 0.79$). Consistently, the S/C ratios are mostly within the range of 0.20-0.29 (average of 0.24). These very high S/C values (Raiswell and Berner, 1986) indicate that the sedimentary system was probably iron-limited with regard to sulfide uptake (with the probable exception of the P-enriched horizons, which have somewhat elevated unsulfidized Fe oxide contents; Fig. 3.6). The marine organic matter deposited

during OAE3 was highly reactive (Arndt et al., 2005; Meyers et al., 2006) and thus prone to effective diagenetic sulfurization, which in combination with iron limitation gives a likely explanation for the high S/C values.

Trace metal systematics

Certain trace metals have proven to be particularly diagnostic for anoxic/sulfidic conditions during deposition of organic matter-rich sediments (e.g. Calvert and Pedersen, 1993; Jones and Manning, 1994; Morford and Emerson, 1999; reviews by Algeo and Maynard, 2004; Brumsack, 2006; Tribovillard et al., 2006). In sediments deposited under such extreme conditions, redox-sensitive trace metals may be strongly enriched (by factors of >100) in comparison to average marine shale. The elements Cd, Mo, V and Zn are regarded as particularly reliable recorders of reducing conditions (e.g. Morford and Emerson, 1999; Nameroff et al., 2004; Brumsack, 2006; Tribovillard et al., 2006).

Cadmium and zinc exist as free cations (Cd^{2+} and Zn^{2+}, or $CdCl^{+}$ and $ZnCl^{+}$) under oxic conditions, and are mainly bound as sulfides (CdS and ZnS) in sediments deposited under sulfidic conditions. It is noteworthy, however, that these elements are not strongly incorporated into pyrite, but form discrete sulfide minerals (Huerta-Diaz and Morse, 1992). In addition, Morse and Luther (1999) found that the formation of CdS and ZnS is faster than, and thus occurs prior to, pyrite formation. Our results agree with these observations, as the correlations of Cd and Zn with pyrite-Fe are poor. The fact that CdS and ZnS form prior to pyrite in the presence of free sulfide provides an explanation for the distinct Cd and Zn peaks directly above their minima (Fig. 3.3). We suggest that periods of anoxic non-sulfidic bottom water conditions during deposition of the P-rich intervals resulted in a relatively low drawdown of Cd and Zn as sulfides. Subsequently, peaks in Fe-S/FeHR shortly after each P-rich horizon (Fig. 3.6) suggest that bottom waters again turned sulfidic. This shift in ocean redox resulted in the rapid and extensive removal of Cd and Zn from the water column (in the form of sulfides), leading to the observed sharp peaks (Fig. 3.3). A gradual upcore decrease in Cd and Zn is observed above each corresponding maximum (Fig. 3.3). However, this does not necessarily suggest a return to non-sulfidic conditions, as total S, TOC and Mo contents are consistently rising through these zones and are punctuated by periods of elevated Fe-S/FeHR ratios, at least implying sulfidic intervals, if not persistent sulfidic conditions, between the P-enriched horizons (Fig. 3.6). We suggest that the seawater pool of Cd and Zn was gradually consumed under sulfidic conditions (and it is also likely that FeHR was periodically limited, at least in terms of the most reactive Fe oxides, possibly leading to the variable Fe-S/FeHR ratios), resulting in the subsequent rise of dissolved sulfide in the lower water

column and stimulating early sulfurization of labile organic matter and the subsequent scavenging of Mo complexes.

Molybdenum displays much stronger enrichment under sulfidic than anoxic conditions (e.g. Algeo and Maynard, 2004; Algeo and Lyons, 2006). It has been suggested (Helz et al., 1996; Zheng et al., 2000; Adelson et al., 2001; Tribovillard et al., 2004) that, beyond a certain H_2S concentration threshold (activity of free hydrogen sulfide a_{HS^-} = 10-3.6-10-4.3 after Helz et al., 1996; ~11 µmol/l H_2S after Zheng et al., 2000), molybdenum is transformed to particle-reactive thiomolybdate ("thiomolybdate switch"), allowing subsequent removal from solution via metal sulfides and organic matter. Thus, under sulfidic conditions, sorption of Mo to sinking matter and transport to the sediment surface is expected to be much more effective than under anoxic conditions, resulting in higher enrichments. Tribovillard et al. (2004) found that Mo was exceptionally enriched in various anoxic sediments due to incorporation into sulfurized organic matter, but there was little correlation with pyrite abundance. In our study, the data suggest that the deep ocean gradually became limited with respect to the most readily sulfide-forming metals (Cd, Zn) and the most highly reactive iron (oxyhydr)oxides (e.g. minerals such as ferrihydrite relative to hematite; see Canfield et al., 1992; Poulton et al., 2004a). This reduced rates of sulfide consumption by metal sulfide formation sufficiently to promote organic matter sulfurization and associated thiomolybdate formation and scavenging. The observed gradual upcore increases in Mo/Al between each P-rich peak (Fig. 3.3), and the robust relationships between Mo/Al and TOC/Al (Figs. 3.2 and 3.3; $R^2 = 0.79$), and Mo/Al and non-sulfide S/Al (not shown here; $R^2 = 0.71$), support this mechanism of dynamic trace metal removal.

Although vanadium is not included in the systematic studies of Huerta-Diaz and Morse (1992) and Morse and Luther III (1999), based on the similarity of its profile to those of Cd and Zn in our sample set (Fig. 3.3), it seems likely that a similar mechanism of V enrichment occurs. The fact that the V peak is not as sharp, and declines more slowly than Cd and Zn, could be explained by (1) the incorporation of some V into another sedimentary fraction (e.g. by formation of organometallic ligands, or incorporation into geoporphyrins; Breit and Wanty, 1991; Morford and Emerson, 1999), or (2) the higher concentration of V in sea water (comparable to modern sea water values, where V = 2.15 µg/l, Zn = 0.32 µg/l, Cd = 0.076 µg/l; Whitfield and Turner, 1987), and thus slower consumption by any removal mechanism, relative to Cd and Zn.

The consistent variations in all proxy parameters clearly suggest rapid changes in bottom water redox conditions. Even in the intervals with lowest trace metal, TOC and sulfur contents, however, the Al-normalised enrichment factors of Cd, Mo, V and Zn are still (strongly) elevated over average shale. This, in combination with $FeHR/Fe_{total}$ ratios (Fig. 3.6) and a continuous lamination, supports

continued anoxia. Neither are there "classical" indications for oxygen "burndown" events (as reported from Mediterranean sapropels; Thomson et al., 1995; Van Santvoort et al., 1996), suggesting re-oxygenation events. We would expect that the effects of such "burndowns" should be visible in the organic matter- and/or sulfide-associated trace metals Cd, Mo, V, Zn, which are removed from the diagenetically oxidized zone due to organic matter remineralization and sulfide re-oxidation, and re-precipitate in a typical secondary redox succession deeper in the sediment (e.g. Wilson et al., 1985; Thomson et al., 1993). As this is not the case, the geochemical records give no indication of bottom water oxygenation at any time over the sampled interval. It remains possible, however, that the redox system fluctuated on time scales much lower than resolved by this study. Thus, redox transformations were maybe even more dynamic than indicated by our data, and in fact the variations observed in the Fe-S/FeHR ratios (Fig. 3.6) for each anoxic interval might imply very rapid transformations between euxinic and non-euxinic conditions. Furthermore, there may have been periods where bottom water conditions were even suboxic to oxic, but they were too short-lived to be reflected in the geochemical record (Algeo and Ingall, 2007).

Fe and P cycling

Under oxygen-free conditions, the oceanic and sedimentary coupling of Fe and P is believed to be of minor importance, as iron (oxyhydr)oxides are rapidly reduced and dissolved, releasing adsorbed phosphate to solution. Furthermore, the regeneration of organic-bound P is also believed to be more efficient in anoxic relative to oxic sediments (e.g. Ingall et al., 1993; Ingall and Jahnke, 1997; Anderson et al., 2001; Filippelli, 2001; Slomp et al., 2004; Slomp and Van Cappellen, 2007). This explains the P depletion relative to average shale throughout most of the investigated interval (Fig. 3.4), as phosphate was effectively recycled from organic matter and Fe oxides, and delivered back to the water column. Through upwelling of deep water into the photic zone, this dissolved phosphate may then have been used to maintain high surface productivity and elevated TOC export to the sediment, thus stabilizing sulfidic conditions at the sediment surface.

However, the studied section documents periods when this positive anoxia-productivity feedback loop was interrupted and P was retained, or even enriched, in the sediment. The sequential P extractions (Table 3.1) give detailed information about the dominant P-carrying phases within the P peak investigated, providing further insight into the sources and sinks of sedimentary phosphate. Overall, we found the extracted fractions from Steps II and III, which is iron-bound P and authigenic apatite, to be dominant over the investigated P peak. The other extraction steps together yielded <15 %

of total P and are thus only of minor importance.

The high contents of authigenic apatite (P_{auth}; extraction step V) in the P-rich samples are not surprising, as the transfer of P from more labile P-carrying phases (organic matter, Fe (oxyhydr)oxides, hydroxyapatite) into this mineral, makes authigenic apatite the dominant and ultimate oceanic P sink with increasing sediment age and burial depth (e.g. Delaney, 1998; Anderson et al., 2001; Slomp and Van Cappellen, 2007). Following this "sink switching" mechanism, the preservation of a large fraction of P still bound to Fe (oxyhydr)oxides is unexpected in OAE3 black shales ~86 Ma old and buried more than 500 m below the sea floor. We suggest that during times of sulfidic bottom waters, scavenging and removal of phosphate by adsorption to iron oxides was inhibited by their rapid syn- or diagenetic transformation to Fe sulfides, and a large pool of dissolved phosphate was able to build up in the deep ocean. As discussed above, however, the redox conditions in the basin repetitively changed from sulfidic to anoxic non-sulfidic. Under these conditions, syngenetic Fe (oxyhydr)oxide precipitation at the chemocline resulted in P removal in the water column, and subsequent deposition at the sea floor. The freshly formed Fe minerals are characterized by a high surface area (e.g. Slomp et al., 1996) and high reactivity (e.g. Feely et al., 1990; Poulton and Canfield, 2006) and are thus regarded as particularly effective in scavenging phosphate (by adsorption and/or co-precipitation) from the water column. During diagenesis, some P was released and subsequently formed apatite during limited sulfidation of Fe (oxyhydr)oxides, while some Fe (oxyhydr)oxides escaped sulfidation and retained adsorbed/co-precipitated phosphate.

Paleoenvironmental implications

Events of massive P deposition, as periodically evident in the studied core interval, could have been triggered by any process that decreases sulfide concentrations in the water column. In the case of the Cretaceous Demerara Rise, we regard repetitive periods of enhanced circulation and admixture of water masses, in an otherwise stratified oceanic basin with limited vertical water exchange, as the most probable explanation for the observed geochemical records. A similar conclusion was drawn by Friedrich and Erbacher (2006), based on benthic foraminiferal assemblages at ODP Sites 1257 and 1259. They argue that during nannofossil biozone CC15, a fluctuation of the oxygen minimum zone at the more shallow parts of Demerara Rise occurred, due to establishment of a shallow-water connection to the South Atlantic via the Equatorial Atlantic Gateway (Wagner and Pletsch, 1999). During CC17, the first deep-water connection was established via this gateway, leading to sea floor ventilation at Site 1259 (Friedrich and Erbacher, 2006). We assume that similar, though relatively shallow, intrusions

of well-oxygenated water from the South Atlantic were responsible for a periodical admixing and oxygenation of the shallow to intermediate water masses (but not bottom waters) at Site 1261 as early as CC14. Such intrusions of oxygenated water masses would have two combined effects on the ocean-sediment system: better admixing of nutrients regenerated from the sediment into the zone of primary productivity, and downward shifting of the oxic-anoxic chemocline to greater water depths. As a result, the observed P-Fe coupling could have become active.

The reason for the termination of sulfidic conditions remains unclear. Factors affecting the rate of sulfide production via microbial sulfate reduction include the amount of organic matter delivered to, and remineralized at, the sea floor; the availablility and replenishment of oxygen at the sea floor; and the availability of sulfate. Decreasing organic matter export is often associated with lower primary productivity in the photic zone, probably caused by decreased nutrient availability. We indeed find a decrease in TOC/Al within the anoxic, non-sulfidic parts of the studied core interval. This may document a more efficient organic matter degradation, but also decreased organic matter fluxes to the sea floor. The amount of oxygen in the shallow and intermediate water column, governed by the penetration depth of oxygenated water, sets an upper boundary to deeper-water sulfidic conditions, as sulfide is oxidized and cannot rise into O_2-containing waters.In modern anoxic basins as the Black Sea, sulfide is even oxidized below oxic surface waters, e.g. by nitrate within the so-called suboxic zone, a layer of more than 20 m thickness between upper (oxic) and lower (sulfidic) water masses (e.g. Murray et al., 1989; Konovalov et al., 2005). In addition, within an oxic water column, organic matter is more effectively remineralized than under sulfidic conditions, leading to lower amounts of reactive organic material reaching the sea floor, less material suitable for sulfate reduction, and subsequently a lower production of hydrogen sulfide.

Another explanation for the disappearance of sulfidic deeper water masses could be a significant drawdown of sea water sulfate, regarded as nearly unlimited in the modern ocean. However, given very high rates of TOC delivery to the sea floor, sulfidic bottom water conditons over time intervals of thousands of years, a still rather restricted Equatorial Atlantic Gateway in the Late Cretaceous (Wagner and Pletsch, 1999; Friedrich and Erbacher, 2006), and lower sulfate concentrations in the Cretaceous oceans relative to today (Hardie, 1996; Horita et al., 2002; Paytan et al., 2004; Wortmann and Chernyasky, 2007), the consumption of sea water sulfate by microbial reduction may have exceeded its supply via continental erosion. We note that each of the observed P peaks (Fig. 3.4) are preceeded by significant peaks in Fe-S/FeHR (although Fe-S/FeHR peaks are not restricted to these horizons; Fig. 3.6), suggesting that increased drawdown of sulfide at these times may well have had an impact on S availability and hence the observed transition to anoxic, non-sulfidic conditions.

Conclusions

The high-resolution geochemical records from OAE3 at ODP Site 1261 provide evidence for persistant bottom water anoxia. However, abrupt and cyclic changes occurred between sulfidic and anoxic non-sulfidic bottom water conditions. Defining the anoxic, non-sulfidic state as the starting point of one redox cycle, redox conditions may have progressively changed as follows: Anoxic, non-sulfidic bottom waters rich in dissolved P and Fe were underlying a relatively expanded oxygenated water mass. At the anoxic-oxic chemocline, phosphate adsorption to, and/or co-precipitation with, freshly precipitated Fe (oxyhyr)oxides created a close Fe-P coupling. Upon sinking, the P-rich iron (oxyhydr)oxide particles were deposited at the sea floor and partly preserved. During these anoxic, non-sulfidic conditions, rates of metal (Cd, Fe, V, Zn) sulfide formation and organic matter sulfurization were at a relative minimum, but "background" contents of trace metals, FeHR, TOC and S remained high relative to average shale. Assuming a linear sedimentation rate (Flögel et al., in review), the duration of the anoxic, non-sulfidic mode is estimated as ~15-25 ka. With increasing TOC deposition and subsequent higher rates of sulfate reduction, bottom waters then became progressively sulfidic, leading to rapid precipitation of Cd, V and Zn sulfides, documented by distinct peaks in these elements. As the relatively limited sea water pool of these trace metals became depleted by sulfide formation, extensive sulfurization of organic matter took over as the main sulfide removal process. This sulfurized organic material then served as a major carrier of Mo (in form of thiomolybdates), which was subsequently enriched and, together with S and organic matter, progressively accumulated on the sea floor. This redox scenario lasted for ~90-100 ka, before anoxic, non-sulfidic bottom waters re-developed, completing one ~120 ka redox cycle. The reasons for the termination of sulfidic bottom water conditions at Demerara Rise, with respect to its paleogeographic location ~86 Ma B.P., may have been a repetitive input of well-oxygenated water masses from the South Atlantic. This could activate the Fe-P coupling, remove phosphate from the upper water column and drawing down primary production, TOC export to the sea floor and, thus, sulfide production. Alternatively, extensive and persistent sulfate reduction in the semi-restricted Proto-Atlantic could have led to sulfate depletion, thereby removing the ultimate sulfur source for sulfide formation.

Acknowledgements

This study used samples from the Ocean Drilling Program. The work of the ODP Leg 207 shipboard party is therefore highly acknowledged, as well as the kind help of W. Hale with sampling the core at the Bremen Core Repository. We are indebted to K. Enneking, S. Hessler, S. Siemer, B. Kockisch, C. Vogt, J. Hoffmann, T. Haarmann and N. Allroggen for sample preparation and laboratory assistance. The manuscript benefited from discussions with G. de Lange, P. Kraal, P. Hofmann. This study was financed by the DFG International Graduate College EUROPROX. Additionally, SWP acknowledges support from a NERC Research Fellowship, and TW from a Royal Society Wolfson Research Award.

References

Adelson, J.M., Helz, G.R., Miller, C.V. (2001) Reconstructing the rise of recent coastal anoxia: Molybdenum in Chesapeake Bay sediments. Geochim. Cosmochim. Acta 65, 237-252.

Algeo, T.J., Maynard, J.B. (2004) Trace element behaviour and redox facies in core shales of the Upper Pennsylvanian Kansas-type cyclothems. Chem. Geol. 206, 289-318.

Algeo, T.J., Lyons, T.W. (2006) Mo-total organic carbon covariation in modern anoxic marine environments: Implications for amalysis of paleoredox and paleohydrographic conditions. Paleoceanography 21, PA 1016.

Algeo, T.J., Ingall, E., (2007) Sedimentary C_{org}:P ratios, paleocean ventilation, and Phanerozoic pO_2. Palaeogeogr. Palaeoclimatol. Palaeoecol. 256, 130-155.

Anderson, L.D., Delaney, M.L., Faul, K.L. (2001) Carbon to phosphorus ratios in sediments: Implications for nutrient cycling. Global Biogeochem. Cycles 15, 65-79.

Anderson, T.F., Raiswell, R. (2004) Sources and mechanisms for the enrichment of highly reactive iron in euxinic Black Sea sediments. Am. J. Sci. 304, 203-233.

Arndt, S., Brumsack, H.-J., Hetzel, A., Wirtz, K. (2006) Cretaceous black shales as active bioreactors: a biogeochemical model for the deep biosphere encountered during ODP Leg 207 (Demerara Rise). Geochim. Cosmochim. Acta 70, 480-425.

Beckmann, B., Flögel, S, Hofmann, P., Schulz, M., Wagner, T. (2005a) Orbital forcing of Cretaceous river discharge in tropical Africa and ocean response. Nature, 437, 241-244.

Beckmann, B., Wagner, T., Hofmann, P. (2005b) Linking Coniacian-Santonian (OAE3) black shale formation to African climate variability: a reference section from the eastern tropical Atlantic at orbital time scales (ODP Site 959, off Ivory Coast/Ghana). In: Harris, N.B. (Ed.) *The Deposition of Organic Carbon-Rich Sediments: Models, Mechanisms, and Consequences*. SEPM Spec. Publ. 82, 125-143.

Beckmann, B., Hofmann, P., März, C., Schouten, S., Sinninghe Damsté, J.S., Wagner, T. (in press) Coniacian-Santonian deep ocean anoxia/euxinia inferred from molecular and inorganic markers: Results from the Demerara Rise (ODP Leg 207). Org. Geochem.

Böttcher, M. E., Hetzel, A., Brumsack, H.-J., Schipper, A. (2006) Sulfur-iron-carbon geochemistry in sediments of the Demerara Rise. In: Mosher, D.C., Erbacher, J., Malone, M.J. (Eds.) *Proc. ODP Sci. Results 207,* 1-23. doi:10.2973/odp.proc.sr.207.108.2006.

Breit, G.N., Wanty, R.B. (1991) Vanadium accumulation in carbonaceous rocks: a review of geochemical controls during deposition and diagenesis. Chem. Geol. 91, 83-97.

Brumsack, H.-J. (1980) Geochemistry of Cretaceous black shales from the Atlantic Ocean (DSDP Legs 11, 14, 36 and 41). Chem. Geol. 31, 1-25.

Brumsack, H.-J. (1986) The inorganic geochemistry of Cretaceous black shales (DSDP Leg 41) in comparison to modern upwelling sediments from the Gulf of California and the Black Sea. Geol. Rundsch. 78, 851-882.

Brumsack, H.-J. (2006) The trace metal content of recent organic carbon-rich sediments: Implications for Cretaceous black shale formation. Palaeogeogr. Palaeoclimatol. Palaeoecol. 232, 344-361.

Calvert, S.E., Pedersen, T.F. (1993) Geochemistry of recent oxic and anoxic marine sediments: implications for the geological record. Mar. Geol. 113, 67-88.

Canfield, D.E., Raiswell, R., Westrich, J.T., Reaves, C.M., Berner, R.A. (1986) The use of chromium reduction in the analysis of reduced inorganic sulfur in sediments and shales. Chem. Geol. 54, 149-155.

Canfield, D.E., Raiswell, R., Bottrell, S. (1992) The reactivity of sedimentary iron minerals towards sulfide. Am. J. Sci. 292, 659-683.

Canfield, D.E., Lyons, T.W., Raiswell, R. (1996) A model for iron deposition to euxinic Black Sea sediments. Am. J. Sci. 296, 818-834.

Canfield, D.E., Poulton, S.W., Narbonne, G.M. (2007) Late-Neoproterozoic deep-ocean oxygenation and the rise of animal life. Science 315, 92-95.

Delaney, M.L. (1998) Phosphorus accumulation in marine sediments and the oceanic phosphorus cycle. Global Biogeochem. Cycles 12, 563-572.

Erbacher, J., Mosher, D.C., Malone, M.J., Shipboard Scientific Party (2004) *Proc. ODP In. Reports 207*, 89 pp.

Feely, R.A., Massoth, G.J., Baker, E.T., Cowen, J.P., Lamb, M.F., Krogslund, K.A. (1990) The effect of hydrothermal processes on modwater phosphorus distributions in the northeast Pacific. Earth Planet. Sci. Lett. 96, 305-318.

Filippelli, G.M. (2001) Carbon and phosphorus cycling in anoxic sediments of the Saanich Inlet, British Columbia. Mar. Geol. 174, 307-321.

Flögel, S., Beckmann, B., Hofmann, P., Bornemann, A., Norris, R.D., Wagner, T. (in review) Evolution of tropical watersheds and continental hydrology during the Late Cretaceous greenhouse; marine carbon burial and possible implications for the future. Earth Planet. Sci. Lett.

Föllmi, K.B. (1996) The phosphorus cycle, phosphogenesis and marine phosphate-rich deposits. Earth-Sci. Rev. 40, 55-124.

Friedrich, O., Erbacher, J. (2006) Benthic foraminiferal assemblages from Demerara Rise (ODP Leg 207, western tropical Atlantic): possible evidence for a progressive opening of the Equatorial Atlantic Gateway. Cretaceous Res. 27, 377-397.

Gingele, F.X., Schulz, H.D. (1993) Authigenic zeolites in Late Pleistocene sediments of the South Atlantic (Angola Basin). Mar. Geol. 111, 121-131.

Hardie, L.A. (1996) Secular variation in sea water chemistry: An explanation for the coupled variation in the mineralogies of marine limestones and potash evaporites over the past 600 my. Geology 24, 279-283.

Helz, G.R., Miller, C.V., Charnock, J.M., Mosselmans, J.F.W., Pattrick, R.A.D., Garner, C.D. Vaughan, D.J. (1996) Mechanism of molybdenum removal from the sea and its concentration in black shales: EXAFS evidence. Geochim. Cosmochim. Acta 60, 3631-3642.

Hofmann, P., Wagner, T., Beckmann, B. (2003) Millennial- to centennial-scale record of African climate variability and organic carbon accumulation in the Coniacian-Santonian eastern tropical Atlantic (Ocean Drilling Program Site 959, off Ivory Coast and Ghana). Geology 31, 135-138.

Horita, J., Zimmermann, H., Holland, H.D. (2002) Chemical evolution of sea water during the Phanerozoic: Implications from the record of marine evaporites. Geochim. Cosmochim. Acta 66, 3733-3756.

Huerta-Diaz, M.G., Morse, J.W. (1992) Pyritization of trace metals in anoxic marine sediments. Geochim. Cosmochim. Acta 56, 2681-2702.

Ingall, E.D., Bustin, R.M., Van Cappellen, P. (1993) Influence of water column anoxia on the burial and preservation of carbon and phosphorus in marine shales. Geochim. Cosmochim. Acta 57, 303-316.

Ingall, E.D., Jahnke, R.A. (1997) Influence of water-column anoxia on the elemental fractionation of carbon and phosphorus during sediment diagenesis. Mar. Geol. 139, 219-229.

Jenkyns, H.C. (1980) Cretaceous anoxic events: from continents to oceans. J. Geol. Soc. London 137, 171-188.

Jones, B., Manning, D.A.C. (1994) Comparison of geochemical indices used for the interpretation of palaeoredox conditions in ancient mudstones. Chem. Geol. 111, 111-129.

Kastner, M. (1980) Zeolites. In: Burns, R. (Ed.) *Marine Minerals*. Rev. Mineral., Mineralogical Society of America 6, 111-122.

Konovalov, S.K., Murray, J.W., Luther III, G.W. (2005) Basic Processes of Black Sea oceanography. Oceanogr. 18, 24-35.

Lyons, T.W., Severmann, S. (2006) A critical look at iron paleoredox proxies: New insights from modern euxinic marine basins. Geochim. Cosmochim. Acta 70, 5698-5722.

Meyers, P.A., Bernasconi, S.M., Forster, A. (2006) Origin and accumulation of organic matter in expanded Albian to Santonian black shale sequences on the Demerara Rise, South American margin. Org. Geochem. 37, 1816-1830.

Morford, J.L., Emerson, S.E. (1999) The geochemistry of redox sensitive trace metals in sediments. Geochim. Cosmochim. Acta 63, 1735-1750.

Morse, J.W., Luther III, G.W. (1999) Chemical influences on trace metal-sulfide interactions in anoxic sediments. Geochim. Cosmochim. Acta 63, 3373-3378.

Mort, H.P., Adatte, T., Föllmi, K.B., Keller, G., Steinmann, P., Matera, V., Berner, Z., Stüben, D. (2007) Phosphorus and the roles of productivity and nutrient recycling during oceanic anoxic event 2. Geology 35, 483-486.

Mosher, D.C., Erbacher, J., Malone, M.J., Shipboard Scientific Party (2007) *Proc. ODP Sci. Results 207*. doi: 10.2973/odp.proc.sr.207.2007.

Murray, J.W., Jannasch, H.W., Hojo, S., Anderson, R.F., Reeburgh, W.S., Top, Z., Friederich, G.E., Codispoti, L.A., Izdar, E. (1989) Unexpected changes in the oxic/anoxic interface in the Black Sea. Nature 338, 411-413.

Nameroff, T.J., Calvert, S.E., Murray, J.W. (2004) Glacial-interglacial variability in the eastern tropical North Pacific oxygen minimum zone recorded by redox-sensitive trace metals. Paleoceanography 19, PA1010.

Nederbragt, A.J., Thurow, J., Vonhof, H., Brumsack, H.-J. (2004) Modelling oceanic carbon and phosphorus fluxes: implications for the cause of the late Cenomanian Oceanic Anoxic Event (OAE2). J. Geol. Soc. London 161, 721-728.

Negri, A., Wagner, T., Meyers, P. (2006) Introduction to "Causes and consequences of organic carbon burial through time". Palaeogeogr. Palaeoclimatol. Palaeoecol. 235, 1-7.

Paytan, A., Kastner, M., Campbell, D., Thiemens, M.H. (2004) Seawater sulfur isotope fluctuations in the Cretaceous. Science 304, 1663-1665.

Poulton, S.W., Raiswell, R. (2002) The low-temperature geochemical cycle of iron: From continental fluxes to marine sediment deposition. Am. J. Sci. 302, 774-805.

Poulton, S.W., Krom, M.D., Raiswell, R. (2004a) A revised scheme for the reactivity of iron (oxyhydr)oxide minerals towards dissolved sulfide. Geochim. Cosmochim. Acta 68, 3703-3715.

Poulton, S.W., Fralick, P.W., Canfield, D.E. (2004b) The transition to a sulphidic ocean ~1.84 billion years ago. Nature 431, 173-177.

Poulton, S.W., Canfield, D.E. (2005) Development of a sequential extraction procedure for iron: implications for iron partitioning in continentally derived particulates. Chem. Geol. 214, 209-221.

Poulton, S.W., Canfield, D.E. (2006) Co-diagenesis of iron and phosphorus in hydrothermal sediments from the southern East Pacific rise: Implications for the evaluation of paleoseawater phosphate concentrations. Geochim. Cosmochim. Acta 70, 5883-5898.

Raiswell, R., Berner, R.A. (1986) Pyrite and organic matter in Phanerozoic normal marine shales. Geochim. Cosmochim. Acta 50, 1967-1976.

Raiswell, R., Buckley, F., Berner, R.A., Anderson, T.F. (1988) Degree of pyritization of iron as a paleoenvironmental indicator of bottom-water oxygenation J. Sed. Petrol. 58, 812-819.

Raiswell, R., Canfield, D.E. (1996) Rates of reaction between silicate iron and dissolved sulfide in Peru Margin sediments. Geochim. Cosmochim. Acta 60, 2777-2787.

Raiswell, R., Canfield, D.E. (1998) Sources of iron for pyrite formation in marine sediments. Am. J. Sci. 298, 219-245.

Raiswell, R., Newton, R., Wignall, P.B. (2001) An indicator of water-column anoxia: resolution of biofacies variations in the Kimmeridge clay (upper Jurassic, U.K.). J. Sed. Res. 71, 286-294.

Redfield, A.C. (1958) The biological control of chemical factors in the environment. Am. Sci. 64, 205-221.

Riquier, L., Tribovillard, N., Averbuch, O., Devleeschouwer, X., Riboulleau, A. (2006) The Late Frasnian Kellwasser horizons of the Harz Mountains (Germany): Two oxygen-deficient periods resulting from different mechanisms. Chem. Geol. 233, 137-155.

Ruttenberg, K.C. (1992) Development of a sequential extraction method for different forms of phosphorus in marine sediments. Limnol. Oceanogr. 37, 1460-1482.

Sageman, B.B., Murphy, A.E., Werne, J.P., Ver Straeten, C.A., Hollander, D.J., Lyons, T.W. (2003) A tale of shales: the relative role of production, decomposition, and dilution in the accumulation of organic-rich strata, Middle-Upper Devonian, Appalachian Basin. Chem. Geol. 195, 229-273.

Schenau, S.J., De Lange, G.J. (2000) A novel chemical extraction method to quantify fish debris in marine sediments. Limnol. Oceanogr. 45, 963-971.

Schenau, S.J., Slomp, C.P., De Lange, G.J. (2000) Phosphogenesis and active phosphorite formation in sediments from the Arabian Sea oxygen minimum zone. Mar. Geol. 169, 1-20.

Schlanger, S.O., Jenkyns, H.C. (1976) Cretaceous oceanic anoxic events: Causes and consequences. Geol. Mijnbouw 55, 179-184.

Schulz, H.D. (2006) Quantification of Early Diagenesis: Dissolved Constituents in Pore Water and Signals in the Solid Phase. In: Schulz, H.D., Zabel, M. (Eds.) *Marine Geochemistry*, 2nd ed. Springer Berlin Heidelberg New York, pp. 73-124.

Shen, Y., Canfield, D.E., Knoll, A.H. (2002) Middle Proterozoic Ocean chemistry: Evidence from the McArthur Basin, Northern Australia. Am. J. Sci. 302, 81-109.

Shen, Y., Knoll, A.H., Walter, M.R. (2003) Evidence for low sulphate and anoxia in a mid-Proterozoic marine basin. Nature 423, 632-635.

Sinninghe Damsté, J.S., De Leeuw, J.W. (1990) Analysis, structure and geochemical significance of organically-bound sulphur in the geosphere: State of the art and future research. Org. Geochem. 16, 1077-1101.

Sinninghe Damsté, J.S., Kok, M.D., Köster, J., Schouten, S. (1998) Sulfurized carbohydrates: an important sedimentary sink for organic carbon? Earth Planet. Sci. Lett. 164, 7-13.

Sinninghe Damsté, J.S., Kuypers, M.M.M., Schouten, S., Schulte, S., Rullkötter, J. (2003) The lycopane/C_{31} n-alkane ratio as a proxy to assess palaeoxicity during sediment deposition. Earth Planet. Sci. Lett. 209, 215-226.

Slomp, C.P., Van der Gaast, S.J., Van Raaphorst, W. (1996) Phosphorus binding by poorly crystalline iron oxides in North sea sediments. Mar. Chem. 52, 55-73.

Slomp, C.P., Thomson, J., De Lange, G.J. (2004) Controls on phosphorus regeneration and burial during formation of the eastern Mediterranean sapropels. Mar. Geol. 203, 141-159.

Slomp, C.P., Van Cappellen, P. (2007) The global marine phosphorus cycle: sensitivity to oceanic circulation. Biogeosciences 4, 155-171.

Stein, R., Rullkötter, J., Welte, D. (1986) Accumulation of organic-carbon-rich sediments in the Late Jurassic and Cretaceous Atlantic Ocean - A synthesis. Chem. Geol. 56, 1-32.

Thomson, J., Higgs, N.C., Croudace, I.W., Colley, S., Hydes, D.J. (1993) Redox zonation of elements at an oxic/post-oxic boundary in deep-sea sediments. Geochim. Cosmochim. Acta 57, 579-595.

Thomson, J., Higgs, N.C., Wilson, T.R.S., Croudace, I.W., De Lange, G.J., Van Santvoort, P.J.M. (1995) Redistribution and geochemical behaviour of redox- sensitive elements around S1, the most recent eastern Mediterranean sapropel. Geochim. Cosmochim. Acta 59, 3487-3501.

Tribovillard, N., Riboulleau, A., Lyons, T., Baudin, F. (2004) Enhanced trapping of molybdenum by sulfurized marine organic matter of marine origin in Mesozoic limestones and shales. Chem. Geol. 213, 385-401.

Tribovillard, N., Algeo, T.J., Lyons, T., Riboulleau, A. (2006) Trace metals as paleoredox and paleoproductivity proxies: An update. Chem. Geol. 232, 12-32.

Turekian, K.K., Wedepohl, K.H. (1961) Distribution of the elements in some major units of the Earth´s crust. Geol. Soc. Am. Bull. 72, 175-192.

Van Santvoort, P.J.M., De Lange, G.J., Thomson, J., Cussen, H., Wilson, T.R.S., Krom, M.D., Ströhle, K. (1996) Active post-depositional oxidation of the most recenet sapropel (S1) in sediments of the eastern Mediterranean Sea. Geochim. Cosmochim. Acta 60, 4007-4024.

Wagner, T., Pletsch, T. (1999) Tectono-sedimentary controls on Cretaceous black shale deposition along the opening Equatorial Atlantic Gateway (ODP Leg 159). In: Cameron, N.R., Bate, R.H., Clure, V.S. (Eds.) *The Oil and Gas Habitats of the South Atlantic*. Geol. Soc. London Spec. Publ. 153, p. 241-265.

Wagner, T., Sinninghe Damsté, J.S., Hofmann, P., Beckmann, B. (2004) Euxinia and primary production in Late Cretaceous eastern equatorial Atlantic surface waters fostered orbitally driven formation of marine black shales. Paleoceanography 19, PA3009.

Whitfield, M., Turner, D.R. (1987) The role of particles in regulating the composition of sea water. In: Stumm, W. (Ed.) *Aquatic Surface Chemistry: Chemical Processes at the Particle-Water Interface*. John Wiley and Sons, New York, pp. 457-493.

Wignall, P.B. (1994) *Black Shales*. Oxford University Press, Geology and Geophysics Monographs 30, 130 p.

Wilson, T.R.S., Thomson, J., Colley, S., Hydes, D.J., Higgs, N.C. (1985) Early organic diagenesis: The significance of progressive subsurface oxidation fronts in pelagic sediments. Geochim. Cosmochim. Acta 49, 811-822.

Wortmann, U.G., Chernyavsky, B.M. (2007) Effect of evaporite deposition on Early Cretaceous carbon and sulphur cycling. Nature 445, 654-656.

Zheng, Y., Anderson, R.F., van Geen, A., Kuwabara, J.S. (2000) Authigenic molybdenum formation in marine sediments: A linkage to pore water sulfide in the Santa Barbara Basin. Geochim. Cosmochim. Acta 64, 4165-4178.

4. Geochemical environment of the Coniacian-Santonian western tropical Atlantic at Demerara Rise

C. März (1*), B. Beckmann (2), C. Franke (3), Christoph Vogt (1),
T. Wagner (4), S. Kasten (5)

(1) Department of Geosciences, University of Bremen, Klagenfurter Str., 28359 Bremen, Germany
*(*corresponding author: Email: cmaerz@uni-bremen.de, Tel.: +49 (0)421 218 3927)*
(2) Institute for Geology and Mineralogy, University of Cologne, Zülpicher Str. 49a, 50674 Cologne, Germany
(3) Laboratoire des Sciences du Climat et de l'Environnement (LSCE), CEA-CNRS-UVSQ, 12 Avenue de la Terrasse, 91198 Gif-sur-Yvette, France
(4) School of Civil Engineering and Geosciences, Newcastle University, Newcastle upon Tyne, NE1 7RU, UK
(5) Alfred Wegener Institute for Polar and Marine Research, Am Handelshafen 12, 27570 Bremerhaven, Germany

Abstract

Organic carbon-rich shales deposited during the Coniacian-Santonian Oceanic Anoxic Event 3 were drilled during ODP Leg 207 at Demerara Rise. We present integrated high-resolution geochemical records of core intervals from ODP Sites 1259 and 1261 both covering nannofossil biozone CC14. Our results reveal systematic variations in marine and detrital sediment contribution, depositional processes, and bottom water redox during black shale formation at two locations on Demerara Rise in different paleo-water depths. A combination of redox proxies (Fe/S, P/Al, C/P, redox-sensitive trace metals Mn, Cd, Mo, Ni, V, Zn) and other analytical approaches (bulk sediment composition, P speciation, electron microscopy, X-ray diffraction) evidence anoxic to sulfidic bottom water and sediment conditions throughout the deposition of black shale. These extreme redox conditions persisted and were periodically punctuated by short-termed periods with less reducing bottom waters irrespective of paleo-water depth. Sediment supply at both sites was generally dominated by marine material (carbonate, organic matter, opal) although relationships of detrital proxies as well as

glauconitic horizons support some influence of turbidites, winnowing bottom currents and/or variable detritus sources, along with less reducing bottom water at the proposed shallower location (ODP Site 1259). At Site 1261, deeper on the continental margin, redox fluctuations were more regular, and steady hemipelagic sedimentation sustained the development of mostly undisturbed lamination in the sedimentary record. Strong similarities of the studied deposits exist with the stratigraphic older Cenomanian-Turonian OAE2 black shale sections at Demerara Rise, suggesting that the primary mechanisms controlling continental supply and ocean redox were time-invariant and kept the western equatorial Atlantic margin widely anoxic over millions of years.

Keywords: Oceanic anoxic event, trace elements, iron, phosphorus, sediment source, redox changes, enrichment factors

Introduction

Since Schlanger & Jenkyns (1976) introduced the original concept of Oceanic Anoxic Events (OAEs), much progress has been made in the understanding of the widespread deposition of organic matter (OM)-rich sediments in the Cretaceous Proto-Atlantic and adjacent seas, in particular on the dynamics and mechanisms of short-term change in ocean redox. During ODP Leg 207 up to 90 m thick Cretaceous black shale deposits, including OAE2 and OAE3 were recovered from Demerara Rise (Erbacher et al., 2004; Mosher et al., 2007). Cenomanian-Turonian OAE2 black shales from ODP Leg 207 have been subject of intensive research (e.g. Erbacher et al., 2005; Friedrich et al., 2006; Hardas and Mutterlose, 2006; Musavu-Moussavou and Danelian, 2006; Forster et al., 2007a; Junium and Arthur, 2007; Nederbragt et al., 2007) whereas far less is known about the development of the later Coniacian-Santonian OAE3 in this critical area of the tropical North Atlantic (Friedrich and Erbacher, 2006; Beckmann et al., in press; März et al., accepted). Given that OAE3 sediments from the adjacent tropical African margin (Deep Ivory Basin, ODP Leg 159) revealed spectacular evidence of astronomically forced sedimentary and redox cycles directly associated with African climate variability (Wagner, 2002; Wagner et al., 2004; Beckmann et al., 2005a, b; Flögel and Wagner, 2006) and the opening of the Equatorial Atlantic (Wagner and Pletsch, 1999; Pletsch et al., 2001) there is scope for more detailed investigation of this stratigraphic interval at Demerara Rise.

First geochemical studies revealed that Demerara Rise black shales are dominated by thermally immature marine OM (Meyers et al., 2006; Forster et al., 2007b). Its slow degradation still produces methane, which is anaerobically oxidized at the top of the Cretaceous black shale succession via sulfate

reduction, resulting in sulfate depletion and long-lasting barite remobilization within the black shale succession (Erbacher et al., 2004; Arndt et al., 2006). High degrees of pyritization, but also sulfurized OM (Böttcher et al., 2006), overall enrichments of Mo, V, Zn, and Mn depletion (Hetzel et al., 2006) indicate overall oxygen-depleted, periodically even sulfidic bottom waters. Overall enrichments of P as well as high amounts of Ba (despite diagenetic barite redistribution and formation of diagenetic fronts) support enhanced nutrient supply and high productivity during black shale deposition (Hetzel et al., 2006; Arndt et al, 2006). We recently explored a broad variety of redox proxies in OAE3 black shales at ODP Site 1261. The records are consistent and show cyclic and rapid redox fluctuations from sulfidic to anoxic, non-sulfidic conditions in bottom waters (März et al., accepted) obviously triggered astronomically by short eccentricity cycles (Flögel et al., in review).

In this study we add evidence to the findings of the Cretaceous low latitude Atlantic by applying a wide analytical spectrum in high temporal resolution to ODP Sites 1259 and 1261 from Demerara Rise. The main goal is to trace changes in deep ocean redox, sediment sources and depositional processes along a bathymetric transect across the S-American continental margin. To achieve these goals we selected nannofossil biozone CC14 intervals from both sites and applied major and trace element geochemistry, P speciation, X-ray diffraction, and scanning electron microscopy. For completeness, some of the results presented by März et al. (accepted). are shown here, however, we emphasize that this study takes the discussion forward by comparing synchronous stratigraphic intervals from two sites, and by adding new information on sediment sources and depositional processes. To place the results from OAE3 into wider perspective we compare them with geochemical properties from OAE2 sections at Demerara Rise, and an average of various OAE2 locations worldwide (Brumsack, 2006).

Material and Methods

The ODP Leg 207 Sites 1259 and 1261 were drilled on Demerara Rise, in modern water depths of 2354 m and 1899 m on the northern and northwestern slope, respectively (Erbacher et al., 2004). For this high-resolution study, we chose core intervals from Sites 1259 (499.60 – 500.61 mcd, 101 cm) and 1261 (570.20 – 571.40 mcd, 120 cm) and sampled them in continuous 1 cm resolution. For comparison we selected intervals from the same stratigraphic nannofossil biozone CC14 (Coniacian-Santonian), using the nannofossil stratigraphy published by Erbacher et al. (2004) that was recently refined by Flögel et al. (in review) for Site 1261 and by Bornemann et al. (2008) for Site 1259. Sedimentation rates were ~5.4 mm/ka at Site 1261 (Flögel et al., in review), and ~2-3 mm/ka at Site 1259 (Bornemann et al., 2008). Thus, both sampled intervals document condensed successions, with sedimentation rates at Site

1261 about twice as high as at Site 1259. Being aware of these differences, our geochemical comparison does not aim at layer-to-layer correlation - although both intervals were deposited during nannofossil biozone CC14, there might still be a significant offset in time between them. We rather compare both sites in terms of general sedimentation patterns and geochemical characteristics of sediments and bottom waters.

Sampling took place at the ODP Core Repository in Bremen, Germany. Sample splits were frozen, freeze-dried and ground in an agate mortar. Total organic carbon (TOC) and carbonate contents were determined with a Leco CS 200. First, total carbon (TC) was measured. After the sediment was decalcified with 12.5% HCl, washed twice and dried at 60°C, TOC content was determined. Finally, the $CaCO_3$ content of the sediment was calculated: $CaCO_3$ (%) = (TC - TOC) x 8.33. Several standards with C contents between 0.5 and 12% were applied to keep the accuracy of the measurement at >97%.

About 50 mg of each sample were subjected to a microwave total acid digestion procedure (3 ml HNO_3, 2ml HCl and 2 ml HF, heated up to ~210° C in pressure-resistant teflon containers). Major and minor elements were measured with an Inductively Coupled Plasma Atomic Emission Spectrometer (ICP-AES, Perkin Elmer 3000) in triplicate to assure a standard deviation of <5 %. For details, we refer to Schulz (2004) and www.geochemie.uni-bremen.de/koelling/MGCmain.html.

A sequential phosphate extraction (modified version of SEDEX, Ruttenberg, 1992; Schenau and De Lange, 2000; Schenau et al., 2000) was applied to selected P-rich samples from both sites (500.13 – 500.53 mcd at Site 1259 and 570.56 – 570.64 mcd at Site 1261). This method enables us to differentiate between various phosphorus-bearing phases in the sediment (Table 1). Extracted P was analysed photometrically (Steps I, III-V) or via ICP-AES (Step II).

X-ray diffraction (XRD) was used to confirm the results of the SEDEX extraction and to reveal the general mineralogy of the core sections. X-ray diffractograms of freeze-dried, ground samples were produced with a Philips X'Pert Pro multipurpose diffractometer equipped with a Cu-tube (k" 1.541, 45 kV, 40 mA), a fixed divergence slit of 1/4° , a 16 samples changer, a secondary monochromator and the X'Celerator detector system. Samples were scanned continuously from 3-85° 2θ, with a calculated step size of 0.016° 2θ (calculated time per step 100 seconds). Mineral identification was done with the Philips software X'Pert HighScore™, which also gave semi-quantitative values for identified minerals (according to their Relative Intensity Ratio values, calculated as ratio of the most intense reflex of a specific mineral phase to most intense reflex of pure corundum; "matrix-flushing method" after Chung, 1974; Vogt et al., 2002; Bender, 2007).

We also applied heavy liquid separation (Franke et al., 2007) to selected samples, extracting the mineral fraction with a density of >3.0 g/cm^3 (e.g. barite, pyrite, calcium-fluorapatite = CFA). We used ~0.5-1 g of freeze-dried, homogenized sediment and a Na-polytungstate solution (3.0 g/cm^3; ~25 ml per sample). Sediment solutions were shaken manually and subsequently dispersed in an ultrasonic bath. Suspensions were centrifuged (20 minutes, 4000 rps), and the heavy liquid mirror and supernatant fraction (<3.0 g/cm^3) were removed with a pipette. The remaining heavy fraction was vacuum-filtered (0.2 µm cellulose acetate filters), and washed several times with bi-distilled water. Filtered heavy mineral extracts were dispersed in bi-distilled water and centrifuged several times to prevent Na-polytungstate contamination. Dried extracts were prepared for Scanning Electron Microscopy (SEM, Philips XL30 SFEG, 12 kV acceleration voltage). Unconsolidated grains were dispersed onto a carbon sticker on a standard Al stub, and covered with a few nm thick carbon layer to prevent surface charging during SEM analysis. Secondary electron (SE) and backscattered electron (BSE) detectors were used for imaging. For elemental composition of single grains, energy-dispersive X-ray spectroscopy (EDS; e.g. Goldstein et al., 1992) was applied and semi-quantification was achieved using the EDAX PhiRhoZ software. All elemental spectra were normalized to their respective oxygen maxima.

Step	Reagents	P component extracted
I	25 ml 2M NH_4Cl (pH 7, shake for 4 h), repetition up to 20x	P_{var}: Pore water phosphate, amorphous Ca-rich apatite precursor mineral, phosphate loosely sorbed to carbonates and clay minerals, fish bones (= biogenic hydroxyapatite)
II	25 ml Na-dithionite solution, citrate-buffered (pH 7.5, shake for 8 h); wash with 25 ml 2M NH_4Cl (shake for 2 h); wash with 25 ml dem. water (shake for 2 h)	P_{iron}: Phosphate bound to iron (oxyhydr)oxides, including secondarily oxidized Fe(II)-phophates as vivianite
III	25 ml 1M Na-acetate solution (pH 4, for 6 h); wash with 25 ml 2M NH_4Cl (shake for 2 h); wash with 25 ml dem. water (shake for 2 h)	P_{auth}: Authigenic apatite (CFA, francolite)
IV	25 ml 1M HCl (shake for 24 h); wash with 25 ml dem. water (shake for 2 h)	P_{det}: Detrital apatite
V	25 ml 1M HCl (shake for 24 h) after ignition at 550°C	P_{org}: Phosphate bound to organic matter

Table 4.1: Different steps of the applied sequential phosphate extraction, the respective extraction solutions and extracted fractions of phosphate.

Results

Lithology

OAE3 sediments at Site 1261 consist of finely laminated black claystone and nannofossil claystone (Erbacher et al., 2004). Visual inspection of the Site 1261 biozone CC14 core section revealed black intervals of few centimeters thickness containing light, roundish components of up to a few mm in diameter. The components are elongate, lense-shaped, and embedded into the stratification and bear no signs of physical disturbance throughout the entire study interval. Similarly, biozone CC14 at Site 1259 displays lamination in the upper ~70 cm of the interval (499.60 – 500.30 mcd), as well as cyclic occurence of layers with round to elliptic, whitish components of up to a few mm in size. However, in the lower part a glauconitic horizon (Erbacher et al. 2004; here referred to as GH) is visible as a sandy, light horizon of ~20 cm thickness, comprising a relatively unsorted framework of white, mm- to cm-sized grains. Under the light microscope, glauconite grains from the GH appear as green to blue-green crystals, fragments or as green-whitish aggregates.

Total organic carbon and carbonate

The investigated deposits are TOC-rich with lowest values around 3 wt% (Fig. 4.1a). The TOC content at Site 1261 is generally higher compared to Site 1259 (average of 7.7 wt% versus 6.1 wt%, respectively), as is the TOC/Al ratio (average of 3.6 versus 2.8; Fig. 4.1b) and carbonate-free TOC (CFB; average of 18.7 wt% versus 15.8 wt%; not shown here), parameters that both correct for variable dilution by biogenic carbonate. The amplitude between TOC maxima and minima is on the order of 7 wt% at both sites, with values of 4.4-11.7 wt% at Site 1261 and 2.9-10.2 wt% at Site 1259 (Fig. 4.1a), without clear repetitive patterns. Different from that, the TOC/Al records show regular cyclic patterns at both sites, with the exception of much lower TOC/Al ratios in the lower part of the 1259 section (below 500.30 mcd; Fig. 4.1b).

The carbonate record at Site 1261 displays background values of ~50-70 wt%, interrupted by four intervals of 5-10 cm thickness, each with carbonate contents of only 20-30 wt% (Fig. 4.1c), coincident with lowest TOC/Al values. In contrast, the carbonate content at Site 1259 does not show the same systematic variations, but varies in a more irregular manner between 30-70 wt% (Fig. 4.1c). Only in the lowest part of the interval (below 500.48 mcd), carbonate contents reach 70-100 wt%.

Detrital elements (Al, K, Mg, Ti, Zr)

Aluminum is mainly incorporated into detrital silicates in continental margin settings like Demerara Rise and thus represents continental input. At Site 1261, background Al values of 15-25 g/kg are interrupted by sharp peaks of 35-40 g/kg (Fig. 4.1d). Calculation on CFB, however, removes these peaks, and documents negligible fluctuations in Al (CFB; data not shown). A clear anti-correlation of Al with carbonate (R^2 = 0.91; correlation coefficients always given as linear correlations; Figs. 4.1d, 4.2a) documents mutual dilution of detrital and biogenic material. At Site 1259, Al contents are within a similar range (10-35 g/kg; Fig. 4.1d), but the Al-carbonate relationship is weaker (R^2 = 0.59; Fig. 4.2a). Terrigenous proxy elements bound to the heavy mineral fraction include Ti and Zr. At Site 1261, correlation coefficients are R^2 = 0.99 for Al with Ti, and R^2 = 0.93 with Zr (Figs. 4.2b, c).

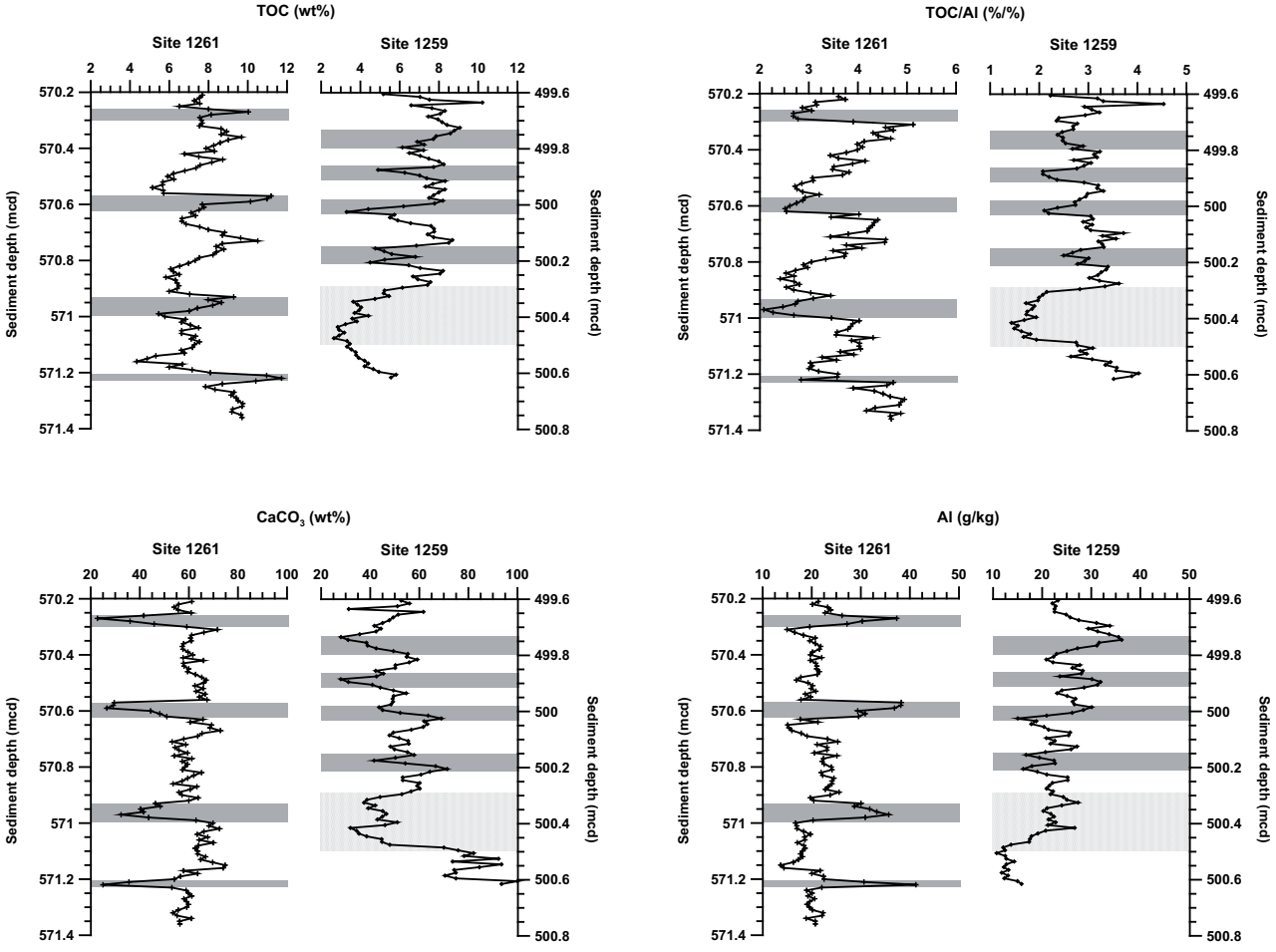

Figure 4.1: Chemical composition of ODP Sites 1261, 570.2-571.4 mcd, and 1259, 499.6-500.7 mcd. (a) Total organic carbon (TOC, wt%), (b) TOC/Al (%/%), (c) carbonate (wt%), (d) Al (g/kg) versus core depth (meters composite depth, mcd). The grey-shaded areas indicate less reducing conditions, the glauconitic horizon (GC) is marked by the dotted area.

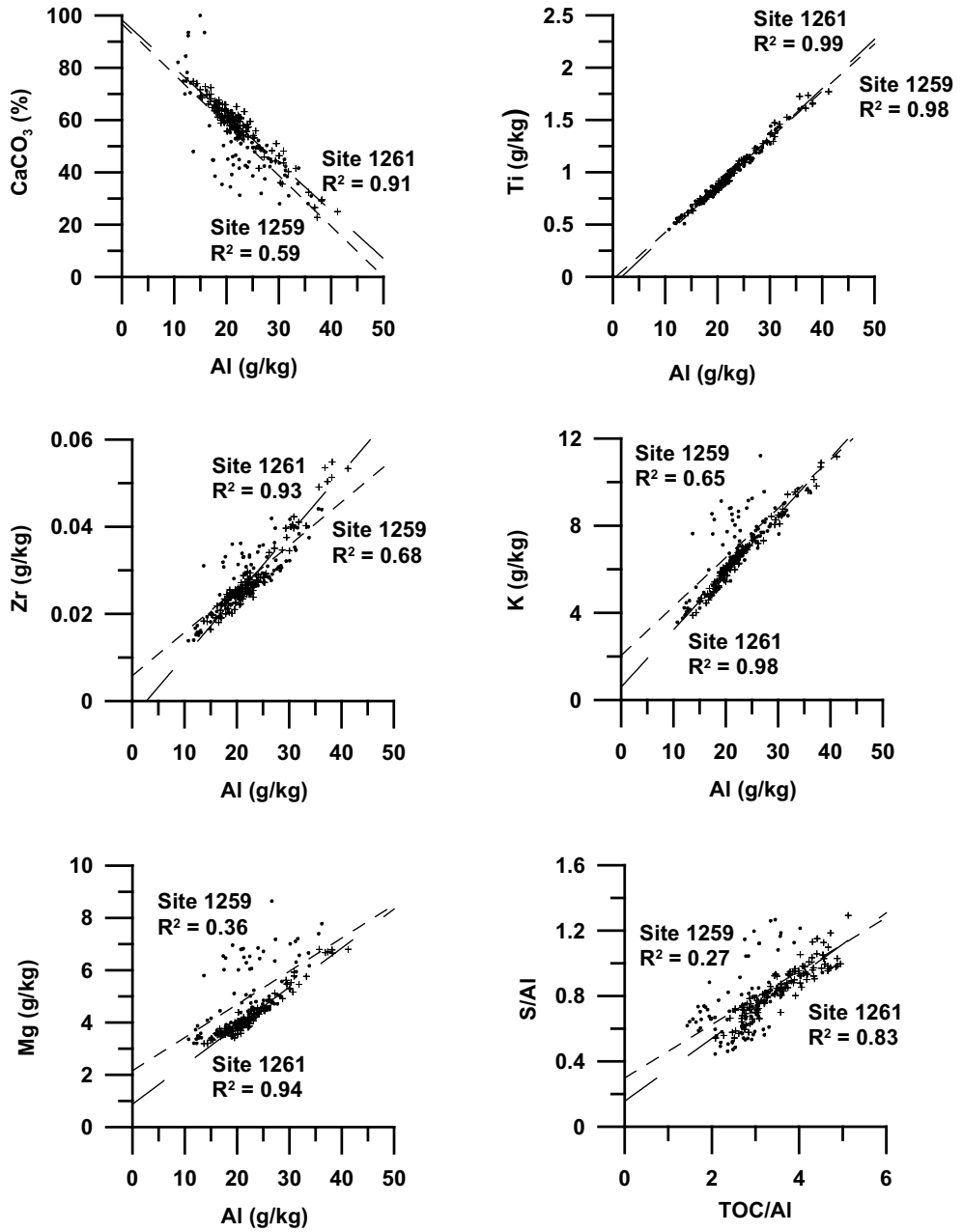

Figure 4.2: Cross plots of: (a) $CaCO_3$ to Al, (b) Ti to Al, (c) Zr to Al, (d) K to Al, (e) Mg to Al, (f) S/Al to TOC/Al for Sites 1259 (dots) and 1261 (crosses), with respective linear correlation coefficients (R^2, Pearson product-moment correlation coefficient).

At Site 1259, the correlation of Al with Ti is strong ($R^2 = 0.98$), but the one of Al with Zr is weaker (Figs. 4.2b, c; $R^2 = 0.63$). Typical elements of light silicates apart from Al are K and Mg, but they are also present in sea water, and Mg can be incorporated in carbonates. Comparable to Ti and Zr, relationships of Al with K and Mg at Site 1261 are strong ($R^2 = 0.98$ for Al with K, 0.94 for Al with Mg; Figs. 4.2d, e). At Site 1259, correlations of Al with K and Mg are overall weaker, with $R^2 = 0.65$ for Al with K, and $R^2 = 0.36$ for Al with Mg (Figs. 4.2d, e).

Redox-sensitive trace elements (Cd, Mn, Mo, Ni, V, Zn)

The investigated trace elements participate strongly in redox reactions and may become authigenically enriched or depleted in sediments deposited under oxygen-free conditions, making them frequently applied tracers of paleoredox conditions (e.g. Francois, 1988; Calvert and Pedersen, 1993; Dean et al., 1997; Morford and Emerson, 1999; recent reviews by Brumsack, 2006; Tribovillard et al., 2006). The degree of enrichment/depletion is calculated as enrichment factor (EF) relative to a standard material (average shale = AS; Turekian and Wedepohl, 1961):

$$EF_{element} = (element/Al)_{sample} / (element/Al)_{average\ shale}$$

The use of AS as reference material may get stressed by non-uniform lithologies in the detrital source area (Van der Weijden, 2002), but this potential bias is uncritical for elements with low contents in AS and/or strong incorporation into biological or authigenic processes, as the presented trace metals (Brumsack, 2006). In the studied core sections we identified two categories of redox-sensitive trace elements.

Manganese: Values of Mn/Al range from ~20-45 ppm/% across the Site 1261 and the upper Site 1259 interval (above 500.10 mcd). Values of ~60-90 ppm/% are reached in the lowest part of the 1259 section (below 500.48 mcd; Fig. 4.3a). Still, despite these overall low Mn/Al ratios, the Mn/Al record displays a rather strong correlation with carbonate (Fig. 4.4a). At Site 1261, correlation coefficients are similar for carbonate-poorer ($R^2 = 0.78$, n = 19) and carbonate-richer ($R^2 = 0.79$, n = 96) samples if the carbonate content threshold is set to 55 wt%. Respective correlations both follow positive trends, but with different slopes. At Site 1259, the Mn/Al to carbonate correlation is only high for carbonate-richer samples ($R^2 = 0.74$, n = 35; Fig. 4.4b). Average EFs for Mn at Sites 1259 and 1261 are ~0.36 (up to 1.0) and ~0.30 (up to 0.49), respectively, indicating Mn depletion throughout the investigated sediment intervals (Tab. 4.2; Fig. 4.5).

Cadmium, molybdenum, nickel, vanadium, zinc: Throughout the study interval at Site 1261 and the upper part at Site 1259 (499.60 – 500.10 mcd) there are cyclic patterns of Cd/Al, Mo/Al, Ni/Al, V/Al and Zn/Al (Fig. 4.3b-f). The cycles are documented more clearly at Site 1261 compared to Site 1259, partly because the latter had a lower sedimentation rate during biozone CC14 (Bornemann et al., 2008). Maximum values of Cd/Al, V/Al and Zn/Al ratios are similar at both sites, but Mo/Al and Ni/Al maxima are much lower at Site 1259 (Fig. 4.3). As further differences between trace element/Al profiles at Site 1261, all trace element/Al ratios are lowest within the carbonate-poor layers (grey bars), but the positions of the maxima vary. While Cd/Al, V/Al and Zn/Al are highest right above the carbonate-poor layers and gradually decrease upsection, Mo/Al and Ni/Al continuously increase

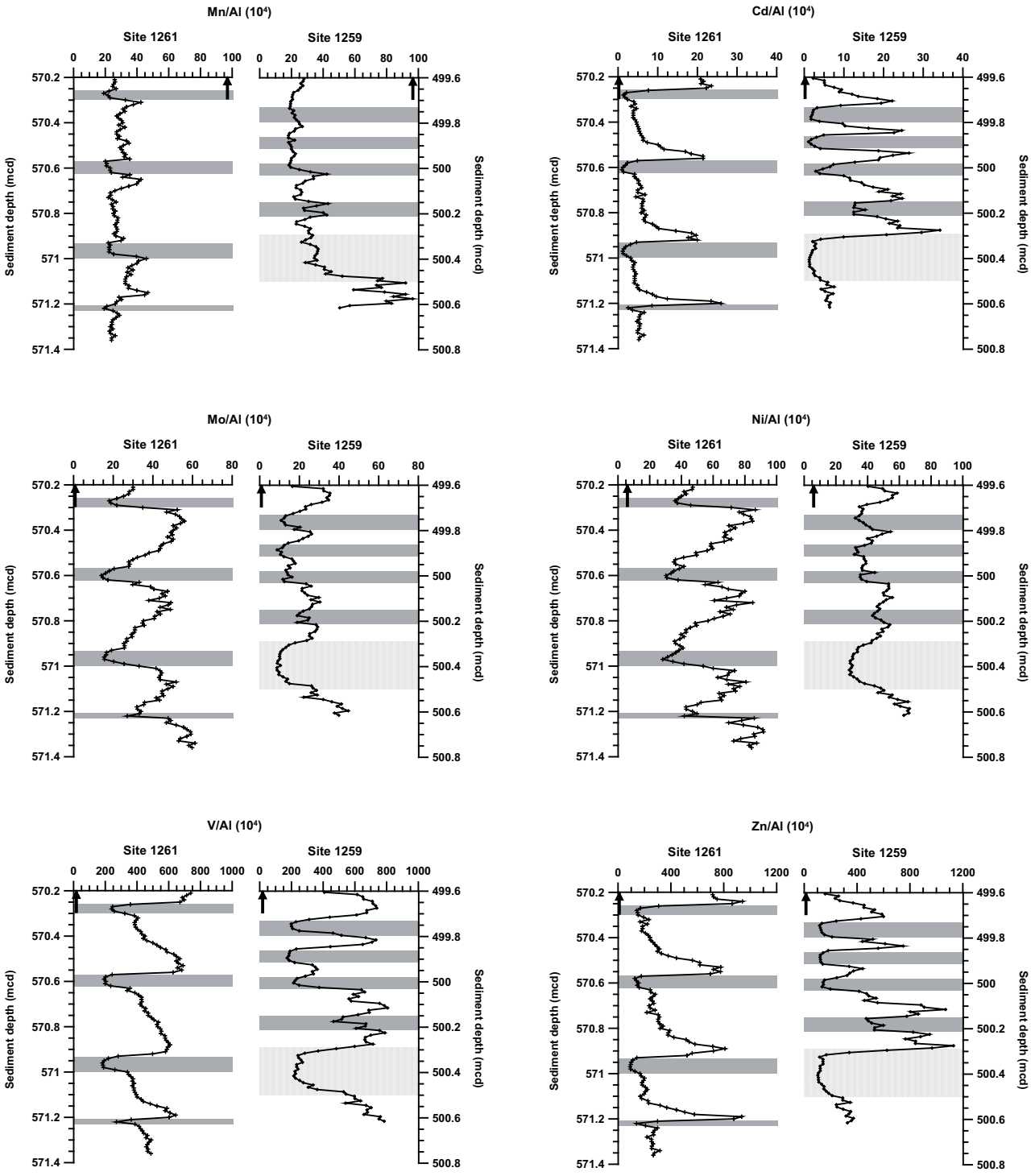

Figure 4.3: Chemical composition of ODP Sites 1261, 570.2-571.4 mcd, and 1259, 499.6-500.7 mcd. (a) Mn/Al, (b) Cd/Al, (c) Mo/Al, (d) Ni/Al, (e) V/Al, (f) Zn/Al (all as ppm/%) versus core depth (mcd). Arrows at X-axis indicate respective element/Al values of average shale (Turekian and Wedepohl, 1961).

upcore and reach maximum values right below the next carbonate-poor layer. Thus, Mo/Al and Ni/Al exhibit rather strong correlations with the TOC/Al and S/Al records (R^2 = 0.73 to 0.89; Figs. 4.4c-f), while there are no significant correlations of Cd/Al, V/Al and Zn/Al with TOC/Al and S/Al (R^2 <0.01).

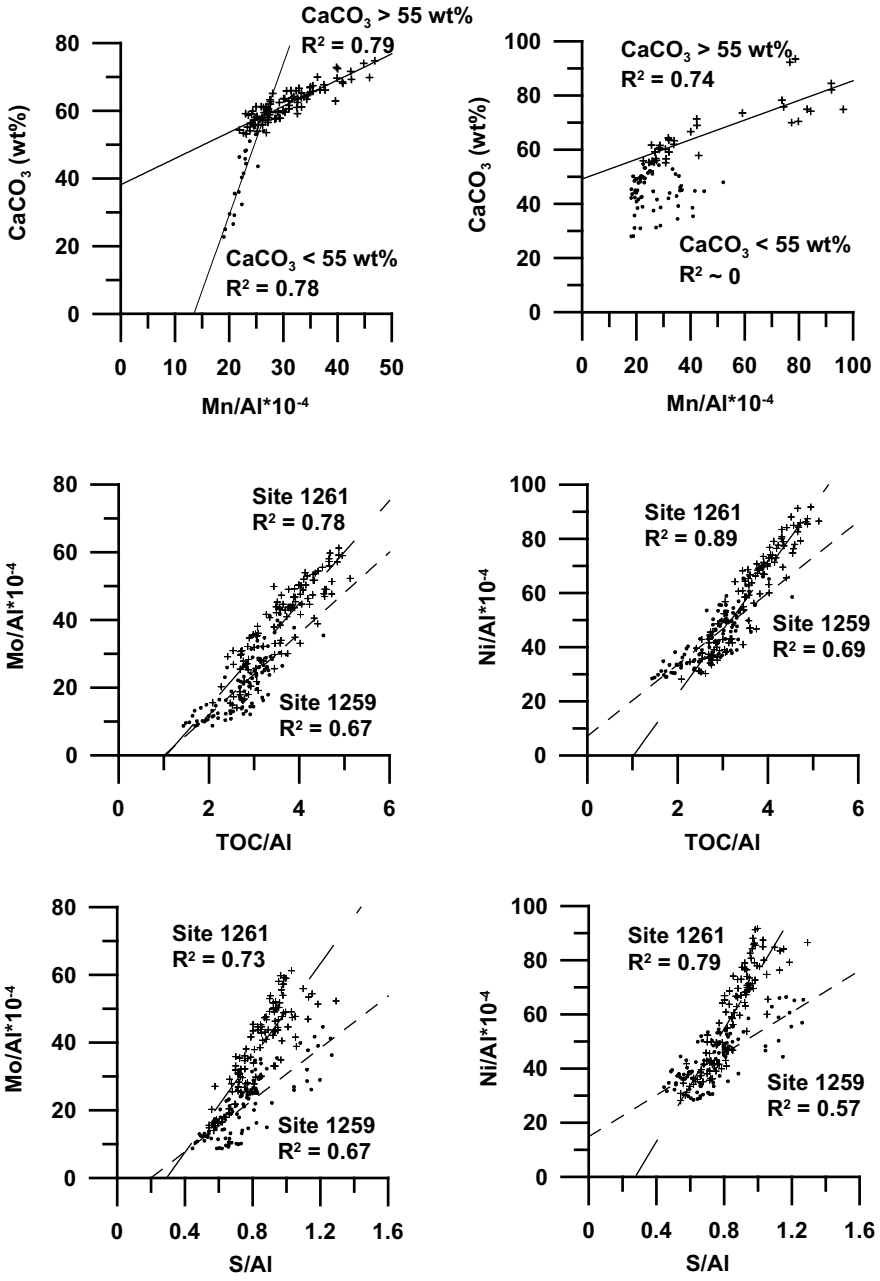

Figure 4.4: Cross plots of: $CaCO_3$ to Mn/Al for Sites 1261 (a) and 1259 (b), respectively, of carbonate-poorer (dots) and -richer (crosses) samples; (c) Mo/Al to TOC/Al, (d) Ni/Al to TOC/Al, (e) Mo/Al to S/Al, (f) Ni/Al to TOC/Al for Sites 1259 (dots) and 1261 (crosses), with respective linear correlation coefficients (R^2, Pearson product-moment correlation coefficient).

Site 1259 exhibits the same general trace element/Al patterns, but trace element/Al minima (grey bars) do not match with carbonate minima as at Site 1261. Average trace element EFs are within the same range at both sites (Tab. 4.2; Fig. 4.5). Notably, even lowest trace element/Al ratios are still (strongly) enriched relative to AS (Fig. 4.3b-f; AS values indicated by black arrows on the X-Axis). The GH is characterised by consistently lower trace element/Al ratios (Fig. 4.3b-f).

Iron and sulfur

Based on sequential iron extraction data, März et al. (accepted) inferred sulfidic bottom water conditions throughout most of the studied interval at Site 1261. Similar to sequential extraction data, the Fe/S ratio can be used as indicator for the amount of sulfide-bound Fe - the lower the ratio, the more Fe is sulfide-bound. The Fe/S ratio at Site 1261 ranges between 0.4 and 0.9, and highest values are reached within the carbonate-poor intervals, from where they gradually decrease upcore (Fig. 4.6a). Thus, highest Fe/S values coincide with lowest trace metal/Al and TOC/Al values. In the upper part of Site 1259 (499.60 – 500.10 mcd), Fe/S correlates with the same parameters as at Site 1261, but Fe/S values are markedly higher (~0.6-1.4), and within the GH, Fe/S reaches maximum values of 2.2 (Fig. 4.6a). The EF of Fe at Site 1261 is ~0.9 on average, with maxima of ~1.1 (Tab. 4.2). At Site 1259, slightly higher average EFs of ~1.3 are observed, but Fe/Al ratios that are consistently >1.0 are mostly confined to the GH, where Fe/Al values are consistently >1.0 (maximum values = 3.1; AS value = 0.54; Tab. 4.2). Notably, S/Al ratios correlate strongly with TOC/Al at Site 1261(R^2 = 0.83; Fig. 4.2f), while the respective correlation is much weaker at Site 1259 (R^2 = 0.27; Fig. 4.2f).

	Mean EF of 1261 vs. AS	*Max. EF of 1261 vs. AS*	*Mean EF of 1259 vs. AS*	*Max. EF of 1259 vs. AS*	*EF of (1) vs. AS*	*EF of (2) vs. AS*
Ba/Al	4.78	5.85	3.04	6.39	2.35	3.10
Cd/Al	212	763	298	1004	170	184
Fe/Al	0.88	1.03	1.28	3.14	1.16	1.44
K/Al	0.96	1.03	1.06	1.85	0.86	0.93
Mg/Al	1.12	1.37	1.35	2.49	1.41	1.29
Mn/Al	0.30	0.49	0.36	0.10	0.44	1.29
Mo/Al	130	207	74.2	164	127	208
Ni/Al	10.4	16.1	8.74	13.7	10.6	11.5
P/Al	13.5	71.8	67.2	418	8.80	5.91
S/Al	30.9	38.8	27.5	46.5	_	_
Ti/Al	0.83	0.85	0.84	0.85	1.01	0.96
V/Al	30.7	46.8	32.7	46.8	33.2	18.4
Zn/Al	30.9	86.7	35.1	86.7	22.8	42.5
Zr/Al	0.67	0.80	0.70	0.80	0.83	0.99

Table 4.2: Maximum and mean elemental enrichment factors (EFs) for the investigated intervals from ODP Sites 1261 and 1259, Demerara Rise. EFs are calculated from element/Al ratios relative to average shale (AS; Turekian and Wedepohl, 1961), and compared to EFs of OAE2 black shales from Demerara Rise (1) and various OAE2 location worldwide (2; Brumsack, 2006).

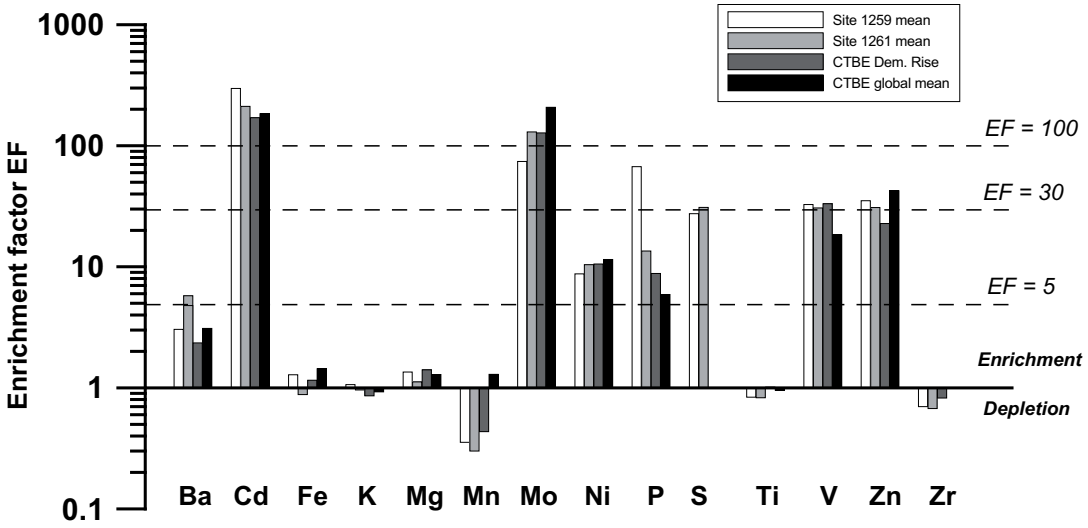

Figure 4.5: Bar plots displaying mean elemental enrichment factors (EFs; note logarithmic scale) of Sites 1259 and 1261, as well as of OAE2 black shale from Demerara Rise (Brumsack, 2006) and CTBE mean (from various OAE2 locations by Brumsack, 2006), relative to average shale (Turekian and Wedepohl, 1961). Dashed lines indicate EFs of 5, 30 and 100.

Phosphorus

At Site 1261, consistently low P contents of <0.1 wt% (75 of 115 samples in total) and P/Al ratios of <0.1 are found (Fig. 4.6b). However, pronounced peaks with P contents of up to 2.5 wt% and high P/Al ratios (up to ~0.8) cyclically occur within the carbonate-poor layers. At Site 1259, we observe P-poor (<0.1 wt%; 22 out of 101 samples) and P-rich layers as well, but their pattern is less regular, P peaks are not as distinct, and P/Al ratios are generally higher than at Site 1261 (Fig. 4.6b). Especially the GH at Site 1259 (499.60-500.10 mcd) is characterized by P contents of >2.0 wt% (up to 5.2 wt%, data not shown), and P/Al ratios of >1.0 (up to 3.3), with higher values at the base of the GH. The TOC to bulk P ratios (C/P), which is ~106:1 in average marine biomass (Redfield, 1958), are variable at both studied sites. C/P ratios range from 3.0 to 301 at Site 1261, and from 0.57 to 372 at Site 1259 (Fig. 4.6c). Generally, highest C/P values coincide with high values of TOC/Al and S/Al, and lowest C/P values with P/Al peaks.

Results of a sequential phosphate extraction yield information about the P speciation (Figs. 4.7a, b). The investigated P peak at Site 1261 (8 samples; Fig. 4.7a) and the upper studied P peak at Site 1259 (7 samples, without GH; Fig. 4.7b) have a similar P speciation: Fish bones (Step I) and OM-bound P (Step V) make up a minor fraction of the bulk P pool (<10 %) at both sites. Detrital apatite (Step IV)

is more significant at Site 1259 (~0-26 %, average of ~9 %) than at Site 1261 (~0.2-9 %, average of ~5 %). Authigenic apatite (Step III) is clearly the dominant fraction at Site 1259 (~17-87 %, average of ~60 %), and is also of major importance at Site 1261 (~16-81 %, average of ~43 %). Iron-bound P (Step II) is the dominant fraction at Site 1261 (~23-66 %, average of ~49 %), while its contribution to the P pool is substantially smaller at Site 1259 (~4-27 %, average of ~17 %). Within the GH at Site 1259 (6 samples; Fig. 4.7b), the fish bone and OM-bound P fractions are likewise rather unimportant (<7 %). The sum of iron-bound P and authigenic apatite (~6-35 % with ~21 % on average, and ~36-88 % ~with 58 % on average, respectively) constitutes the majority of the P pool. In relation to the other P peaks, detrital apatite is more significant within the GH (~1-42 %, average of ~22 %).

SEM and XRD results

The majority of particles of the density fraction >3.0 g/cm^3 were calcium-fluorapatite (CFA), Fe sulfides (mostly pyrite), Zn sulfides and barite. Despite their limited number, the analysed samples are considered representative in terms of composition, size and morphology of the dominant heavy minerals.

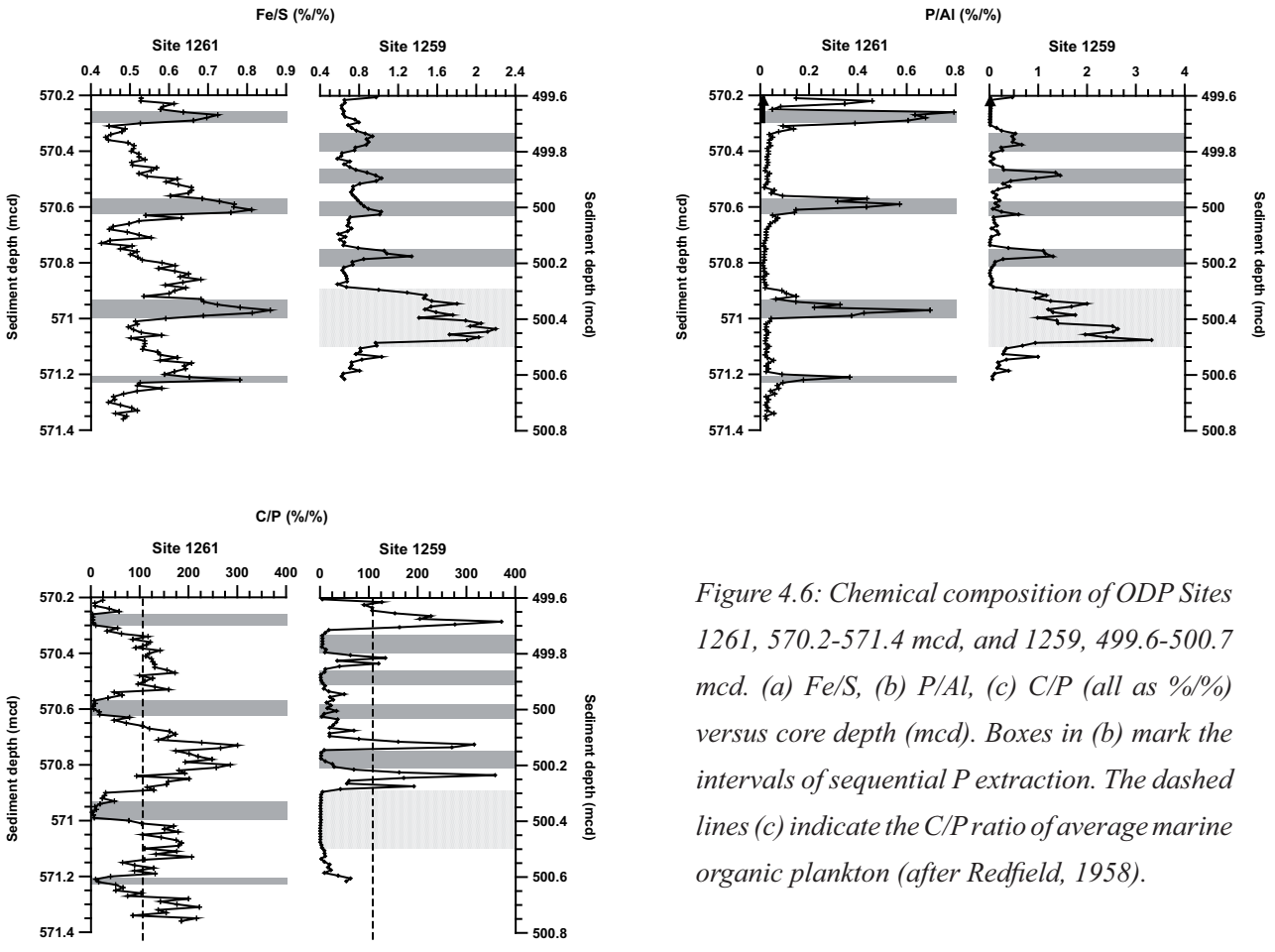

Figure 4.6: Chemical composition of ODP Sites 1261, 570.2-571.4 mcd, and 1259, 499.6-500.7 mcd. (a) Fe/S, (b) P/Al, (c) C/P (all as %/%) versus core depth (mcd). Boxes in (b) mark the intervals of sequential P extraction. The dashed lines (c) indicate the C/P ratio of average marine organic plankton (after Redfield, 1958).

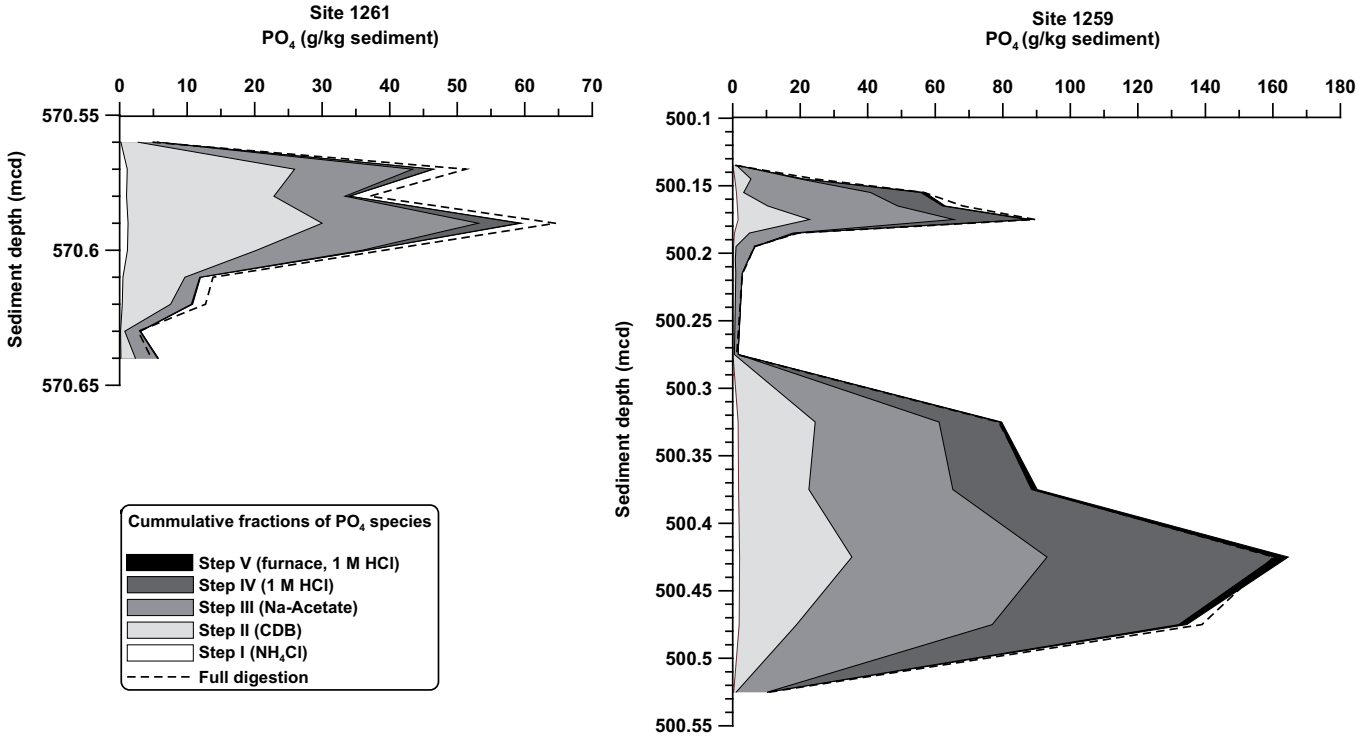

Figure 4.7: Cummulative extracted P fractions at (a) Site 1261 (570.56-570.64 mcd) and (b) Site 1259 (500.1-500.53 mcd) in g PO_4/kg sediment versus core depth (mcd). Explanation of extraction steps in Table 1.

Pyrite and other Fe sulfides are frequently observed in all samples, and occur as euhedral or cubic crystals of ~2-20 µm in diameter or as framboids of similar size range (Fig. 4.8a). The atomic Fe:S ratios of the Fe sulfides range between 1.0 and 0.5 according to the applied quantification software, indicating the presence of greigite and mackinawite next to pyrite. Zinc sulfides were observed in the Zn-rich samples (Site 1259, 499.82 and 499.88 mcd) as idiomorphic stochiometric ZnS crystals of 1-5 µm diameter. Crystals were found either dispersed or in framboid-like aggregates of ~15 µm diameter (Figs. 4.8b, c).

Barite is present in most of the samples, but rather dispersed, and was observed in the grain size range of 2-30 µm. Most of the barites appear as either flat, platy crystals with clear signs of dissolution (Fig. 4.9a), or uneven, angular, massive grains with signs of fractures (Fig. 4.9b). The latter are most likely fragments of larger grains that were broken into smaller pieces during sediment grinding.

Apatite grains represent the dominant heavy mineral in the P-rich samples, while they are absent in the P-poor ones. They cover a wide range of grain sizes, from few µm to several 100 µm in diameter. Irregular aggregates of smaller crystals are most likely of authigenic origin (Fig. 4.9c). However, most apatite particles have a massive, compact morphology and partly medium to strong rounding, probably due to transportation (Fig. 4.9d).

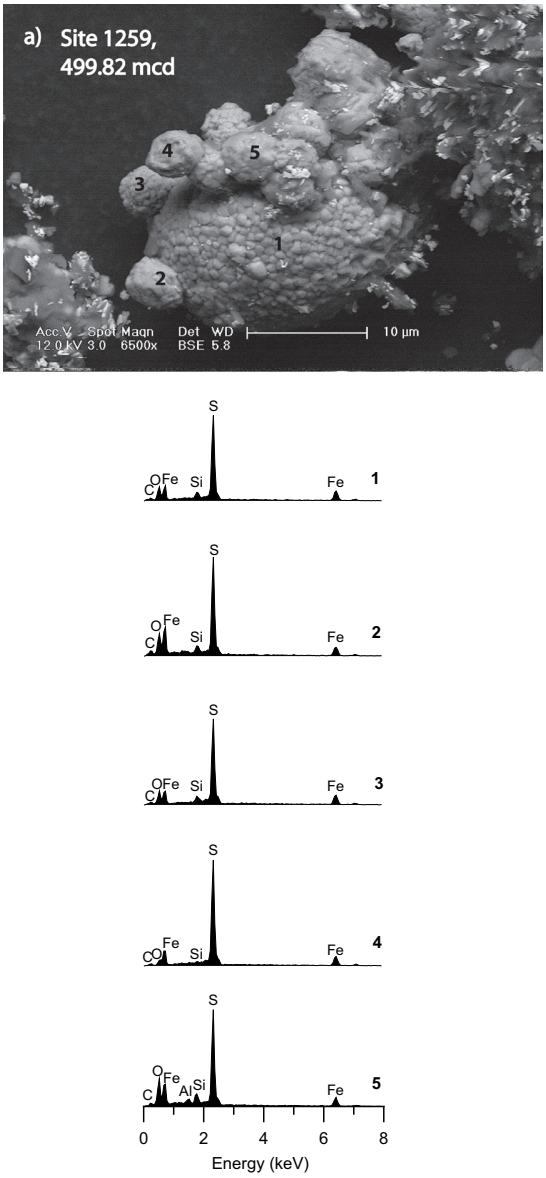

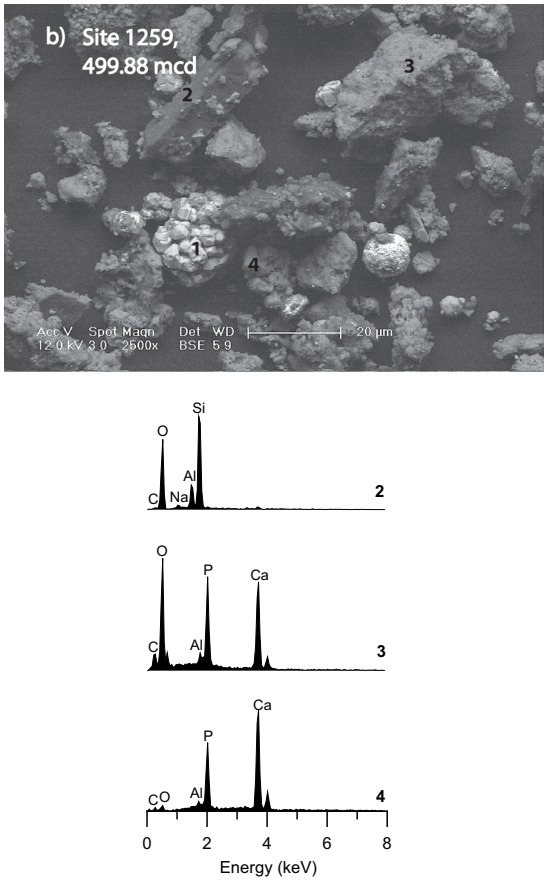

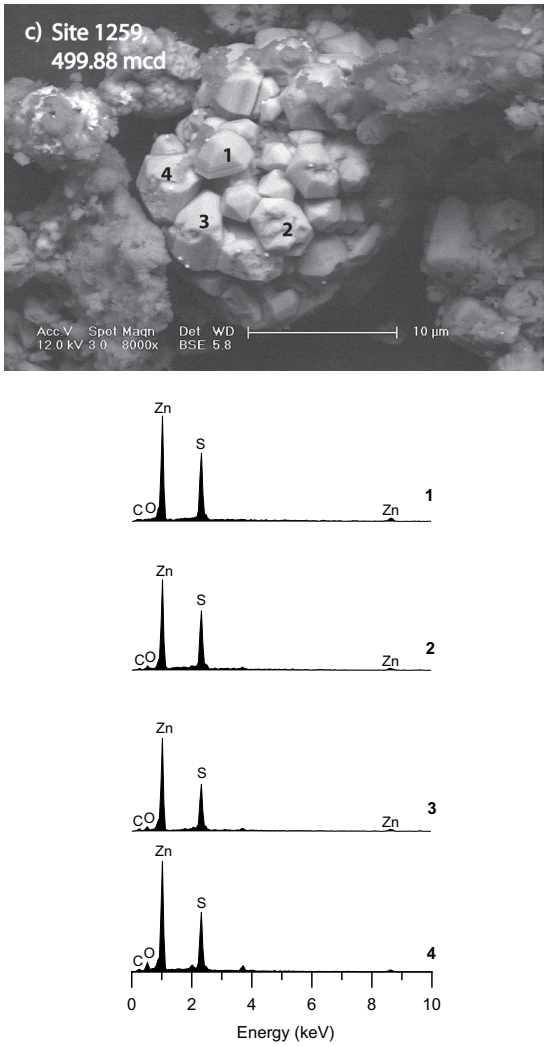

Figure 4.8: SEM micrographs in BSE mode and respective elemental spectra from representative particles. (a) Fe sulfide framboids (1-5); (b) aggregate/framboid of idiomorphic Zn-sulfide crystals (1), Na feldspar (2), CFA (3, 4); (c) closeup of particle 1 in (d), idiomorphic ZnS crystals (1-4). EDS spectra numbers correspond to the spot analyses of the respective numbered particles.

In support of the sequential P extraction, large amounts of CFA were detected via structural analysis with X-ray diffraction. Other common minerals apart from CFA encountered in all analysed samples via X-ray diffraction were calcite (confirming the geochemical analysis) and clinoptilolite ($(Na,K,Ca)_{2-3}Al_3(Al,Si)_2Si_{13}O_{36}\bullet 12(H_2O)$). Clinoptilolite is one of the most common zeolite minerals in marine pelagic sediments, and has previously been described in Cretaceous black shales from the North Atlantic (Thurow, 1988). It is formed authigenically by dissolution of amorphous SiO_2 (volcanic glass, opal tests as Si source) during burial diagenesis (e.g. Kastner, 1980).

Discussion

Terrigenous versus marine sediment input

Contribution of Al, K, Mg, Ti and Zr at Sites 1259 and 1261 was rather low, with e.g. Al constituting only ~1-4 wt% of bulk sediment. Persistent lamination and strong correlation of Al with K, Mg, Ti and Zr (R^2 >0.9) at Site 1261 support steady sedimentation without bioturbation or mass wasting, and probably one single detrital source area. Depositional conditions were different at Site 1259 as indicated by weaker relationships between the detrital proxy elements. They support repeated interruptions of sedimentation by mass wasting or winnowing of light particles (Nederbragt et al., 2007) and/or change of the detrital source area. A possible explanation for the little continental material reaching Sites 1259 and 1261, which are regarded more proximal than the other ODP Leg 207 sites (Mosher et al., 2007; Nederbragt et al., 2007), could be the high sea level during deposition, trapping most detrital matter on the flooded shelf area, or transport by coast-parallel currents.

The observed cyclicity of the Al record, particularly at Site 1261, is attributed to variable dilution of the detrital signal by biogenic material, in particular by calcium carbonate which constitutes ~30-70 wt% of bulk sediment at both sites, supporting a strong influence of carbonate productivity on sedimentation. X-ray diffraction data from both sites reveal the presence of large amounts of clinoptilolite.

In Demerara Rise black shales, preservation of siliceous radiolarian tests is generally poor (Erbacher et al., 2004; Musavu-Moussavou and Danelian, 2006; Nederbragt et al., 2007), which is most probably related to extensive silica diagenesis in these deeply buried sediments (e.g. Kastner, 1980; Thurow, 1988). Karpoff et al. (2007) regarded clinoptilolite as a diagnostic proxy for paleoproductivity in a Miocene marine setting. We therefore assume that clinoptilolite in the studied samples is derived from dissolution-reprecipitation reactions of biogenic silica, and thus indicative of high opal

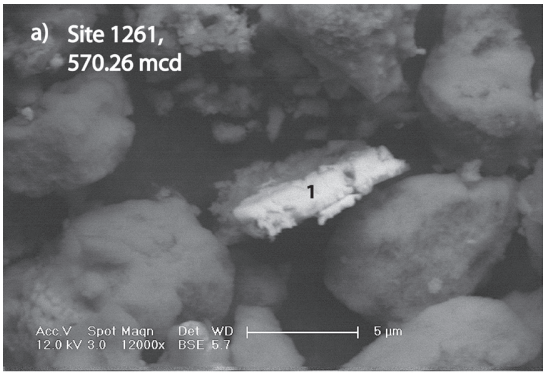
a) Site 1261,
570.26 mcd
1
Acc.V Spot Magn Det WD
12.0 kV 3.0 12000x BSE 5.7
5 µm

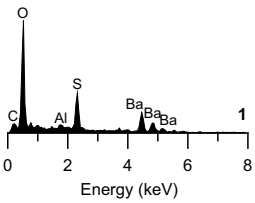
O
S
C
Al
Ba
Ba
Ba
1
0 2 4 6 8
Energy (keV)

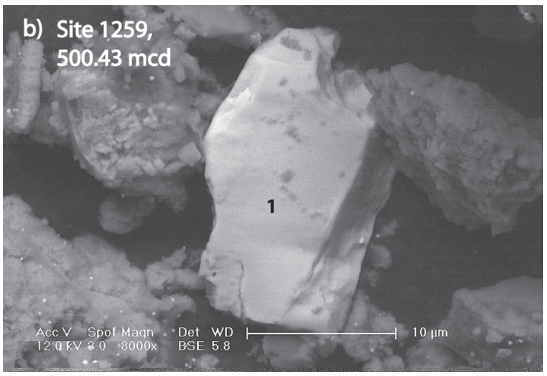
b) Site 1259,
500.43 mcd
1
Acc.V Spot Magn Det WD
12.0 kV 3.0 8000x BSE 5.8
10 µm

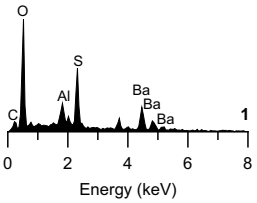
O
S
Al
C
Ba
Ba
Ba
1
0 2 4 6 8
Energy (keV)

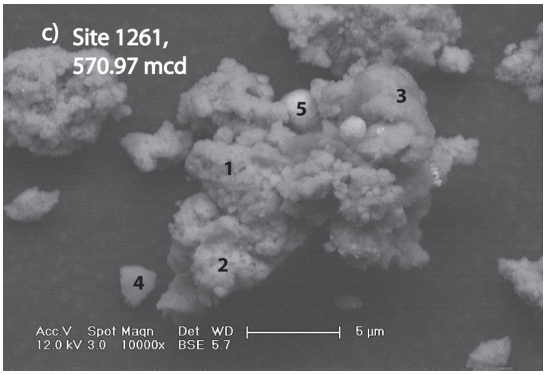
c) Site 1261,
570.97 mcd
5
3
1
2
4
Acc.V Spot Magn Det WD
12.0 kV 3.0 10000x BSE 5.7
5 µm

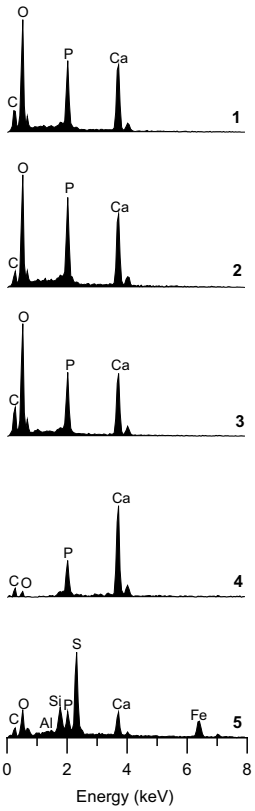
O
P
Ca
C
1
O
P
Ca
C
2
O
P
Ca
C
3
Ca
P
C O
4
S
O
Si P
Ca
Fe
C
Al
5
0 2 4 6 8
Energy (keV)

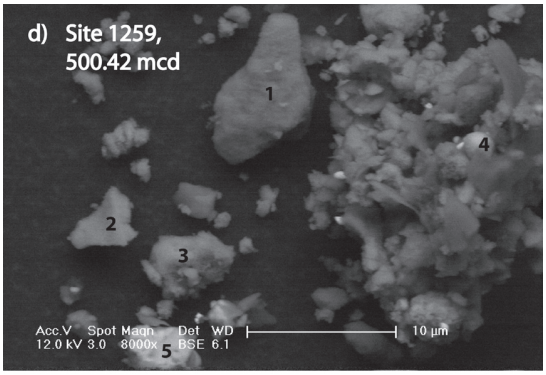
d) Site 1259,
500.42 mcd
1
4
2
3
5
Acc.V Spot Magn Det WD
12.0 kV 3.0 8000x BSE 6.1
10 µm

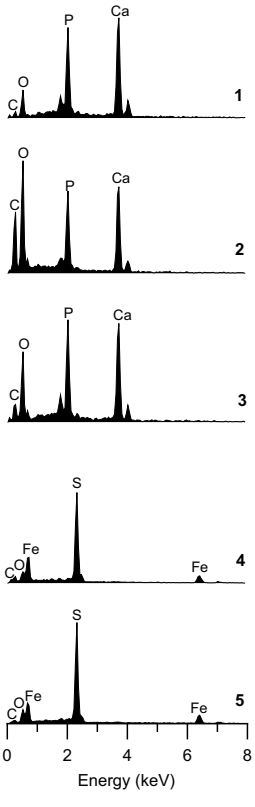
P
Ca
O
C
1
O
P
Ca
C
2
P
Ca
O
C
3
S
Fe
O
C
Fe
4
S
O Fe
C
Fe
5
0 2 4 6 8
Energy (keV)

productivity at the Coniacian-Santonian Demerara Rise. A weak anti-correlation of carbonate and clinoptilolite is observed suggesting periodic changes in the association of primary producers from carbonate to opal assemblages. In further support for elevated marine primary paleoproductivity, organic geochemical studies within Cretaceous black shales at Demerara Rise (e.g. Meyers et al., 2006; Forster et al., 2007b; Beckmann et al., in press) proved an overall high contribution of fresh marine OM to the bulk sediment.

Taking all these results into account we infer a depositional regime at both ODP Sites that was dominated by strong biogenic marine input, at least during the Coniacian nannofossil biozone CC14. This conclusion is consistent with interpretations for OAE3 black shales from the Deep Ivory Basin (ODP Site 959) and OAE2 black shale from the Tarfaya shelf basin off SW Morocco (e.g. Wagner, 2002; Wagner et al., 2004; Beckmann et al., 2005a, b). Estimates of paleoproductivity during Demerara Rise black shale deposition based on the barite record are hampered by diagenesis. Pore water profiles of SO_4^{2-} and Ba^{2+} (Erbacher et al., 2004) indicate sulfate depletion throughout the black shales at Demerara Rise, resulting in barite dissolution in this interval for the last ~86 Ma (Arndt et al., 2006). Despite overall Ba enrichment relative to AS in both studied intervals (Fig. 4.5), SEM analyses of samples from ODP Sites 1259 and 1261 did not identify any biogenic barite crystals, which are generally smaller than the diagenetic ones (0.5-5 μm versus 20-700 μm), and form elliptical or euhedral crystals or aggregates (Torres et al., 1996; Paytan et al., 2004; Paytan and Griffith, 2007). Instead, we detected numerous (fragments of) most probably diagenetic barite particles (Fig. 4.9a, b). The Ba enrichment and the Ba/Al records at both sites (data not shown) therefore document a diagenetic rather than a biogenic signal, making their interpretation in terms of paleoproductivity impossible.

Redox-sensitive elements

Combining records of different redox-sensitive (trace) elements is a well established approach for reconstructing past redox conditions. The interpretation of redox-sensitive (trace) metals investigated at Demerara Rise will be preceded by a short introduction into its behaviour under variable redox conditions.

Figure 4.9: SEM micrographs in BSE mode and respective elemental spectra from representative particles; (a) platy barite crystal showing clear signs of dissolution; (b) angular barite grain, probably fragment of larger diagenetic barite aggregates; (c) aggregate of fine CFA crystals (1-4), Fe sulfide with clay coating (5); (d) rounded, massive, most probably detrital CFA grain (1), angular CFA particles (2, 3), Fe sulfide framboid (4), angular Fe sulfide particle (5). EDS spectra numbers correspond to the spot analyses of the respective numbered particles.

Manganese: This element has a low solubility in oxic water and forms solid Mn (oxyhydr)oxides. While being preserved in oxic sediments, Mn (oxyhydr)oxides are utilized microbially as electron acceptor (dissimilatory Mn reduction) under suboxic conditions, leading to liberation of Mn^{2+} into the pore water, and potential reprecipitation at the oxic/suboxic boundary (Froelich et al., 1979; Lovley, 1991; Burdige, 1993). Below sub- or anoxic waters, Mn^{2+} is reductively leached from the sediment and, due to higher solubility, may reach high concentrations in the water (e.g. Klinkhammer and Bender, 1980; Lewis and Landing, 1991; Morford and Emerson, 1999). In a stratified anoxic water body, Mn^{2+}/Mn (oxyhydr)oxide cycling can occur at the oxic/anoxic transition, as in the Black Sea or Cariaco Basin (Tebo, 1991; Percy et al., in press; Yakushev et al., 2007). At such transitions, Mn (oxyhydr)oxides may precipitate and scavenge other particle-reactive trace element species in the water column, and thus act as shuttles to the oxygen-depleted sea floor - due to rapid settling of Mn (oxyhydr)oxide particles even in anoxic water columns (e.g. Morford et al., 2005; Brumsack, 2006; Tribovillard et al., 2006). In an anoxic water body related to an open margin oxygen minimum zone (OMZ), Mn^{2+} leached from the underlying sediment is initially concentrated in OMZ waters, but may partly diffuse out of the OMZ (e.g. Klinkhammer and Bender, 1980; Lewis and Luther, 2000; Brumsack, 2006). Manganese leaching results to its depletion in the underlying sediment. The significant Mn depletion within the studied OAE3 intervals (except for the lowest part of the 1259 interval) indicates sedimentary Mn leaching under constantly sub-/anoxic depositional conditions (Fig. 4.5).

Despite overall Mn depletion, however, the low amounts of sedimentary Mn appear to be bound to carbonate as indicated by a strong correlation between carbonate and Mn/Al at least for carbonate-rich samples (Figs. 4.4a, b). This Mn to carbonate coupling is most obvious in the bottom part of the 1259 section (below 500.48 mcd; Fig. 4.2a), where both Mn/Al and carbonate reach maximum values, implying substantial Mn carbonate formation. The formation of Mn carbonates is most probably a diagenetic process close to the sediment surface, where OM degradation and Mn (oxyhydr)oxide reduction increase alkalinity and Mn^{2+} concentration in the pore water (e.g. Baltic Sea anoxic deeps; Huckriede and Meischner, 1996; Neumann et al., 2002). However, Brumsack (2006) stated that close carbonate-Mn correlation might also be obtained syngenetically by Mn-carbonate overgrowths on carbonate tests within a Mn^{2+}-enriched anoxic water body. The latter process could have been important during biozone CC14 at Sites 1259 and 1261, as the former mechanism would require at least periodically oxic conditions at the sea floor, which is regarded as improbable (see discussion below and Beckmann et al., in press; März et al., accepted). Only the layers with strongly elevated Mn/Al and carbonate contents at the bottom of 1259 might indicate intermittent and minor influence of oxygen. Precipitation of Mn sulfides is generally neglected as Mn sink in black shales, as

is Mn incorporation into pyrite or organic phases (Huerta-Diaz and Morse, 1992; Algeo and Maynard, 2004).

Cadmium and zinc: These elements are present under oxic to suboxic conditions as soluble anions ($CdCl^+$; Zn^{2+}, $ZnCl^+$; Tribovillard et al., 2004). In addition, Cd and Zn are micronutrients incorporated into marine plankton biomass, which is also their major carrier to the sea floor (e.g. Bruland et al., 1991; Ho, 2006). Already at very low HS^- concentrations, Cd and Zn may form sulfides (CdS, ZnS) at the sea floor, due to lower solubility products and faster water exchange kinetics than other metal (e.g. iron) sulfides (Jacobs and Emerson, 1982; Rosenthal et al., 1995; Morse and Luther, 1999; Scholz and Neumann, 2007). Indeed, in the studied 1259 and 1261 intervals, Zn and Cd exhibit sharp peaks right above their minima (Figs. 4.3b, f), most probably documenting precipitation as CdS, and ZnS under weakly sulfidic bottom waters (Morse and Luther, 1999; März et al., accepted). This assumption is assured by SEM detection of pure idiomorphic ZnS crystals (Figs. 4.8c, d). In samples with high Zn contents, also Fe sulfides were observed which do not contain Cd and Zn, supporting that incorporation of these trace elements into pyrite is negligable (Huerta-Diaz and Morse, 1992; Scholz and Neumann, 2007). In addition, weak correlations of Cd/Al and Zn/Al with both TOC/Al and S/Al indicate that no significant fraction of sedimentary Cd and Zn is bound to sulfurized OM, despite their primary transport pathway to the sea floor via OM.

Molybdenum and nickel: These elements form soluble anions (Ni^{2+}, $NiCl^+$) or oxy-anions (MoO_4^{2-}) under oxic to suboxic conditions. Nickel is also a micronutrient taken up by primary producers and transported to the sea floor mainly by OM (e.g. Bruland et al., 1991; Ho, 2006). Molybdenum is conservative towards biological processes, but may be strongly coupled to Mn (oxyhydr)oxides, which can act as Mo shuttles to the sea floor under non-sulfidic conditions (e.g. Adelson et al., 2001; Dellwig et al., 2007). After algal blooms, a transport of Mo to the sea floor via organic macromolecules forming in the water column has been reported (e.g. Lunau et al., 2006; Dellwig et al., 2007). In sulfidic environments, Mo oxy-anions are transformed to particle-reactive thiomolybdates above a certain HS^- threshold ("thiomolybdate switch"; Helz et al., 1996; Zheng et al., 2000; Adelson et al., 2001), and scavenged from the water column by e.g. sinking OM. Different from Mo, incorporation into pyrite can be an important Ni sink at higher HS^- concentrations in the sediment (Huerta-Diaz and Morse, 1992; Algeo and Maynard, 2004). In addition, during OM sulfurization or formation of geoporphyrins in sulfidic sediments, a secondary coupling of Ni and Mo to OM can be created (e.g. Lewan and Maynard, 1982; Breit and Wanty, 1991; Algeo and Maynard, 2004; Tribovillard et al., 2004). The distinct correlations of Mo/Al and Ni/Al not only with TOC/Al, but also with S/Al at Sites 1259 and 1261 (Figs. 4.4c-f) imply that these trace metals were mainly incorporated into (sulfurized) OM

during early diagenesis. A close coupling of Mo to sulfurized OM was found by Tribovillard et al. (2004) and Algeo and Lyons (2006) in several black shale deposits. In contrast, we assume that Ni was rather incorporated into organic tissue as a micronutrient already during primary production and is not as strongly related to OM sulfurization as Mo. This is indicated by slightly stronger correlation of Ni/Al with TOC/Al than with S/Al at both sites, while Mo/Al is correlated with TOC/Al and S/Al to the same degree.

Vanadium: Under oxic to suboxic conditions, V is present as an oxy-anion (HVO_4^{2-}, $H_2VO_4^-$). Manganese (oxyhydr)oxides can play a significant role for its transport to the sea floor (e.g. Wehrli and Stumm, 1989; Hastings et al., 1996). However, different from other trace metals, V does not form sulfides, but - via a two-step reaction pathway - hydroxyl species ($VO(OH)_3^-$) and insoluble hydroxides ($VO(OH)_2$) under anoxic, and insoluble hydroxides ($V(OH)_3$) and oxides (V_2O_3) under sulfidic conditions (e.g. Breit and Wanty, 1991; Tribovillard et al., 2004). Incorporation of V into pyrite under sulfidic conditions is regarded as negligible (e.g. Dellwig et al., 2002; Scholz and Neumann, 2007). Under sulfidic conditions, V can also be incorporated into geoporphyrins (Lewan and Maynard, 1982; Breit and Wanty, 1991), and thus be coupled to OM similar to Ni. At Sites 1259 and 1261, the V/Al records (Fig. 4.3e) show patterns intermediate between Cd/Al and Zn/Al on one side, and Mo/Al and Ni/Al on the other side, making the V speciation in the studied intervals hard to determine. We suggest that precipitation of V (hydr)oxides at relatively low HS^- concentrations may have caused the initial V/Al peaks paralleled by Cd/Al and Zn/Al, while increasing incorporation of V into geoporphyrins could be responsible for keeping V/Al values relatively high (while Cd/Al and Zn/Al rapidly declined) even after initial V/Al peak formation (Breit and Wanty, 1991; Algeo and Maynard, 2004). Initial V (hydr)oxide formation was probably limiting sedimentary Ni enrichment, as the reduction from V(IV) to V(III) at low HS^- concentrations is known to inhibit Ni incorporation into geoporphyrins (Lewan, 1984; Breit and Wanty, 1991).

Iron: In oxic water, Fe has a low solubility and is present mainly as solid Fe (oxyhydr)oxides (e.g. Byrne and Kester, 1976; Liu and Millero, 2002). Under oxygen- and nitrate-free conditions, Fe (oxyhydr)oxides are progressively reduced (Froelich et al., 1979; review by Burdige, 1993), either chemically (e.g. Stone and Morgan, 1987; Stumm and Sulzberger, 1992) or biologically (dissimilatory iron reduction; e.g. Lovley, 1987; Nealson and Myers, 1992). In both cases, Fe^{2+} is liberated to the surrounding pore water, and re-precipitates as iron (oxyhyr)oxides as soon as nitrate or oxygen is available again. If free HS^- is present, Fe (oxyhydr)oxides are reduced (e.g. Morse et al., 1987; Yao and Millero, 1996) via variable pathways and transformed to Fe sulfides, mostly pyrite (FeS_2; e.g. Berner, 1984; Schoonen, 2004). However, if the pool of the most sulfide-reactive Fe minerals (e.g. ferrihydrite,

goethite, hematite; Poulton et al., 2004) is exhausted, HS^- may start to react with fresh OM in the sediment during OM sulfurization or natural vulcanisation (e.g. Sinninghe Damsté and de Leeuw, 1990; Sinninghe Damsté et al., 1998). Excess HS^- may also diffuse out of the sediment, creating sulfidic conditions at the sea floor and in the (lower) water column.

Sequential Fe extraction results obtained in an earlier study (März et al., accepted) indicated repeated shifts from sulfidic to anoxic, non-sulfidic bottom water conditions at Site 1261. Similar information can be obtained from the sedimentary Fe/S ratios, available for both Sites (Fig. 4.6a). Periodic increases in Fe/S ratios at Sites 1259 and 1261 indicate higher amounts of non-sulfide-bound sedimentary Fe. Indeed, März et al. (accepted) found an increase in Fe-oxides in the intervals with highest Fe/S values at Site 1261. Thus, we infer that also Fe/S peaks at Site 1259 document elevated amounts of oxide-bound Fe. Co-occurrence of Fe/S peaks with lowest - but compared to AS still enriched - trace element/Al, lowest TOC/Al, and highest P/Al values points to less reducing, but still anoxic conditions during their formation. Much higher Fe/S ratios within the GH are probably a combined effect of elevated Fe-oxide contents (6-35 % of total P bound to Fe-oxides) and the occurrence of glauconite ($(K,Na)(Fe^{3+},Al,Mg)_2(Si,Al)_4O_{10}(OH)_2$, containing ~20 % Fe). Another finding of März et al. (accepted) was that only about 15-35 % of bulk S at Site 1261 are bound to pyrite (see also Böttcher et al., 2006). Most of the remaining S fraction is attributed to sulfurized fresh marine OM, indicated by a strong TOC-S correlation. However, based on weaker TOC to S correlations at Site 1259, we assume that OM and S are not as strongly coupled as at Site 1261, i.e. OM sulfurization was probably occurring, but less intense than at Site 1261. The reason for that could be higher input of detrital Fe (oxyhydr)oxides, or of more refractory terrigenous OM with a lower potential for HS^- formation and sulfurization. Concluding, enhanced OM preservation via early diagenetic sulfurization was at least partly responsible for the high TOC contents of the studied sediments at both sites.

Phosphorus: In the ocean, P is mainly present as the stable phosphate oxy-anion HPO_4^{2-}, which is not redox-sensitive itself, but strongly coupled to the cycles of Fe and OM. Fresh iron (oxyhydr)oxides can not only adsorb large amounts of phosphate ions, but phosphate may also be co-precipitated during Fe (oxyhydr)oxide formation. Thus, Fe (oxyhydr)oxides can play a major role in the transport of P to the sea floor (e.g. Feely et al., 1990; Slomp et al., 1996; Poulton and Canfield, 2006). Another P carrier to the sea floor is marine OM, as marine phytoplankton contains a relatively stable amount of P (with a mean C/P ratio of 106:1; Redfield, 1958). Under reducing conditions at the sea floor, a decoupling of P from both the Fe and the OM cycles takes place: Dissolution of Fe (oxyhydr)oxides liberates phosphate to the surrounding water. Thus, the Fe-P coupling can only be active if iron (oxyhydr)oxides are formed in/delivered to marine waters and sediments under oxic to at least anoxic, non-sulfidic conditions

(März et al., accepted). Furthermore, under anoxic conditions there is a preferential regeneration of organic P from organic material in relation to organic carbon (e.g. Ingall et al., 1993; Ingall and Jahnke, 1997), resulting in low P burial capacities of anoxic sediments and C/P ratios of >106 (e.g. Anderson et al., 2001; review by Algeo and Ingall, 2007).

Our bulk sediment P data indicate P depletion over large parts of the investigated intervals, resulting in high C/P ratios, and P/Al values lower than AS (Fig. 4.6b, c). This implies a very effective regeneration of both Fe (oxyhydr)oxide- and OM-bound P from the sediment under anoxic, probably even sulfidic bottom water conditions. However, P/Al enrichments at both sites, with very low C/P ratios and Fe-bound P as one of the major fractions (Figs. 4.6b, c; 4.7a, b), document conditions favorable for P burial, and even (partial) preservation of Fe-oxides (and the Fe-P coupling), in the sediment. During these periods, bottom waters are assumed to have been free of HS^-, but free of oxygen as well, as indicated by TOC, S and redox-sensitive trace metal data (anoxic, non-sulfidic conditions according to März et al., accepted). Partial transfer of Fe-bound P, and nearly complete transfer of OM-bound P, to authigenic apatite is consistent with the "sink switching" hypothesis, i.e. P transfer from rather labile binding forms into authigenic apatite as the ultimate oceanic P sink (e.g. Delaney, 1998; Filippelli, 2001). The high P content of the GH is probably a mixed signal of originally larger amounts of Fe oxide-bound P transformed to the now dominant authigenic CFA, and higher input of older, well-crystallized authigenic and/or detrital apatite (Fig. 4.7b). The fact that many of the apatite grains identified under the SEM in GH samples are more or less rounded (Fig. 4.9d) points to re-deposition or movement of at least part of the apatite grains by bottom currents.

Geochemistry at Sites 1259 and 1261 – Similarities and differences

Comparing quasi age-equivalent records from the two drill sites on Demerara Rise in terms of a paleo-water depth transect bears a fundamental complication; Cretaceous water depths may have been different than at present due to subsidence and tilting of the Demerara Rise during progressive rifting in the South Atlantic since the earliest Cretaceous (Erbacher et al., 2004). In this context, Erbacher et al. (2005) stated that transgressive Cretaceous black shale deposition at Site 1259 started later than at all other ODP Leg 207 sites (including Site 1261, where black shales started to develop before the OAE2), implying that during the Cretaceous Site 1259 was situated in shallower water depths than Site 1261. Also benthic foraminiferal assemblages support that re-oxygenation of the Demerara Rise sea floor occurred first at Site 1259 followed by the other ODP Leg 207 sites (Friedrich and Erbacher, 2006).

Sediment source: From the high-resolution profiles presented in this study, it appears that the cyclicity of the carbonate, Al and TOC/Al records, and thus the overall sedimentary input is much more regular at Site 1261 compared to Site 1259. Based on Al and carbonate data, we infer that variable dilution by marine carbonate was the main process leading to the observed fluctuations in carbonate, Al and TOC/Al. Well-preserved mm-scale lamination at Site 1261 excludes physical and biological disturbance of the sediment. The strong correlation between all terrigenous "marker elements" such as Al, K, Mg, Ti and Zr (Figs. 4.2a-e) implies a stable detrital source area at Site 1261. Terrestrial-sourced elements (Fe, K, Mg, Ti, Zr) normalized to Al support that the mineralogical composition of the detrital source material is close to AS composition (Fig. 4.5), consistent with the findings of Hetzel et al. (2006). At Site 1259, however, the terrestrial-sourced elements are overall slightly more enriched than at Site 1261 (Tab. 4.2; Fig. 4.5), implying a stronger detrital influence, and thus a more proximal location of Site 1259 during the Coniacian-Santonian consistent with Erbacher et al. (2005) and Friedrich and Erbacher (2006). Alternatively, the input of marine biogenic carbonate could have been lower at Site 1259. The weaker carbonate-Al anti-correlation as well as weaker correlations of the detrital elements support that the interplay of marine versus terrigenous dilution was disrupted by mass wasting, winnowing of fine particles, and/or varying sources of lithogenic input. The periodic, potentially erosional activity of winnowing bottom currents would also offer an explanation for lower sedimentation rates at Site 1259 than at Site 1261, where continuous hemipelagic sedimentation is documented. The occurrence of glauconitic horizons, as observed at Site 1259, is interpreted by Friedrich and Erbacher (2006) and Nederbragt et al. (2007) as an indication for extremely low sedimentation rates, possibly periodic erosion due to increased bottom currents at Site 1259. Indeed, coarser grain size, enrichment of heavy mineral-bound Zr (data not shown), association of glauconite and detrital apatite (identified by sequential P extraction and SEM analysis; Fig. 4.7a; 4.9e), and low carbonate contents within the GH support this conclusion. Still, enrichments of K/Al, Mg/Al, and depletion of Ti/Al are no typical features of a winnowing horizon, but rather suggest an import of detrital material from a different source area with a K- and Mg-richer, but Ti-poorer lithology. Unfortunately we cannot be more precise in that respect due to limited knowledge about the detrital source area or related drainage systems to Demerara Rise.

Redox cycles: Rapid and cyclic bottom water redox fluctuations at Site 1261 were suggested to document variations between sulfidic and anoxic, non-sulfidic conditions in an earlier work of März et al. (accepted). Comparing the records of Cd/Al, Mo/Al, Ni/Al, V/Al and Zn/Al at Site 1261 and the part of 1259 above the GH, the variations from maxima to minima (Fig. 4.3b-f) are similar at both sites, despite lower time resolution at Site 1259. Also the respective trace element EFs (Fig. 4.5) are

very similar at both sites. This indicates that at least the upper part of Site 1259 (499.60 - 500.10 mcd) experienced very similar redox variations as Site 1261. Detection of variable, but overall anoxic redox conditions not only at the supposedly shallower Site 1259, but also at the deeper Site 1261 suggests that indeed large parts of the continental margin at Demerara Rise were affected by bottom water anoxia during OAE3. However, more detailed comparison of redox-sensitive proxy records reveals slight differences between both sites. Compared to the four nearly identical redox cycles at Site 1261 (regular cyclicity, very similar maximum and minimum element/Al values in each cycle, repetitive "sawtooth" patterns), Site 1259 displays more irregular variations, with some element/Al minima (500.15-500.22 mcd; Fig. 4.3b-f) and maxima (499.92-499.98 mcd; Fig. 4.3b-f) that are less pronounced than expected. Thus, we conclude that although redox cyclicity at Site 1259 above the GH was similar to Site 1261, the intensity of anoxia/euxinia and the regularity of redox changes were less pronounced. A major difference between both sites is the occurrence of the GH horizon at Site 1259 (dotted bar, Figs. 4.1, 4.3, 4.6). The relatively low Al ratios of Cd, Ni, Mo, V and Zn throughout the GH (Fig. 3b-f), in combination with lower TOC/Al (Fig. 4.1b) and high Fe/S (Fig. 4.3a) ratios point to less reducing conditions during its deposition than during the overlying section of Site 1259. In support of this, the P/Al and C/P records within the GH show highest (0.6-3.3) respectively lowest (0.3-2.9) values of all samples (Fig. 4.6b, c), proving enhanced P retention in the sediment under at least non-sulfidic conditions. In addition, ~20% of all P measured in the GH is Fe oxide-associated (Fig. 4.7a). We assume that depositional conditions during formation of the GH were probably influenced by enhanced bottom current activity, introducing less reducing bottom waters and winnowing fine particles.

The sediment section below the GH at Site 1259 (below 500.48 mcd) is the only interval where Mn/Al reaches values comparable to AS (Fig. 4.3a). This Mn/Al maximum is paralleled by highest overall carbonate contents of up to ~100 wt% (Fig. 4.1c). As discussed earlier, Mn carbonate formation requires elevated Mn^{2+} levels in the pore water, which are induced by reductive dissolution of Mn (oxyhydr)oxides. Deposition of Mn (oxyhydr)oxides requires periodically oxic bottom water conditions. Indeed, less reducing bottom water conditions are implied by relatively low Cd/Al and Zn/Al ratios (Fig. 4.3b, f). Also low C/P ratios indicate P burial in the sediment under oxic conditions (Fig. 4.6c). However, V/Al and especially Mo/Al and Ni/Al exhibit very high values (Fig. 4.3c-e), standing in contrast to oxic conditions. Notably, the trace elements highly enriched below the GH are those associated to OM (which is in support of the high TOC/Al values in the respective interval), while sulfide-bound Cd and Zn are relatively low. Despite these two contradictory interpretations for the interval below the GH, its redox development did obviously not follow the regular systematics as the redox cycles above the GH and the ones at Site 1261.

Comparison of EFs at 1259 and 1261 with values reported for the CTBE (Tab. 4.2; Fig. 4.5) shows that for most trace elements, EFs are very similar to CTBE black shales at Demerara Rise, which were deposited ~10 Ma prior to OAE3, during OAE2. Thus, despite the more limited spatial extention of OAE3 (tropical and subtropical North Atlantic), at Demerara Rise both OAEs have obviously developed in a similar dramatic way, and are comparable to each other in terms of high OM production and/or preservation, low detrital input, and anoxic to sulfidic bottom waters. This supports the lower-resolution data of Hetzel et al. (2006), reporting a sediment composition for Demerara Rise black shales very similar to our OAE3 data. Böttcher et al. (2007) found very similar Fe-S systematics in OAE2 black shales at Demerara Rise, indicating an Fe-limited system, a high degree of pyritization and intensive OM sulfurization. We conclude that Middle and Late Cretaceous black shale formation at Demerara Rise took place under very similar paleoenvironmental conditions.

Conclusion

During Coniacian-Santonian time ODP Sites 1261 and 1259 were dominated by marine (calcareous and opal) sedimentation and burial of large amounts of OM, which at least partly related to elevated OM preservation by diagenetic OM sulfurization. The presented new geochemical data support the conclusion that both sites were affected by similar bottom water redox conditions throughout the investigated intervals, which were generally anoxic, and even sulfidic for prolonged periods. However, bottom water and sediment redox were subject to relatively rapid and cyclic variations, which occurred at both sites. This observation suggests that prevailing redox conditions affected large parts of the continental margin at Demerara Rise during OAE3. The sedimentary record documents that redox fluctuations were regular in frequency and degree of changes at the deeper Site 1261. At the shallower position of Site 1259 sedimentation instead was stronger affected by variations in detrital supply and/or winnowing of bottom currents, and probably periodic erosion, together supporting a more proximal location. In contrast, steady hemipelagic sedimentation prevailed at Site 1261, consistent with a greater water depth. Especially during the formation of the glauconitic horizon at Site 1259, the depositional regime was physically disturbed, and bottom waters were most probably better oxygenated. Speciation of P indicates that at both sites Fe oxide-bound P and authigenic apatite are the dominant sedimentary P species, while detrital apatite seems to be of higher importance within the GH. Only minor P contributions are related to fish bones and organic P. Geochemically, the studied OAE3 deposits are well-comparable to the CTBE black shales from the same sites, indicating that both anoxic events created very similar paleoenvironmental conditions at Demerara Rise.

Acknowledgements

We are indebted to Walter Hale for sampling assistance, and to Britt Kockisch, Silvana Pape, Susanne Siemer and Karsten Enneking for analytical and logistic assistance. Help of Kathrin Küster, Jan Hoffmann and Niklas Allroggen with the phosphate extraction is highly appreciated. Electron microscopy was performed at the EMU (Utrecht University), and we thank Martin Drury for his support. CM thanks Gert de Lange and the Geochemistry group at Utrecht University for great hospitality during his research stay. TW acknowledges the Royal Society-Wolfson Research Merit Award. This study was funded by the DFG via the International Graduate College EUROPROX.

Literatur

Adelson, J.M., Helz, G.R., Miller, C.V. (2001) Reconstructing the rise of recent coastal anoxia: Molybdenum in Chesapeake Bay sediments. Geochim. Cosmochim. Acta 65, 237-252.

Algeo, T.J., Maynard, J.B. (2004) Trace element behaviour and redox facies in core shales of the Upper Pennsylvanian Kansas-type cyclothems. Chem. Geol. 206, 289-318.

Algeo, T.J., Lyons, T.W. (2006) Mo-total organic carbon covariation in modern anoxic marine environments: Implications for analysis of paleoredox and paleohydrographic conditions. Paleoceanography 21, PA 1016.

Algeo, T.J., Ingall, E. (2007) Sedimentary C_{org}:P ratios, paleocean ventilation, and Phanerozoic pO_2. Palaeogeogr. Palaeoclimatol. Palaeoecol. 256, 130-155.

Anderson, L.D., Delaney, M.L., Faul, K.L. (2001) Carbon to phosphorus ratios in sediments: Implications for nutrient cycling. Global Biogeochem. Cycles 15, 65-79.

Arndt, S., Brumsack, H.-J., Wirtz, K. (2006) Cretaceous black shales as active bioreactors: a biogeochemical model for the deep biosphere encountered during ODP Leg 207 (Demerara Rise). Geochim. Cosmochim. Acta 70, 480-425.

Beckmann, B., Flögel, S, Hofmann, P., Schulz, M., Wagner, T. (2005a) Orbital forcing of Cretaceous river discharge in tropical Africa and ocean response. Nature, 437, 241-244.

Beckmann, B., Wagner, T., Hofmann, P. (2005b) Linking Coniacian-Santonian (OAE3) black shale formation to African climate variability: a reference section from the eastern tropical Atlantic at orbital time scales (ODP Site 959, off Ivory Coast/ Ghana). In: Harris, N.B. (Ed.) *The Deposition of Organic Carbon-Rich Sediments: Models, Mechanisms, and Consequences*. SEPM Spec. Publ. 82, pp. 125-143.

Beckmann, B., Hofmann, P., März, C., Schouten S., Sinninghe Damsté, J.S., Wagner, T. (in press) Coniacian-Santonian deep ocean anoxia/euxinia inferred from molecular and inorganic markers: Results from the Demerara Rise (ODP Leg 207). Org. Geochem.

Bender, V.B. (2007) *Evolution of the Galicia mud belt from sediment cores and sediment acoustic profiles*. Unpublished Master Thesis, University of Bremen, Bremen, 59 pp.

Berner, R.A. (1984) Sedimentary pyrite formation: An update. Geochim. Cosmochim. Acta 48, 605-615.

Böttcher, M.E., Hetzel, S., Brumsack, H.-J., Schipper, A. (2006) Sulfur-iron-carbon geochemistry in sediments of the Demerara Rise. In: Mosher, D.C., Erbacher, J., Malone, M.J. (Eds.) *Proc. ODP, Sci. Results 207*, 1-23. doi:10.2973/odp.proc.sr.2007.108.2006.

Bornemann, A., Friedrich, O., Beckmann, B., Hofmann, P., Schouten, S., Sinninghe Damsté, J.S., Vogel, J., Wagner, T., Norris, R.D. (2008) Isotopic evidence for a glaciation event during the early Late Cretaceous super-greenhouse episode. Science 319, 189-192.

Breit, G.N., Wanty, R.B. (1991) Vanadium accumulation in carbonaceous rocks: a review of geochemical controls during deposition and diagenesis. Chem. Geol. 91, 83–97.

Bruland, K.W., Donat, J.R., Hutchins, D.A. (1991) Interactive influences of bioactive trace metals on biological production in oceanic waters. Limnol. Oceanogr. 36, 1555–1577.

Brumsack, H.-J. (2006) The trace metal content of recent organic carbon-rich sediments: Implications for Cretaceous black shale formation. Palaeogeogr. Palaeoclimatol. Palaeoecol. 232, 344-361.

Burdige, D.J. (1993) The biogeochemistry of manganese and iron reduction in marine sediments. Earth-Sci. Rev. 35, 249-284.

Byrne, R.H., Kester, D.R. (1976) Solubility of hydrous ferric oxide and iron speciation in sea water. Mar. Chem. 4, 255-274.

Calvert, S.E., Pedersen, T.F. (1993) Geochemistry of recent oxic and anoxic marine sediments: implications for the geological record. Mar. Geol. 113, 67-88.

Chung, F.H. (1974) Quantitative interpretation of X-ray diffraction patterns, I. Matrix-flushing method of quantitative multicomponent analysis. J. Appl. Crystallogr. 7, 513-519.

Dean, W.E., Gardner, J.V., Piper, D.Z. (1997) Inorganic geochemical indicators of glacial–interglacial changes in productivity and anoxia on the California continental margin. Geochim. Cosmochim. Acta 61, 4507-4518.

Delaney, M.L. (1998) Phosphorus accumulation in marine sediments and the oceanic phosphorus cycle. Global Biogeochem. Cycles 12, 563-572.

Dellwig O., Böttcher M. E., Lipinski M., Brumsack H.-J. (2002) Trace metals in Holocene coastal peats and their relation to pyrite formation (NW Germany). Chem. Geol. 182, 423-442.

Dellwig, O., Beck, M., Lemke, A., Lunau, M., Kolditz, K., Schnetger, B., Brumsack, H.-J. (2007) Non-conservative behaviour of molybdenum in coastal waters: Coupling geochemical, biological, and sedimentological processes. Geochim. Cosmochim. Acta 71, 2745-2761.

Erbacher, J., Mosher, D.C., Malone, M.J., Shipboard Scientific Party (2004) *Proc. ODP In. Reports 207*, doi:10.2973/odp.proc.ir.207.2004.

Erbacher, J., Friedrich, O., Wilson, P.A., Birch, H., Mutterlose, J. (2005) Stable organic carbon isotope stratigraphy across Oceanic Anoxic Event 2 of Demerara Rise, western tropical Atlantic. Geochem. Geophys. Geosyst. 6, Q06010, doi:10.1029/2004GC000850.

Feely, R.A., Massoth, G.J., Baker, E.T., Cowen, J.P., Lamb, M.F., Krogslund, K.A. (1990) The effect of hydrothermal processes on midwater phosphorus distributions in the northeast Pacific. Earth Planet. Sci. Lett. 96, 305-318.

Filippelli, G.M. (2001) Carbon and phosphorus cycling in anoxic sediments of the Saanich Inlet, British Columbia. Mar. Geol. 174, 307-321.

Flögel, S., Wagner, T. (2006) Insolation-control on the Late Cretaceous hydrological cycle and tropical African climate - global climate modelling linked to marine climate records. Palaeogeogr. Palaeoclimatol. Palaeoecol. 235, 288-304.

Flögel, S., Beckmann, B., Hofmann, P., Bornemann, A., Norris, R.D., Wagner, T. (in review) Evolution of tropical watersheds and continental hydrology during the Late Cretaceous greenhouse; marine carbon burial and possible implications for the future. Earth Planet. Sci. Lett.

Forster, A., Schouten, S., Moriya, K., Wilson, P.A., Sinninghe Damsté, J.S. (2007a) Tropical warming and intermittent cooling during the Cenomanian/Turonian oceanic anoxic event 2: sea surface temperature records from the equatorial Atlantic. Paleoceanography 22, PA1219, doi:10.1029/2006PA001349.

Forster, A., Schouten, S., Baas, M., Sinnighe Damsté, J.S. (2007b) Mid-Cretaceous (Albian-Santonian) sea surface temperature records of the tropical Atlantic Ocean. Geology 35, 919-922.

François, R. (1988) A study on the regulation of the concentrations of some trace metals (Rb, Sr, Zn, Pb, Cu, V, Cr, Ni, Mn and Mo) in Saanich Inlet sediments, British Columbia, Canada. Mar. Geol. 83, 285–308.

Franke, C., Frederichs, T., Dekkers, M.J. (2007) Efficiency of heavy liquid separation to concentrate magnetic particles. Geophys. J. Int., doi: 10.1111/j.1365-246X.2007.03489.

Friedrich, O., Erbacher, J. (2006) Benthic foraminiferal assemblages from Demerara Rise (ODP Leg 207, western tropical Atlantic): possible evidence for a progressive opening of the Equatorial Atlantic Gateway. Cretaceous Res. 27, 377-397.

Friedrich, O., Erbacher, J., Mutterlose, J. (2006) Paleoenvironmental changes across the Cenomanian/Turonian boundary event (oceanic anoxic event 2) as indicated by benthic foraminifera from the Demerara Rise (ODP Leg 207). Rev. Micropaleontol. 49, 121–139.

Froelich, P.N., Klinkhammer, G.P., Bender, M.L., Luetge, N.A., Heath, G.R., Cullen, D., Dauphin, P. (1979) Early oxidation of organic matter in pelagic sediments of the eastern equatorial Atlantic: suboxic diagenesis. Geochim. Cosmochim. Acta 43, 1075-1090.

Goldstein, J.I., Newbury, D.E., Echlin, P., Joy, D.C., Romig, A.D. Jr., Lyman, C.E., Fiori, C., Lifshin, E. (1992) *Scanning electron microscopy and X-Ray microanalysis*, 2nd ed.. Plenum Press, New York, 820 pp.

Hardas, P., Mutterlose, J. (2006) Calcareous nannofossil biostratigraphy of the Cenomanian/Turonian boundary interval of Leg 207 at the Demerara Rise. Rev. Micropaleontol. 49, 165–179.

Hastings, D.W., Emerson, S.R., Mix, A.C. (1996) Vanadium in foraminiferal calcite as a tracer for changes in the areal extent of reducing sediments. Paleoceanography 11, 665–678.

Helz, G.R., Miller, C.V., Charnock, J.M., Mosselmans, J.F.W., Pattrick, R.A.D., Garner, C.D. , Vaughan, D.J. (1996) Mechanism of molybdenum removal from the sea and its concentration in black shales: EXAFS evidence. Geochim. Cosmochim. Acta 60, 3631-3642.

Hetzel, A., Brumsack, H.-J., Schnetger, B., Böttcher, M., (2006) Inorganic geochemical characterization of lithologic units recovered during ODP Leg 207 (Demerara Rise). In: Mosher, D.C., Erbacher, J., Malone, M.J. (Eds.) *Proc. ODP Sci. Results 207*, 1-37. doi:10.2973/odp.proc.sr.207.107.2006.

Ho, T.Y. (2006) The trace metal composition of marine microalgae in cultures and natural assemblages. In: Subba Rao, D.V. (Ed.) *Algal cultures: Analogues of blooms and applications*. Science Publishers, pp. 271–299

Huckriede H., Meischner D. (1996) Origin and environment of manganese-rich sediments within black shale basins. Geochim. Cosmochim. Acta 60, 1399-1413.

Huerta-Diaz, M.G., Morse, J.W. (1992) Pyritization of trace metals in anoxic marine sediments. Geochim. Cosmochim. Acta 56, 2681-2702.

Ingall, E.D., Jahnke, R.A. (1997) Influence of water-column anoxia on the elemental fractionation of carbon and phosphorus during sediment diagenesis. Mar. Geol. 139, 219-229.

Ingall, E.D., Bustin, R.M., Van Cappellen, P. (1993) Influence of water column anoxia on the burial and preservation of carbon and phosphorus in marine shales. Geochim. Cosmochim. Acta 57, 303-316.

Jacobs, E., Emerson, S. (1982) Trace metal solubility in an anoxic fjord. Earth Planet. Sci. Lett. 60, 237-252.

Junium, C. K., Arthur, M.A. (2007) Nitrogen cycling during the Cretaceous, Cenomanian-Turonian Oceanic Anoxic Event II. Geochem. Geophys. Geosyst. 8, Q03002, doi:10.1029/2006GC001328.

Karpoff, A.M., Destrigneville, C., Stille, P. (2007) Clinoptilolite as a new proxy of enhanced biogenic silica productivity in lower Miocene carbonate sediments of the Bahamas platform: Isotopic and thermodynamic evidence. Chem. Geol. 245, 285-304.

Kastner, M. (1980) Zeolites. In: Burns, R. (Ed.) *Marine Minerals*. Rev. Mineral., Mineralogical Society of America 6, pp. 111-122.

Klinkhammer, G.P., Bender, M.L. (1980) The distribution of manganese in the Pacific Ocean. Earth Planet. Sci. Lett. 46, 361– 384.

Lewan, M.D. (1984) Factors controlling the proportionality of vanadium to nickel ratios in crude oils. Geochim. Cosmochim. Acta 48, 2231-2238.

Lewan, M.D., Maynard, J.B. (1982) Factors controlling the enrichment of vanadium and nickel in the bitumen of organic sedimentary rocks. Geochim. Cosmochim. Acta 46, 2547–2560.

Lewis, B.L., Landing, W.M. (1991) The biogeochemistry of Mn and Fe in the Black Sea. Deep-Sea Res. 38, 773-803.

Lewis, B.L., Luther, G.W. (2000) Processes controlling the distribution and cycling of manganese in the oxygen minimum zone of the Arabian Sea. Deep-Sea Res. II 47, 1541-1561.

Liu, X., Millero, F.J. (2002) The solubility of iron in seawater. Mar. Chem. 77, 43-54.

Lovley, D.R. (1987) Organic matter remineralization with the reduction of ferric iron: a review. Geomicrobiol. J. 5, 375-399.

Lovley, D.R. (1991) Dissimilatory Fe(III) and Mn(IV) reduction. Microbiol. Rev. 55, 259-287.

Lunau M., Lemke A., Dellwig O., Simon M. (2006) Physical and biogeochemical controls of microaggregate dynamics in a tidally affected coastal ecosystem. Limnol. Oceanogr. 51, 847–859.

März, C., Poulton, S.W., Beckmann, B., Küster, K., Wagner, T., Kasten, S. (accepted) Redox sensitivity of P cycling during marine black shale formation - dynamics of sulfidic and anoxic, non-sulfidic bottom waters. Geochim. Cosmochim. Acta.

Meyers, P.A., Bernasconi, S.M., Forster, A. (2006) Origins and accumulation of organic matter in expanded Albian to Santonian black shale sequences on the Demerara Rise, South American margin. Org. Geochem. 37, 1816-1830.

Morford, J.L., Emerson, S.E. (1999) The geochemistry of redox sensitive trace metals in sediments. Geochim. Cosmochim. Acta 63, 1735-1750.

Morford, J.L., Emerson, S.R., Breckel, E.J., Kim, S.H. (2005) Diagenesis of oxyanions (V, U, Re, and Mo) in pore waters and sediments from a continental margin. Geochim. Cosmochim. Acta 69, 5021-5032.

Morse, J.W., Luther III, G.W. (1999) Chemical influences on trace metal-sulfide interactions in anoxic sediments. Geochim. Cosmochim. Acta 63, 3373-3378.

Morse, J.W., Millero, F.J., Cornwell, J.C., Rickard, D. (1987) The chemistry of hydrogen sulphide and iron sulphide systems in natural waters. Earth-Sci. Rev. 24, 1-42.

Mosher, D.C., Erbacher, J., Malone, M.J., Shipboard Scientific Party (2007) *Proc. ODP Sci. Results 207*. doi:10.2973/odp.proc.sr.207.2007.

Musavu-Moussavou, B., Danelian, T. (2006) The radiolarian response to oceanic anoxic event 2 in the southern part of the Northern proto-Atlantic (Demerara Rise, ODP Leg 207). Rev. Micropal. 49, 141-163.

Nealson, K.H., Myers, C.R. (1992) Microbial reduction of manganese and iron: new approaches to carbon cycling. Appl. Environ. Microbiol. 58, 439-443.

Nederbragt, A.J., Thurow, J., Pearce, R. (2007) Sediment composition and cyclicity in the Mid-Cretaceous at Demerara Rise, ODP Leg 207. In: Mosher, D.C., Erbacher, J., Malone, M.J. (Eds.) *Proc. ODP Sci. Results 207*, 1-31, doi:10.2973/odp.proc.sr.207.103.2007

Neumann, T., Heiser, U., Leosson, M.A., Kersten, M. (2002) Early diagenetic processes during Mn-carbonate formation: Evidence from the isotopic composition of authigenic Ca-rhodochrosites of the Baltic Sea. Geochim. Cosmochim. Acta 66, 867-879.

Paytan, A., Griffith, E.M. (2007) Marine barite: Recorder of variations in ocean export productivity. Deep-Sea Res. II 54, 687-705.

Paytan, A., Kastner, M., Campbell, D., Thiemens, M.H. (2004) Seawater sulfur isotope fluctuations in the Cretaceous. Science 304, 1663-1665.

Percy, D., Li, X., Taylor, G.T., Astor, Y., Scranton, M.I. (in press) Controls on iron, manganese and intermediate oxidation state sulfur compounds in the Cariaco Basin. Mar. Chem.

Pletsch, T., Erbacher, J., Holbourn, A.E.L., Kuhnt, W., Moullade, M., Oboh-Ikuenobede, F.E., Söding, E., Wagner, T., 2001. Cretaceous separation of Africa and South America: the view from the West African margin (ODP Leg 159). J. S. Am. Earth Sci. 14, 142-174.

Poulton, S.W., Krom, M.D., Raiswell, R. (2004) A revised scheme for the reactivity of iron (oxyhyr)oxide minerals towards dissolved sulfide. Geochim. Cosmochim. Acta 68, 3703-3715.

Poulton, S.W., Canfield, D.E. (2006) Co-diagenesis of iron and phosphorus in hydrothermal sediments from the southern East Pacific rise: Implications for the evaluation of paleoseawater phosphate concentrations. Geochim. Cosmochim. Acta 70, 5883-5898.

Redfield, A.C. (1958) The biological control of chemical factors in the environment. Am. Sci. 64, 205-221.

Rosenthal., Y., Lam, P., Byle, E.A., Thomson, J. (1995) Authigenic cadmium enrichments in suboxic sediments: Precipitation and postdepositional mobility. Earth Planet. Sci. Lett. 132, 99-111.

Ruttenberg, K.C. (1992) Development of a sequential extraction method for different forms of phosphorus in marine sediments. Limnol. Oceanogr. 37, 1460-1482.

Schenau, S.J., De Lange, G.J. (2000) A novel chemical extraction method to quantify fish debris in marine sediments. Limnol. Oceanogr. 45, 963-971.

Schenau, S.J., Slomp, C.P., De Lange, G.J. (2000) Phosphogenesis and active phosphorite formation in sediments from the Arabian Sea oxygen minimum zone. Mar. Geol. 169, 1-20.

Schlanger, S.O., Jenkyns, H.C. (1976) Cretaceous oceanic anoxic events: Causes and consequences. Geol. Mijnbouw 55, 179-184.

Scholz, F., Neumann, T. (2007) Trace element diagenesis in pyrite-rich sediments of the Achterwasser lagoon, SW Baltic Sea. Mar. Chem. 107, 516-532.

Schoonen, M.A.A. (2004) Mechanisms of sedimentary pyrite formation. In: Amend, J.P., Edwards, K.J., Lyons, T.W. (Eds.) *Sulfur Biogeochemistry – Past and Present*. GSA Spec. Pap. 379, pp. 117-134.

Schulz, H.D. (2006) Quantification of early diagenesis: Dissolved constituents in pore water and signals in the solid phase. In: Schulz, H.D., Zabel, M. (Eds.) *Marine Geochemistry*, 2nd ed. Springer, pp. 73-124.

Sinninghe Damsté, J.S., De Leeuw, J.W. (1990) Analysis, structure and geochemical significance of organically-bound sulphur in the geosphere: State of the art and future research. Org. Geochem. 16, 1077-1101.

Sinninghe Damsté, J.S., Kok, M.D., Köster, J., Schouten, S. (1998) Sulfurized carbohydrates: an important sedimentary sink for organic carbon? Earth Planet. Sci. Lett. 164, 7-13.

Slomp, C.P., Van der Gaast, S.J., Van Raaphorst, W. (1996) Phosphorus binding by poorly crystalline iron oxides in North sea sediments. Mar. Chem. 52, 55-73.

Stone, A.T., Morgan, J.J. (1987) Reductive dissolution of metal oxides. In: Stumm, W. (Ed.) *Aquatic Surface Chemistry*. Wiley, Chichester, pp. 221-254.

Stumm, W., Sulzberger, B. (1992) The cycling of iron in natural environments: Considerations based on laboratory studies of heterogeneous redox processes. Geochim. Cosmochim. Acta 56, 3233-3257.

Tebo, B.M. (1991) Manganese(II) oxidation in the suboxic zone of the Black Sea. Deep-Sea Res. 38 (Suppl. 2), 883-905.

Thurow, J. (1988) Diagenetic history of Cretaceous radiolarians, North Atlantic Ocean (ODP Leg 103 and DSDP Holes 398D and 603B). In: Boillot, G., Winterer, E.L. (Eds.) *Proc. ODP Sci. Results 103*, 531-555.

Torres, M.E., Brumsack, H.J., Bohrmann, G., Emeis, K.C. (1996) Barite fronts in continental sediments: a new look at barium remobilization in the zone of sulfate reduction and formation of heavy barites in authigenic fronts. Chem. Geol. 127, 125-139.

Tribovillard, N., Riboulleau, A., Lyons, T., Baudin, F. (2004) Enhanced trapping of molybdenum by sulfurized marine organic matter of marine origin in Mesozoic limestones and shales. Chem. Geol. 213, 385-401.

Tribovillard, N., Algeo, T.J., Lyons, T., Riboulleau, A. (2006) Trace metals as paleoredox and paleoproductivity proxies: An update. Chem. Geol. 232, 12-32.

Turekian, K.K., Wedepohl, K.H. (1961) Distribution of the elements in some major units of the Earth´s crust. Geol. Soc. Am. Bull. 72, 175-192.

Van der Weijden, C. (2002) Pitfalls of normalization of marine geochemical data using a common divisor. Mar. Geol. 184, 167-187.

Vogt, C., Lauterjung, J., Fischer, R.X. (2002) Investigation of the clay fraction (<2 μm) of the clay mineral society reference clays. Clay. Clay Miner. 50, 388-400.

Wagner, T. (2002) Late Cretaceous to early Quaternary organic sedimentation in the eastern Equatorial Atlantic. Palaeogeogr. Palaeoclimatol. Palaeoecol. 179, 113-147.

Wagner, T., Pletsch, T., 1999. Tectono-sedimentary controls on Cretaceous black shale deposition along the opening Equatorial Atlantic Gateway (ODP Leg 159). In: Cameron, N., Bate, R., Clure, V. (Eds.) *The Oil and Gas Habitats of the South Atlantic*. Geol. Soc. London. Spec. Pub. 153, 241-265.

Wagner, T., Sinninghe Damsté, J.S., Hofmann, P., Beckmann, B. (2004) Euxinia and primary production in Late Cretaceous eastern equatorial Atlantic surface waters fostered orbitally driven formation of marine black shales. Paleoceanography 19, PA3009. doi:10.1029/2003PA000898.

Wehrli, B., Stumm, W. (1989) Vanadyl in natural waters: adsorption, and hydrolysis promote oxygenation. Geochim. Cosmochim. Acta 53, 69-77.

Yakushev, E.V., Pollehne, F., Jost, G., Kuznetsov, I., Schneider, B., Umlauf, L. (in press) Analysis of the water column oxic/anoxic interface in the Black and Baltic seas with a numerical model. Mar. Chem.

Yao, W., Millero, F.J. (1996) Oxidation of hydrogen sulfide by hydrous Fe(III) oxides in seawater. Mar. Chem. 52, 1-16.

Zheng, Y., Anderson, R.F., van Geen, A., Kuwabara, J.S. (2000) Authigenic molybdenum formation in marine sediments: A linkage to pore water sulfide in the Santa Barbara Basin. Geochim. Cosmochim. Acta 64, 4165-4178.

5. Coniacian-Santonian deep ocean anoxia/euxinia inferred from molecular and inorganic markers: Results from the Demerara Rise (ODP Leg 207)

Britta Beckmann (1*), Peter Hofmann (1), Christian März (2), Stefan Schouten (3), Jaap S. Sinninghe Damsté (3), Thomas Wagner (4)

*(1) Institute for Geology and Mineralogy, University of Cologne, Zülpicher Str. 49a, 50674 Köln, Germany (bbeckman@uni-koeln.de, peter.hofmann@uni-koeln.de, * corresponding author, Tel.: +49 421 2188938; fax: +49 421 2187431)*

(2) Department of Geosciences, University of Bremen, Klagenfurter Str., 28359 Bremen, Germany (cmaerz@uni-bremen.de)

(3) Department of Marine Biogeochemistry and Toxicology, Royal Netherlands Institute for Sea Research, P.O. Box 59, 1790 Den Burg, Texel, The Netherlands (schouten@nioz.nl, damste@nioz.nl)

(4) School of Civil Engineering and Geosciences, University of Newcastle, Newcastle upon Tyne, NE1 7RU, United Kingdom (thomas.wagner@newcastle.ac.uk)

Abstract:

We investigated Coniacian to early Santonian sediments from ODP site 1261, Demerara Rise, using organic, inorganic and molecular methods to reconstruct the development of ocean water anoxia/euxinia. High lycopane/n-C_{31} ratios of up to 4.5 suggest oxygen-depleted conditions in the water column for most of the time. Lower ratios (~1) across the early to mid Coniacian transition probably mark a period of better oxygenation. In two higher-resolution intervals we observe strong enrichment in Zn, concurrent with an increase in the lycopane/n-C_{31} ratio, identifying the onset of euxinic bottom waters, whereas decreases in lycopane/n-C_{31} ratio and in Ni enrichment characterize the termination of sulfidic conditions. Photic zone euxinia (PZE) appears to be restricted to the early Coniacian interval, as isorenieratene derivates were exclusively detected in the lowermost part of the section, supporting progressive weakening of upwelling intensities from the mid-Coniacian onwards.

Keywords: Oceanic anoxic event 3, black shale, anoxia, euxinia, isorenieratane, lycopane, trace metals, Demerara Rise, ODP Site 1261

6. Are the Kimmeridge Clay deposits affected by "burn-down" events? A palynological and geochemical approach

Monika Kodrans-Nsiah (1) *, Christian März (1), Ian C. Harding (2), Sabine Kasten (3), Karin A. F. Zonneveld (1)

(1) Fachbereich 5-Geowissenschaften, University of Bremen, Postfach 330440, D-28334 Bremen, Germany (Corresponding author: mknsiah@uni-bremen.de, tel. +49 4212183975, fax +49 4212184451)*

(2) School of Earth and Ocean Science, National Oceanographic Centre, European Way, SO14 3ZH, Southampton, UK

(3) Alfred Wegener Institute for Polar and Marine Research, Am Handelshafen 12, 27570 Bremerhaven, Germany

Abstract

Two independent analytical approaches, palynological and inorganic geochemical, were applied to identify potential oxygenation "burn-down" events in the upper Kimmeridge Clay Formation (KCF) deposited in the Jurassic Wessex Basin. The KCF interval spanning 121.82-122.72 m depth was sampled from the Swanworth Quarry 1 borehole (Dorset, UK) at 2.5-5.0 cm resolution. Samples were analysed for total organic carbon (TOC), palynofacies components, organic-walled dinoflagellate cysts (dinocysts), and concentrations of elements that are known to be productivity- and/or nutrient-related (e.g. Cu, P), detrital (e.g. Al, Ti, Zr) and redox-sensitive/sulfide-forming (e.g. Fe, Mn, S). Overall, TOC contents exceed 2 wt%, with a maximum of 8.8 wt% at 122.37 cm depth and elevated values in the central part of the investigated interval. This interval of relatively higher TOC values correlates well with the maximum recovery of marine palynomorph absolute abundances and low Al values, suggesting that TOC is primarily of marine organic matter. As the amount of marine palynomorphs and TOC content diminishes from the middle part of the studied section upwards, species-specific changes in dinocyst assemblages can be observed. In particular, abundances of Circulodinium spp., Cyclonephelium spp., Sirmiodinium grossi, Senoniasphaera jurassica and Systematophora spp. decrease rapidly in comparison to other species, such as

Glossodinium dimorphum and Cribroperidinium sp. 1. Sharp changes in Fe/Al, Mn/Al and S at 122.37 m depth mark a shift from anoxic/euxinic conditions in the lower and middle part of the studied interval to more oxic conditions in its upper part. Such a shift could explain the high TOC and marine palynomorphs abundances as a result of better preservation, and the subsequent drop in abundances as an effect of a "burn-down", i.e. organic matter oxidation. Although the shift in redox-sensitive elements is very sharp and the major changes in TOC and marine palynomorphs occur at the same level, the changes in TOC and marine palynomorphs are gradual and less pronounced. We suggest that enhanced organic matter preservation due to anoxic/euxinic conditions was the reason for high TOC and marine palynomorphs values in the central part of the studied interval. Oxygenation of bottom and pore waters within the sediment was most probably the cause for decreasing TOC values and reduced recovery of marine palynomorphs towards the top of the studied interval.

Keywords: Kimmeridge Clay Formation, preservation, productivity, palynofacies, organic-walled dinoflagellate cysts, trace metals, oxidation front

7. Conclusions and perspectives

In this work, we used the great potential of combining different redox-sensitive geochemical parameters in combination with high sample resolution. This approach revealed primary and diagenetic effects of rapid paleoenvironmental changes on sediment composition in different marine depositional regimes and at different times of Earth history. In particular, combining high-resolution sequential Fe and P extractions gave important and new insights into their biogeochemical cycling under various bottom water and sediment redox conditions. Most important amongst our findings in terms of paleoredox conditions in the Late Cretaceous deep ocean was the phosphate coupling to Fe (oxyhydr)oxides under obviously anoxic bottom water conditions, and in particular the preservation of this coupling within deeply buried Late Cretaceous black shales. In addition, detailed investigations of redox-sensitive trace element (Cd, Mo, Ni, V, Zn) systematics in these black shales not only enabled us to distinguish between subtle variations at the lower end of the bottom water redox scale, namely sulfidic and anoxic, non-sulfidic bottom water conditions. They also gave interesting insights into coupling of trace elements to different sedimentary phases, i.e. Mo and Ni mostly bound to (sulfurized) organic matter, Cd and Zn forming pure sulfides. In Zambesi deep-sea fan deposits, the diagenetic re-distribution of Fe(III)-adsorbed phosphate within the sulfate/methane transition, and its transformation to authigenic Fe(II)-phosphate minerals as vivianite below it has not been described before in such detail. Preliminary findings in continental slope sediments off the Amazon and Rio de La Plata show very similar pore water, solid phase and P speciation patterns as off the Zambesi, indicating that vivianite precipitation below the SMT might be a globally important P sink in such settings. Notably, this focussed P re-distribution at a certain diagenetic front has to be recognized as a process different than the rather gradual P „sink switching“ to authigenic apatite in marine sediments during deep sediment burial.

The results of this study lead to some potentially important recommendations for investigating rapid paleoclimatic changes in aquatic sediments. A major point is that working in high sampling resolution not only in (sub)recent, but also in ancient marine deposits is one of the keys to successfully identify sedimentary signals of paleoenvironmental changes in their full scope - most of our findings would not have been possible without high sampling resolution. However, sampling and studying paleoenvironmental key sections in sedimentary succession in high resolution is only sensible if there is already a lower-resolution framework of background

information available. Choosing the most suitable interval for a more detailed look is crucial for a successful paleoenvironmental interpretation, as applying high-resolution geochemical analyses e.g. to a whole ODP core is normally limited by time and money. Another important point to mention is that working on deep-sea drill cores - in contrast to outcrop samples - yields sample material usually much less affected by external physicochemical processes like weathering, and thus has a much higher potential to identify original primary and diagenetic sediment properties.

Geochemical analyses are usually resting on a basis of elemental concentrations in sediments or ionic species in pore waters. In ancient sediments, pore water data are often scarce, and if available, they rather document the present-day redox state of a sediment instead of paleoredox conditions. In such cases, but also in addition to pore water analyses in (sub)recent sediments, valuable information about the speciation (and thus the redox state, reactivity and bioavailability) of certain sediment components can be gained by sequential extraction techniques. Especially Fe and P speciation data of a sediment can tell a lot about bottom water and sediment redox conditions during its deposition, about its post-depositional (diagenetic) redox development, and about authigenic mineral formation. In combination with more traditional redox parameters - such as certain trace metal (Cd, Mn, Mo, Ni, V, Zn) contents, enrichments or depletions -, a detailed redox scheme can be established that has the potential to trace even subtle changes at the lower end of the redox scale, i.e. anoxic non-sulfidic versus sulfidic. In addition, the combination of purely inorganic-geochemical analyses with other mineralogical and optical techniques as X-ray diffraction or scanning electron microscopy provides a more comprehensive picture of a sediment´s primary mineralogy and authigenic mineral formation.

Danksagung

Mein ganz besonderer Dank gilt meiner lieben Chefin und Mutti PD Dr. Sabine Kasten, und nicht nur für Vergabe und exzellente Betreuung meiner Arbeit. Sie hat mir ausserdem eine immer spannende, produktive Zusammenarbeit auf Augenhöhe ermöglicht, bei der der Spass nie zu kurz kam. Ob im Kühlkeller der Meteor oder am Schreibtisch - die Entscheidung, von Heidelberg nach Bremen gekommen zu sein, habe ich nie bereut.

Dem zweiten Initiator meines Doktorandenprojektes, Prof. Dr. Gert de Lange aus Utrecht, danke ich für sein stetes Interesse an meinen aktuellen Arbeiten, seine hervorragenden Ideen in fachlichen Fragen und einen ausgesprochen angenehmen Humor.

Professor Dr. Horst Schulz möchte ich vielmals danken für die Übernahme des zweiten Gutachtens, für fachliche Tips und Anregungen, sowie für seine wie selbstverständliche Gastfreundschaft in den Büros und Labors der Arbeitsgruppe Hydrogeologie und Geochemie, in der ich mich sehr wohl gefühlt habe.

Ich möchte weiterhin allen aktuellen und ehemaligen Mitgliedern der erwähnten Arbeitsgruppe danken, die zu der freundschaftlichen, fast familiären Atmosphäre beigetragen haben (Karsten, Silvana, Susanne, Luzie, André, Jens, Veith, Tobi, Kathrin, Natascha, Katharina, Michael, Kerstin, Maik, Fanni, Jens, Simone, Niklas, Tim, Jan, Martin, Jürgen, Kay, Matthias, Frau Haack). Sie haben mir den Einstieg in die Arbeit in einer neuen Umgebung sehr erleichtert, und waren in drei Jahren stets mit Rat, Tat und viel Kaffee eine grosse Hilfe. Danke vor allem an Veith, Tobi und Kathrin, meine Bürogenossen während der vergangenen drei Jahre in Raum 3040 - sie haben massgeblich dazu beigetragen, dass ich jeden Morgen gern zur Arbeit gekommen.

Der Arbeitsgruppe Geochemistry an der Universität Utrecht (Tom, Shauna, Vincent, Goulven, Sandra, José, Sokratis, Iana, Peter, Haydon, Babek, Constantin, Martin, Susann, Doug, Vasso, Claudette, Pien, Caroline, Gert) möchte ich für die freundliche Aufnahme danken, für die gute Gesellschaft beim sogenannten Mittagessen und für die Einblicke in eine so internationale Arbeitsgruppe in den Niederlanden über 2 Monate.

Mein grosser Dank geht weiterhin nach Newcastle, wo mir Dr. Simon Poulton und Prof. Dr. Tom Wagner einen Monat lang und darüber hinaus eine kaum zu überschätzende Hilfe im Labor und beim Schreiben waren. Danke auch an Leonie, Thomas, Gianna und Alessia Rutten, die mir in diesem Monat eine wunderbare „Familie“ waren.

Das beste Labor ist nichts ohne Leute, die damit umgehen können – danke an Karsten Enneking,

Silvana Pape, Susanne Siemer und Britt Kockisch für stets herausragenden Einsatz für meine Analysen und immer mal einen Spass nebenbei. Tim Haarmann, Niklas Allroggen und vor allem Jan Hoffmann standen mir als wissenschaftliche Hilfskräfte im Labor ausgesprochen hilfreich zur Seite.
Das Internationale Graduiertenkolleg EUROPROX, in dessen Rahmen meine Doktorarbeit stand, habe ich immer als eine konzeptionell sehr sinnvolle Einrichtung empfunden, auch wenn interdisziplinäres Arbeiten in der Praxis nicht immer leicht ist. Danke an Professor Dr. Helmut Willems als Sprecher des Graduiertenkollegs, sowie an Prof. Dr. Thilo von Dobeneck und PD. Dr. Karin Zonneveld als Vize-Sprecher. Mindestens genauso wichtig einzuordnen ist die Arbeit von von Maria Petrogiannis und Marion Milling-Goldbach im EUROPROX-Sekretariat. Herzlichen Dank und natürlich viel Erfolg auch an alle anderen EURPROX-Doktoranden und -Postdocs, die ein wirklich nettes und fachliches sehr gutes Team waren und sind.
Wer mich kennt, weiss auch, dass es ohne Sport für mich nicht geht - daher vielen Dank an alle Mitglieder der Unisport-Teams, bei denen ich in den letzten Jahren Mitglied war - insbesondere der Hochschulsportgruppe Turnen. Und danke auch an meine Donnerstag-Bürgerpark-Kicker und Freitags-Sportgarten-Kicker.
Mein Freund und Mitbewohner Tjark hatte immer ein offenes Ohr für Probleme, und seine Gesellschaft in der Küche, vor dem Fernseher, unterwegs im Viertel oder in Frankreich war immer eine echte Bereicherung meines Tages - danke, Grosser.
Meine lieben Eltern haben es geschafft, mir sogar über 600 Kilometer ein Gefühl der Sicherheit und des Vertrauens zu vermitteln, das mich die ganze Zeit über unterschwellig begleitet und mich stets und in allen Lagen motiviert hat - ich danke Euch. Die räumliche Distanz zu meinem Bruder war zwar oft bedauerlich, hat aber unserer Verbundenheit zueinander keinen Abbruch getan - danke, Matze.
Meine Süsse musste in der Endphase der Doktorarbeit zwar des öfteren um ihr Recht in meinem Leben kämpfen, aber ich bin ungemein froh und dankbar dafür, dass ich sie habe und sie mir in allen Dingen den Rücken stärkt und mein Leben unschätzbar bereichert - danke, mein Kleines.